The Abdus Salam
International Centre for Theoretical Physics

United Nations
Educational, Scientific and
Cultural Organization

IAEA
International Atomic Energy Agency

2031-1

Joint ICTP/IAEA School on Novel Synchrotron Radiation Applications

16 - 20 March 2009

Powder Diffraction - Overview and Applications

P. Scardi
University of Trento
Italy

Joint ICTP/IAEA School on Novel Synchrotron Radiation Applications
Trieste, March 16-20, 2009

Powder Diffraction

overview and applications

Prof. Paolo Scardi

Department of Materials Engineering and Industrial Technologies,

University of Trento

PRESENTATION OUTLINE

PART 1

- Basic elements of crystallography and X-ray diffraction (XRD) theory
- Some advantages and peculiarities of synchrotron radiation XRD (SRXRD)

PART 2

- SRXRD from nanocrystalline and highly deformed materials

STRUCTURE & MICROSTRUCTURE

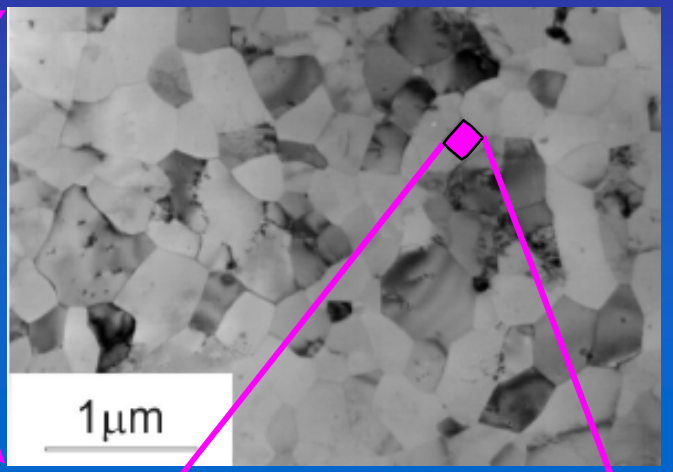

Al

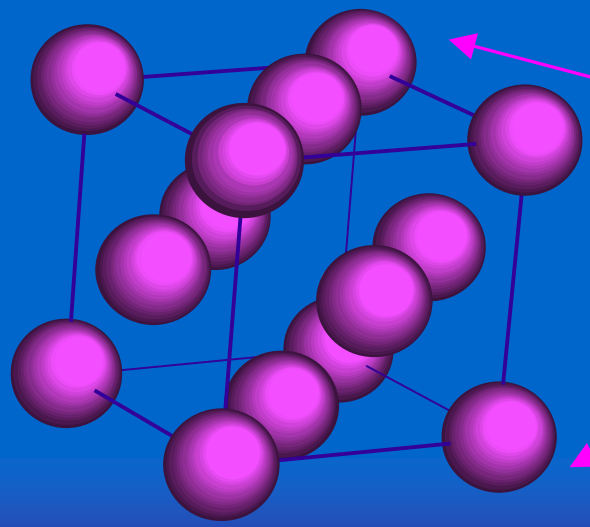

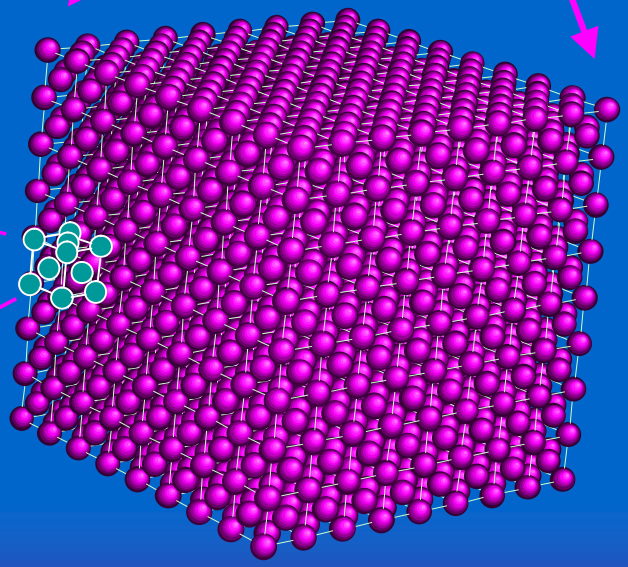

P. Scardi, University of Trento, March 2009 - © Do not copy – Do not reproduce

ATOMIC PLANES AND DIFFRACTION CONDITION

$$\lambda = 2\, d_{hkl} \sin\theta_B$$

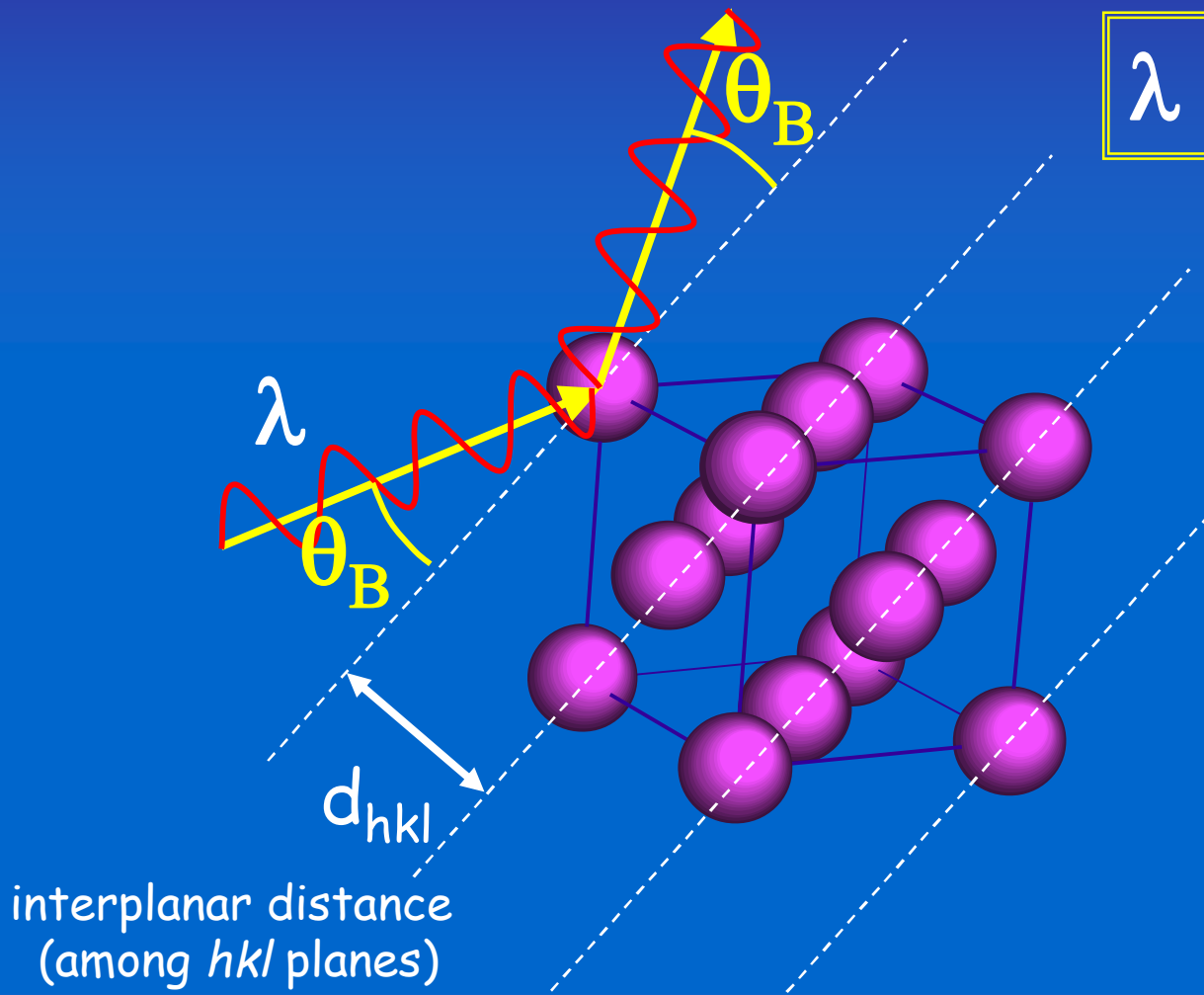

Miller indices (hkl)

(111)

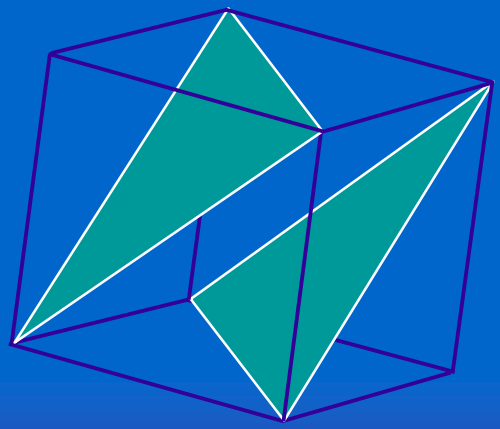

ATOMIC PLANES AND DIFFRACTION CONDITION

$$MP + PN = 2d_{hkl} \sin\theta = n\lambda$$ Bragg Law

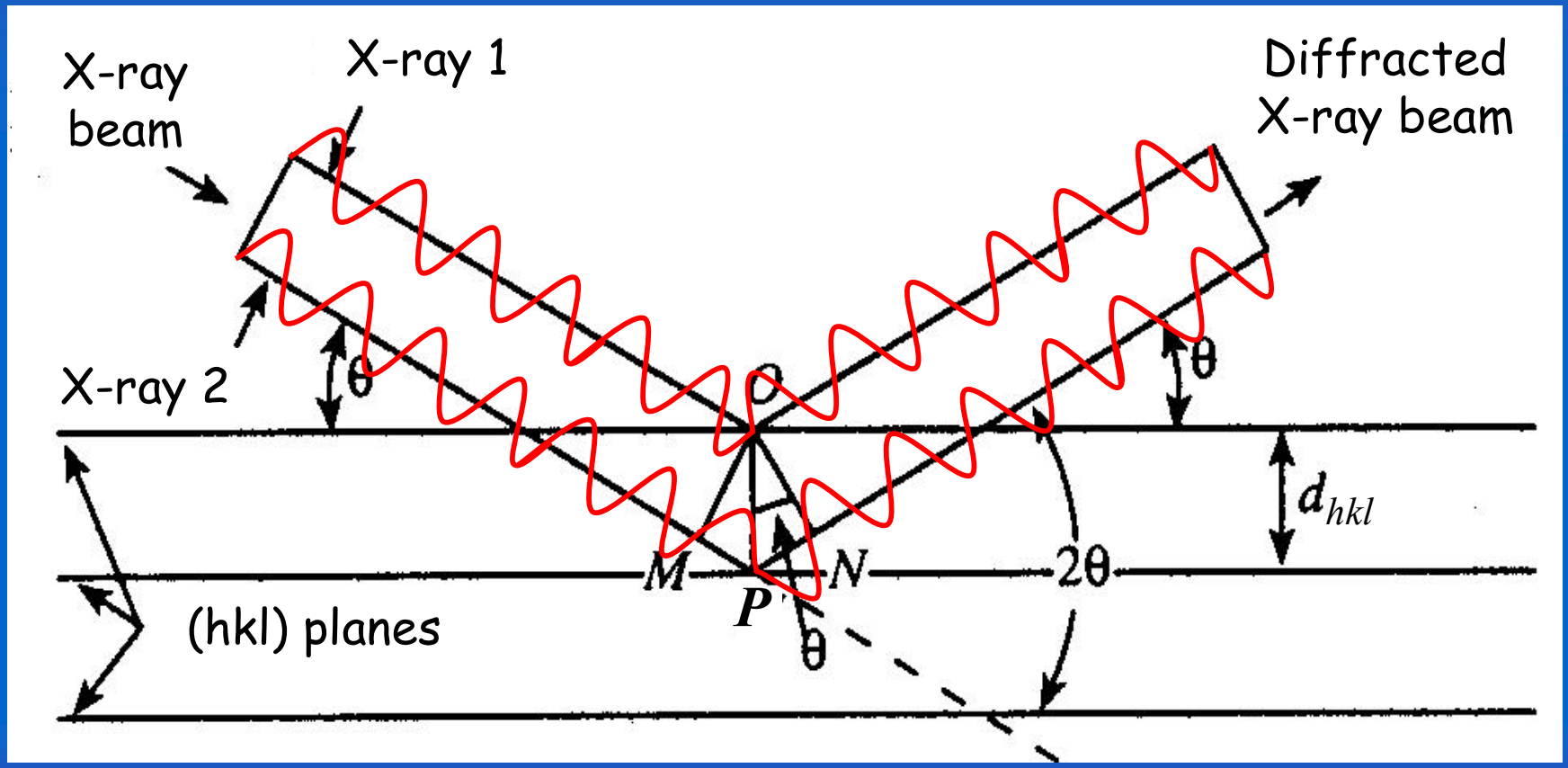

ATOMIC PLANES AND DIFFRACTION CONDITION

Interplanar distance, d_{hkl}

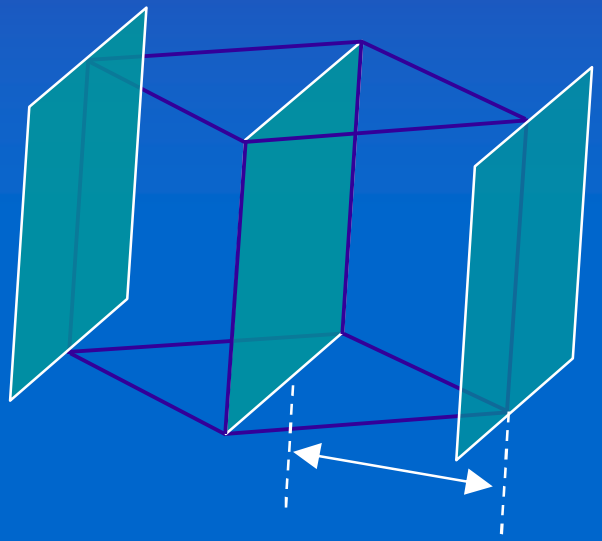

$$d_{110} = \frac{a}{\sqrt{1^2 + 1^2}} = a/\sqrt{2}$$

(110)

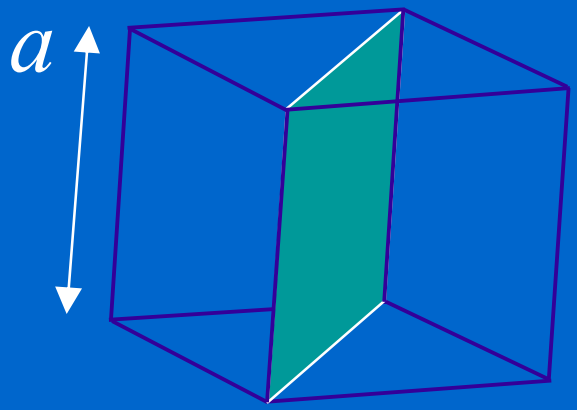

For cubic materials: $d_{hkl} = \frac{a}{\sqrt{h^2 + k^2 + l^2}}$

COHERENT vs INCOHERENT SCATTERING

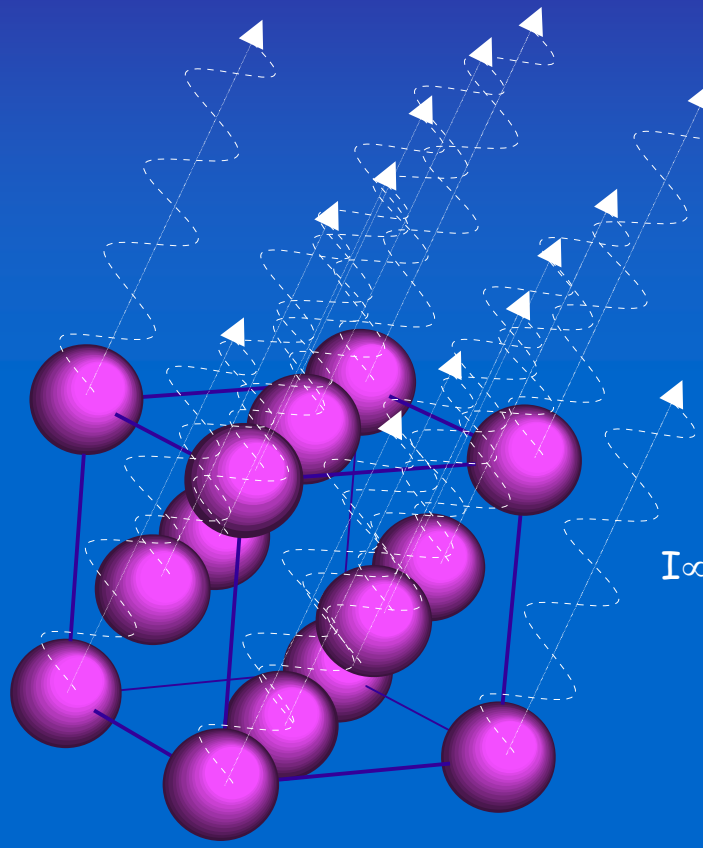

$$\lambda = 2\, d_{hkl} \sin\theta_B$$

Coherent (*diffraction*):

$I \propto (1+1+1+1+1+1+1+1+1+1+1+1+1+1+1)^2$

Incoherent (*reflection*)

$I \propto 1^2+1^2+1^2+1^2+1^2+1^2+1^2+1^2+1^2+1^2+1^2+1^2+1^2+1^2+1^2$

In diffraction conditions the scattered intensity is proportional to the **square of the sum of the amplitudes**

(all atoms are 'in phase')

DIRECT AND RECIPROCAL SPACE

For a perfect (infinite) crystal the ***reciprocal lattice*** is made of *infinitely small* points representing sets of planes of Miller indices *hkl* ***(↓ 2D projection)***

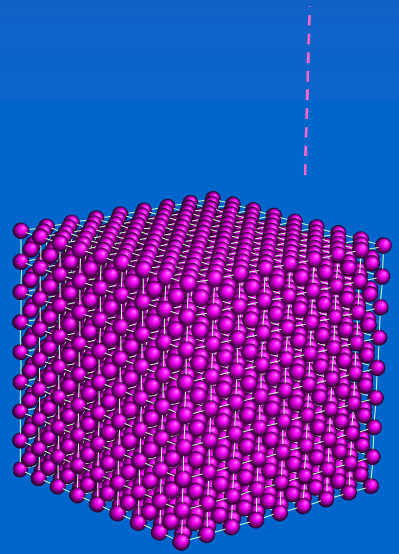

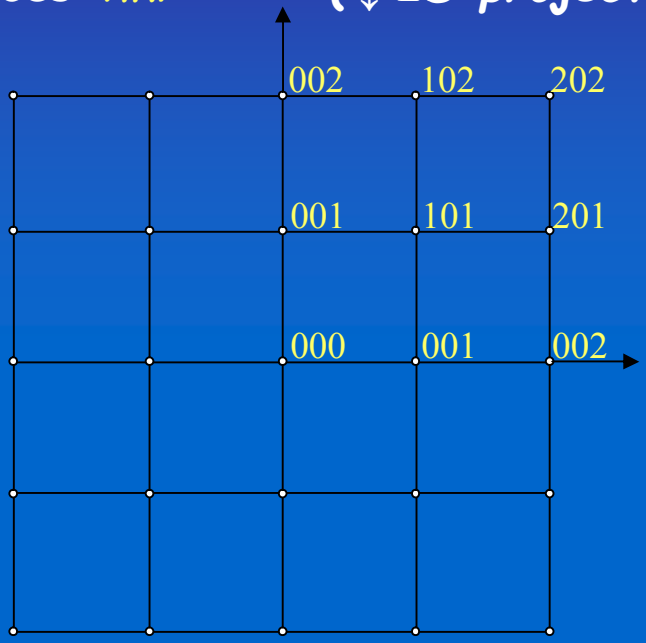

The distance d^*_{hkl} from the 000 origin to a *hkl* point is the ***inverse of the interplanar distance***

$$d^*_{hkl} = \left|\underline{d}^*_{hkl}\right| = \frac{1}{d_{hkl}}$$

DIFFRACTION FROM A SINGLE CRYSTAL

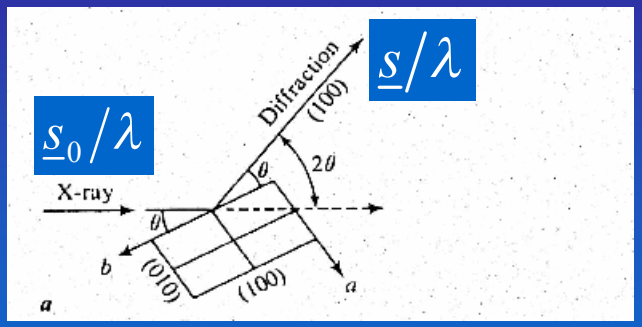

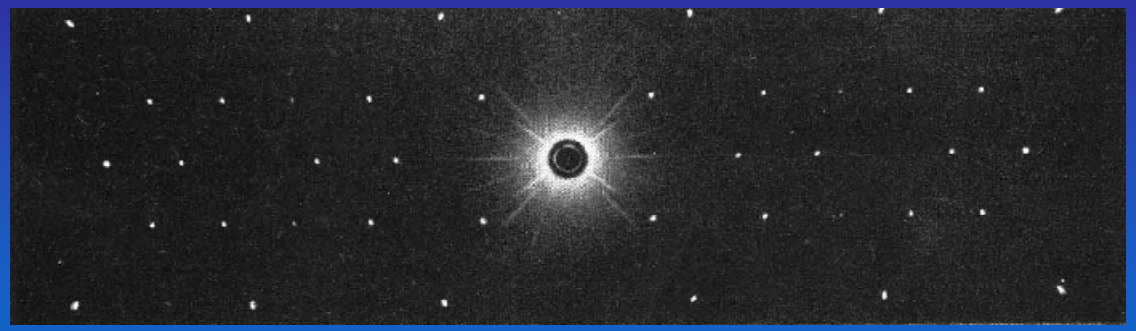

Diffraction conditions correspond to the scattering vector $(\underline{s}-\underline{s}_0)/\lambda$ being equal to:

$$\frac{\underline{s}}{\lambda}-\frac{\underline{s}_0}{\lambda}=\underline{d}^*_{hkl}$$

$$\lambda = 2\, d_{hkl} \sin\theta$$

Bragg law

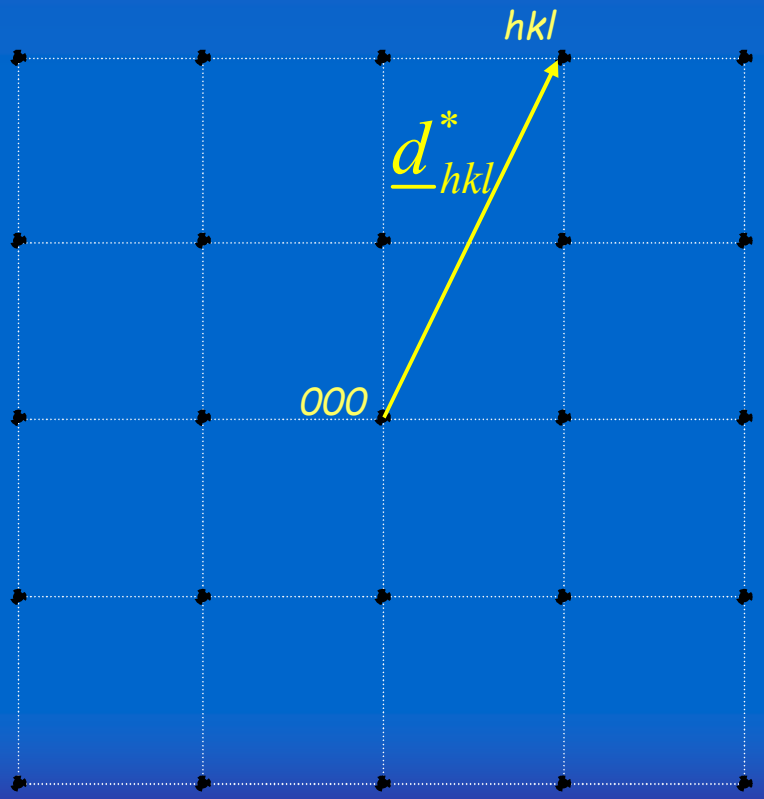

RECIPROCAL LATTICE: DIFFRACTION CONDITIONS

For a given wavelenght, the Bragg law sets a limit to the interplanar distances for which diffraction is observed:

$$\sin\theta = \lambda/2d = \lambda d^*/2 \leq 1$$

$$d^* \leq \frac{2}{\lambda}$$

All points representing planes that can diffract are inside a sphere of finite radius, ***2/λ*** ***(limiting sphere)***

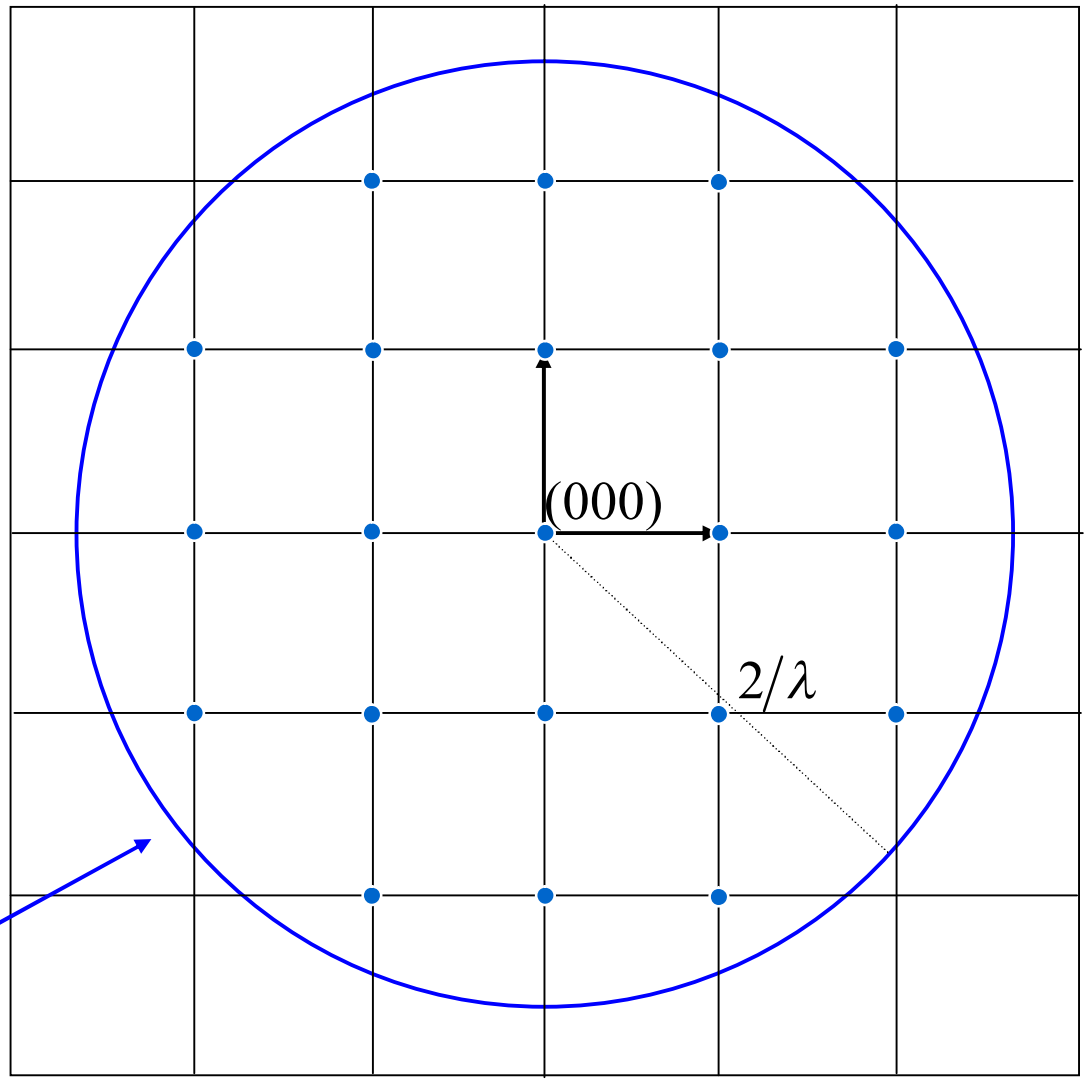

DIFFRACTION: SINGLE CRYSTAL AND POWDER

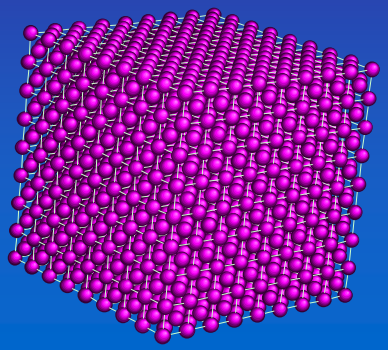

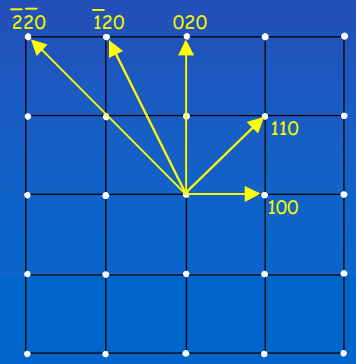

single crystal

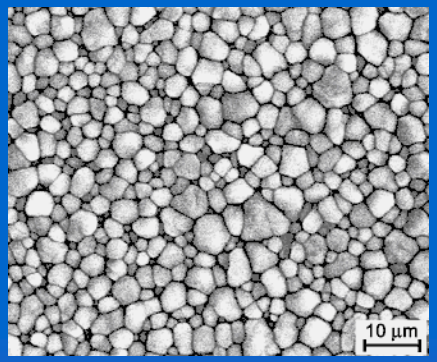

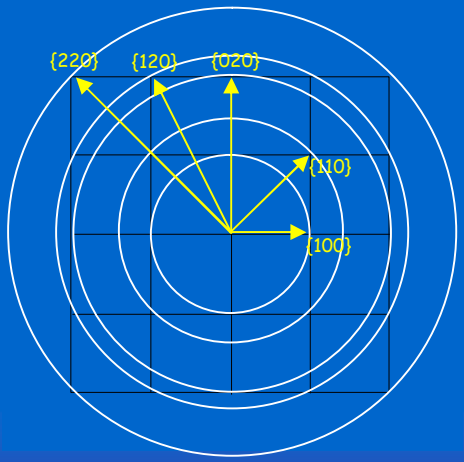

powder
(bulk polycrystalline)

DIFFRACTION: SINGLE CRYSTAL AND POWDER

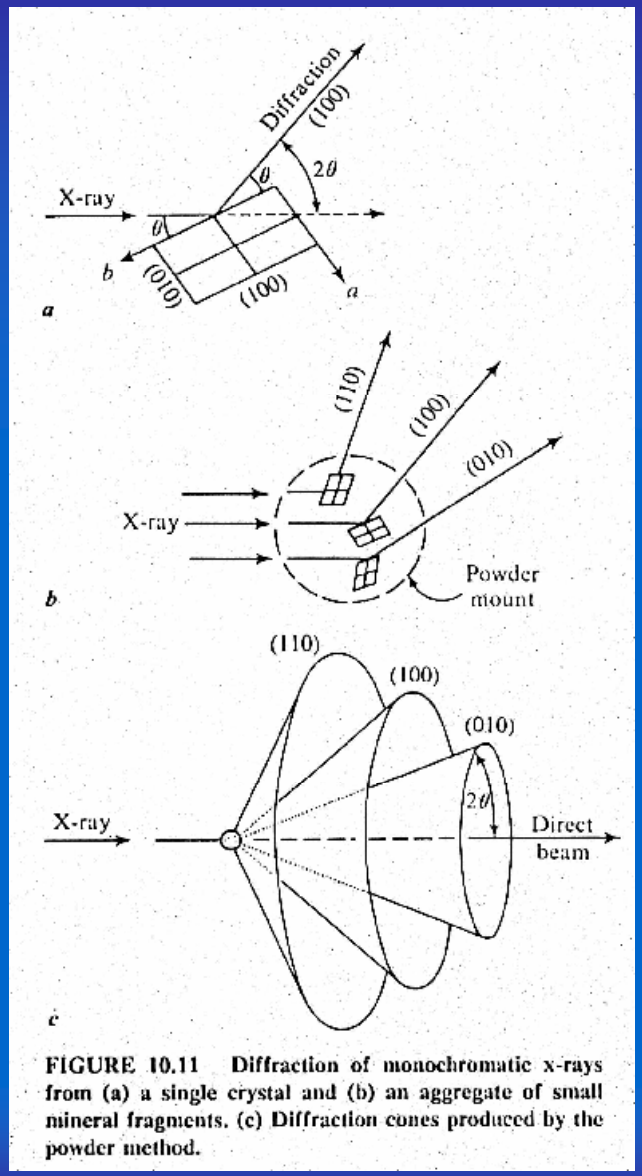

FIGURE 10.11 Diffraction of monochromatic x-rays from (a) a single crystal and (b) an aggregate of small mineral fragments. (c) Diffraction cones produced by the powder method.

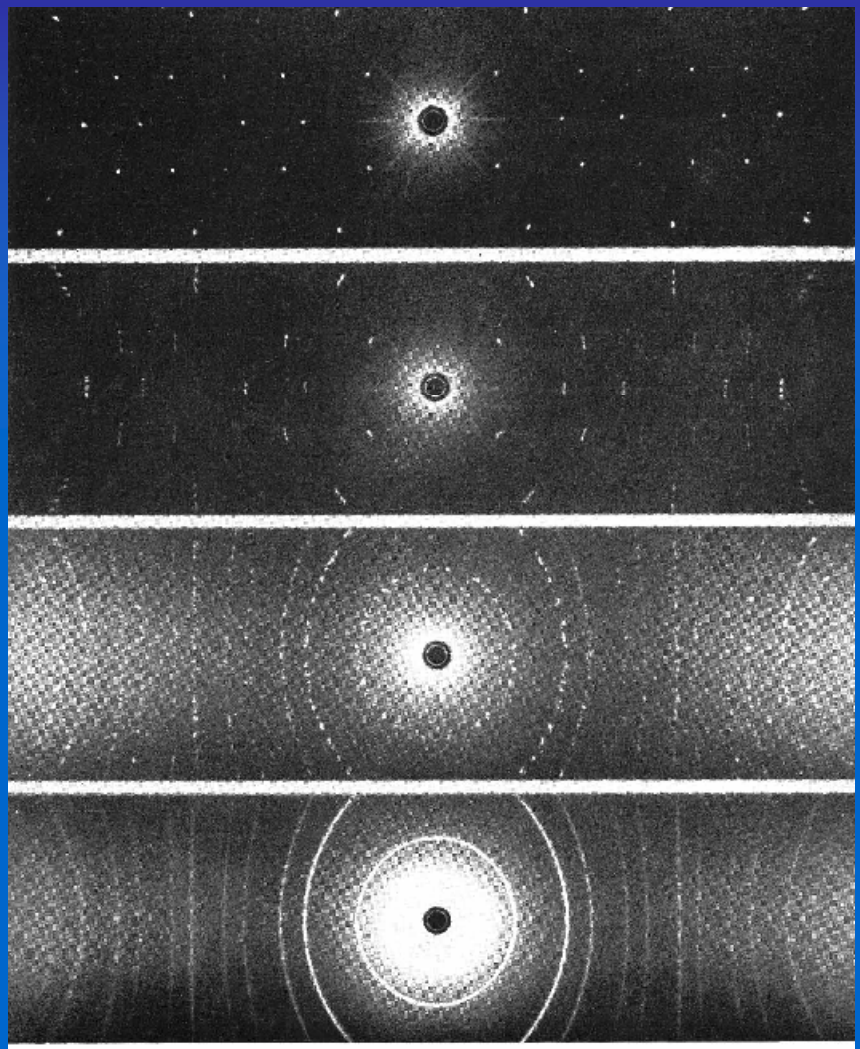

(From top to bottom). Fig. 197: Single-crystal rotation photograph of fluorite [100] vertical: Fig. 198: Single-crystal rotation photograph of fluorite [100] 2° to vertical: Fig. 199; X-ray photograph of five randomly oriented crystals of fluorite: Fig. 200; Powder photograph of fluorite.

DEBYE-SCHERRER GEOMETRY

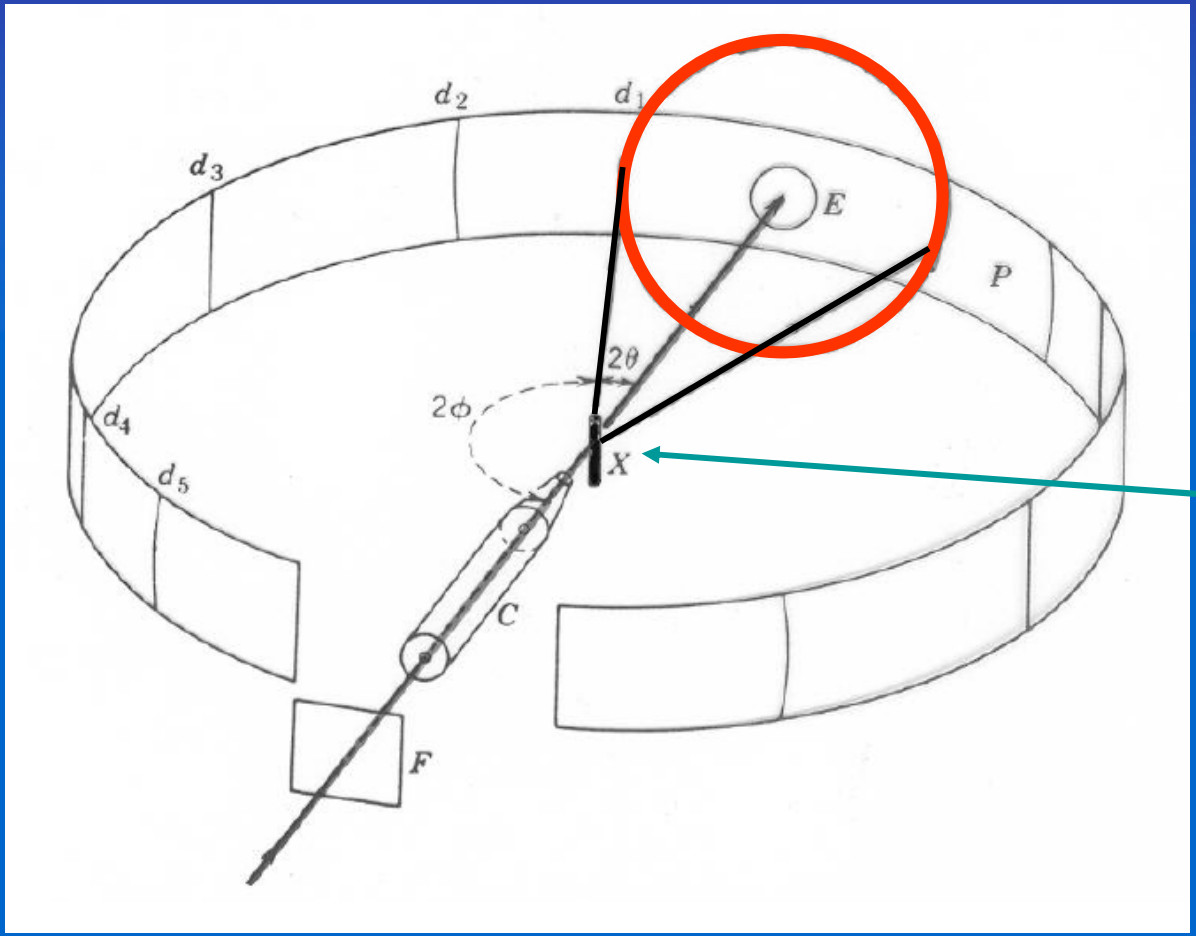

POWDER

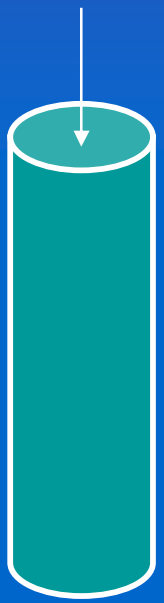

SRXRD POWDER GEOMETRY: A TYPICAL EXAMPLE

Parallel beam geometry at ID31 (ESRF)

ID31 Goniometer and nine-crystal analyzer

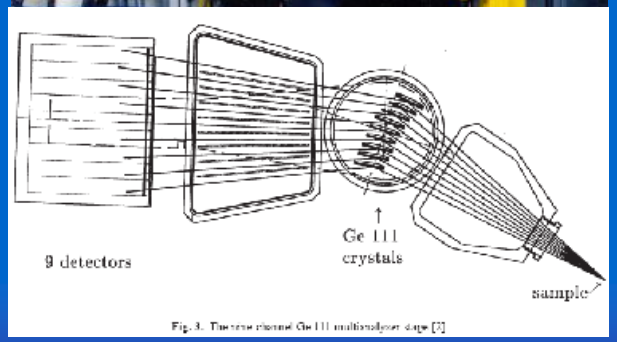

capillary holder / high temperature blower

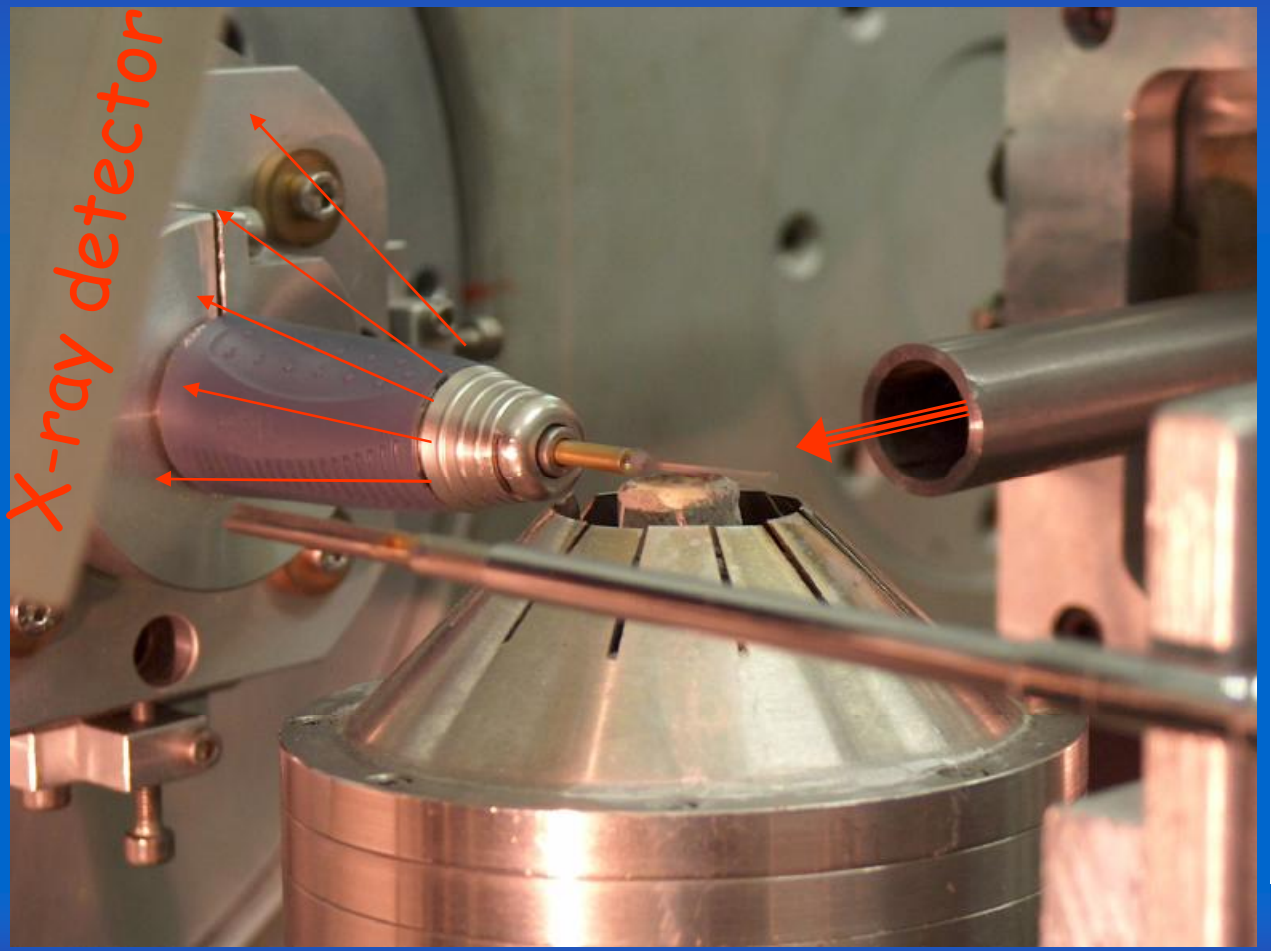

TYPICAL LAB GEOMETRY: BRAGG-BRENTANO (POWDER)

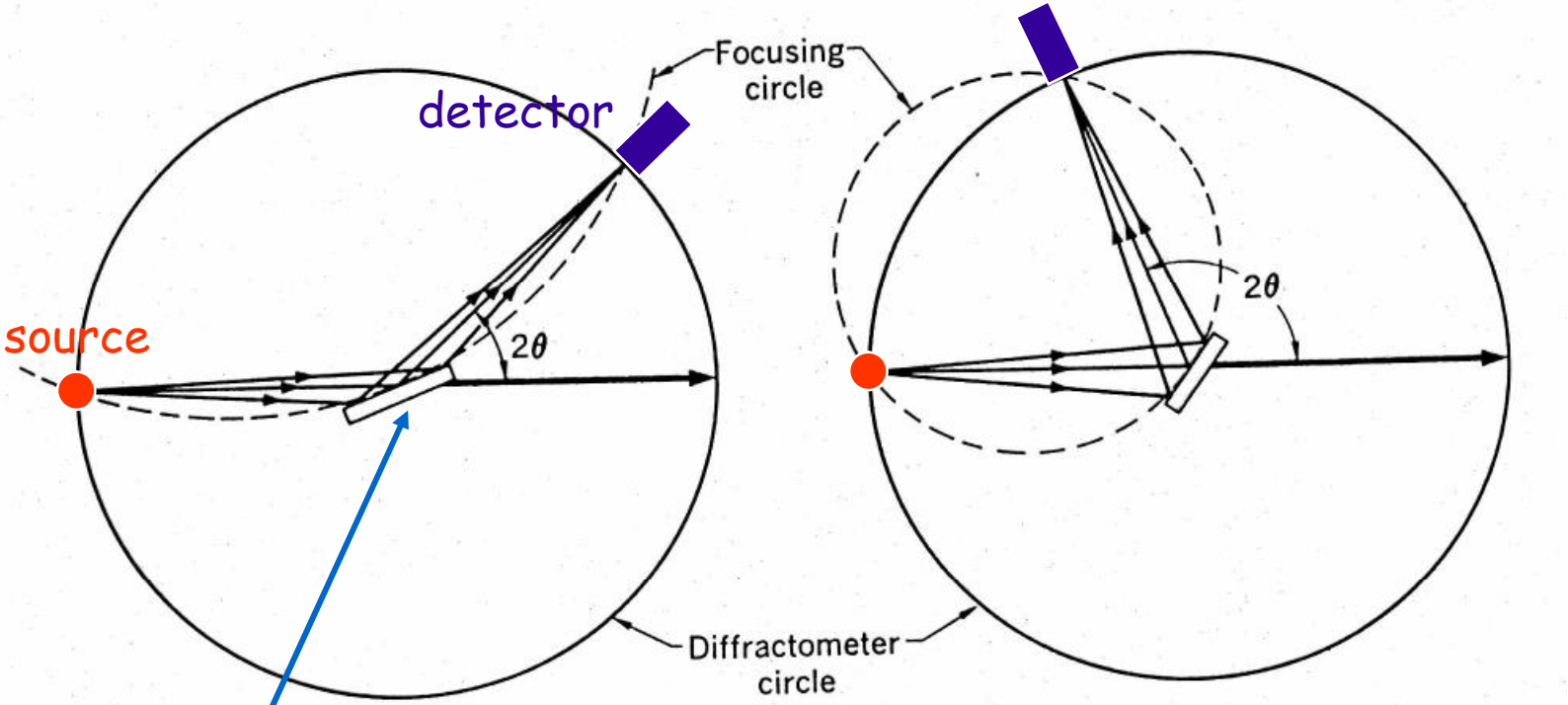

BULK or
POWDER

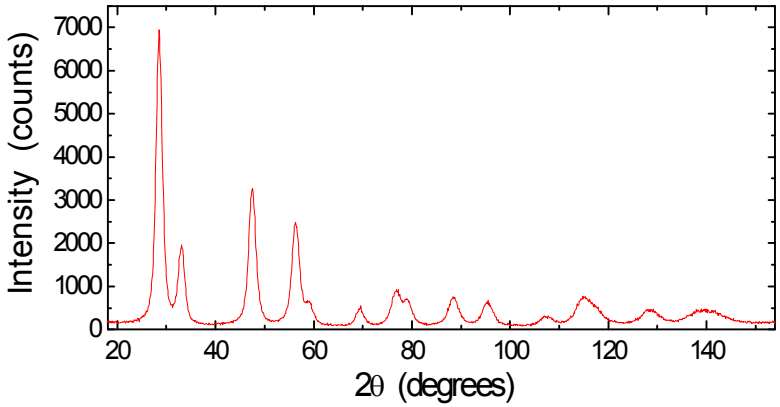

SOME ADVANTAGES OF SRXRD

1) High brillance, much better counting statistics / shorter data collection time (→ fast kinetics, in situ studies)

Ball mille FeMo

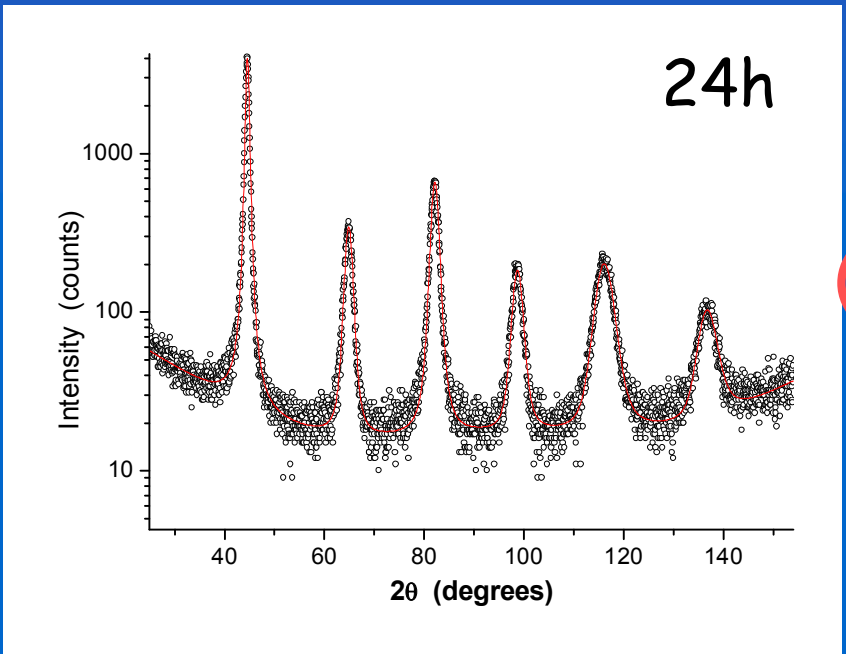

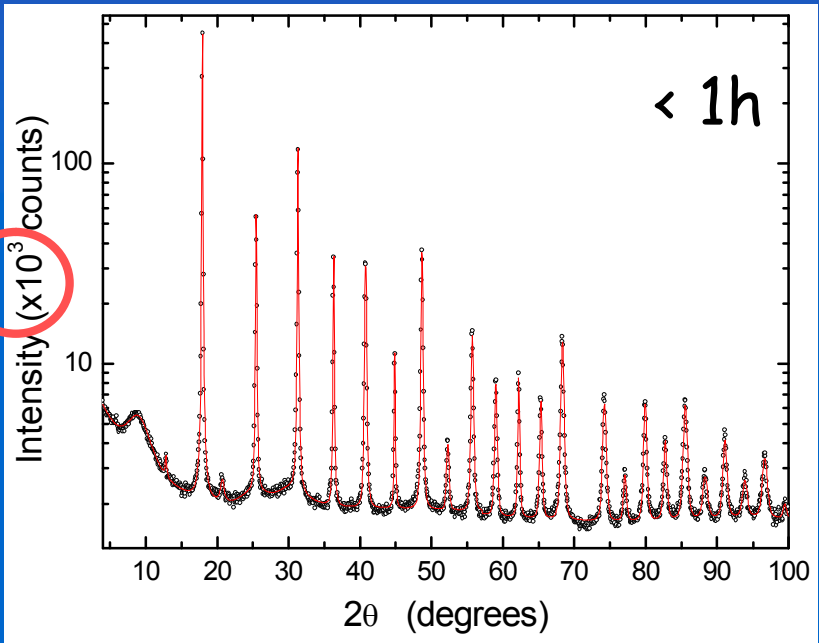

CuKα λ=0.15406 nm

ESRF ID31 λ=0.0632 nm

M. d'Incau,. Leoni & P. Scardi, J. Materials Research 22 (2007) 1744-1753.

SOME ADVANTAGES OF SRXRD

2) With proper selection of optics, very narrow instrumental profile: increased resolution and accuracy in the measurement of peak position, intensity and profile width/shape.

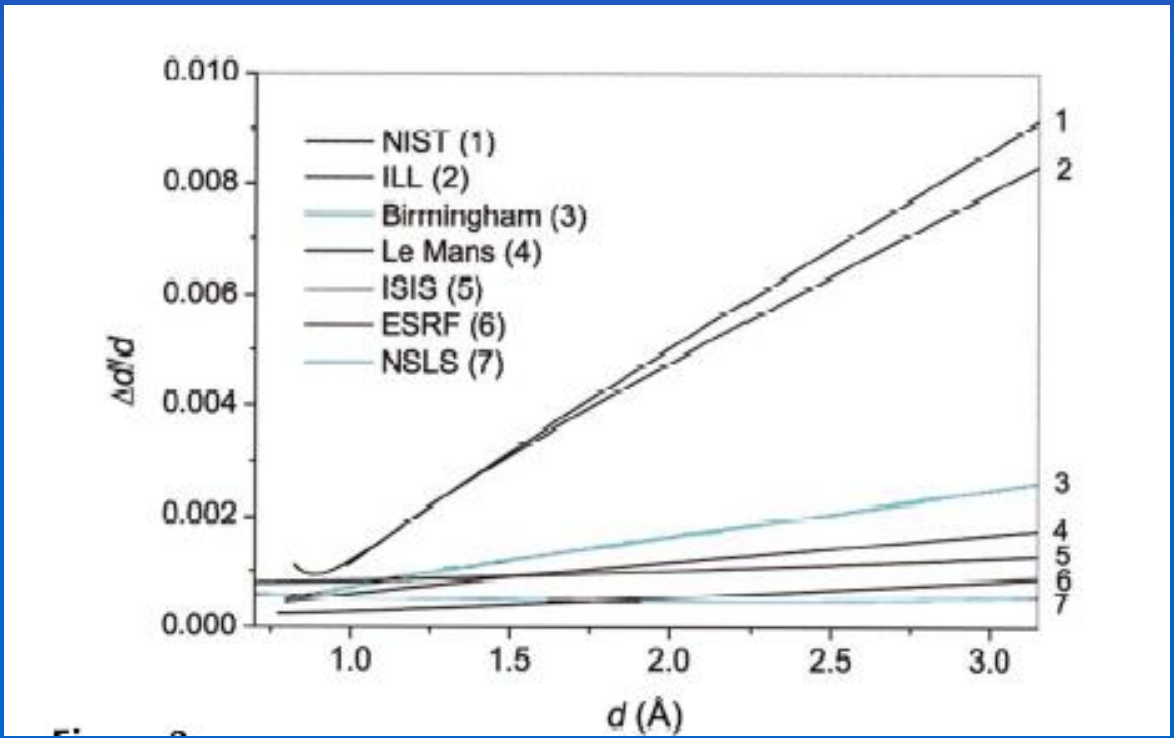

Lab instrument: FWHM≈0.05-0.1°

ID31 @ESRF: FWHM≈0.003-0.004°

SOME ADVANTAGES OF SRXRD

3) Extending the accessible region of reciprocal space well beyond what traditional lab instruments can make

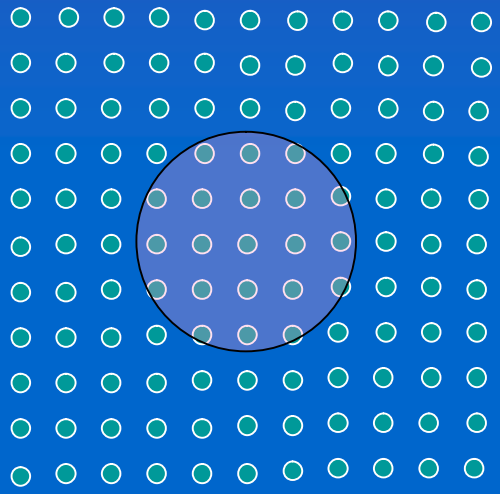

λ_1

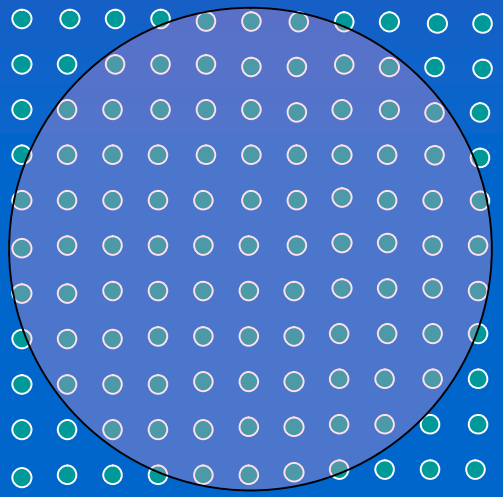

$\lambda_2 < \lambda_1$

SOME ADVANTAGES OF SRXRD

3) Extending the accessible region of reciprocal space well beyond what traditional lab instruments can make

Ball mille FeMo

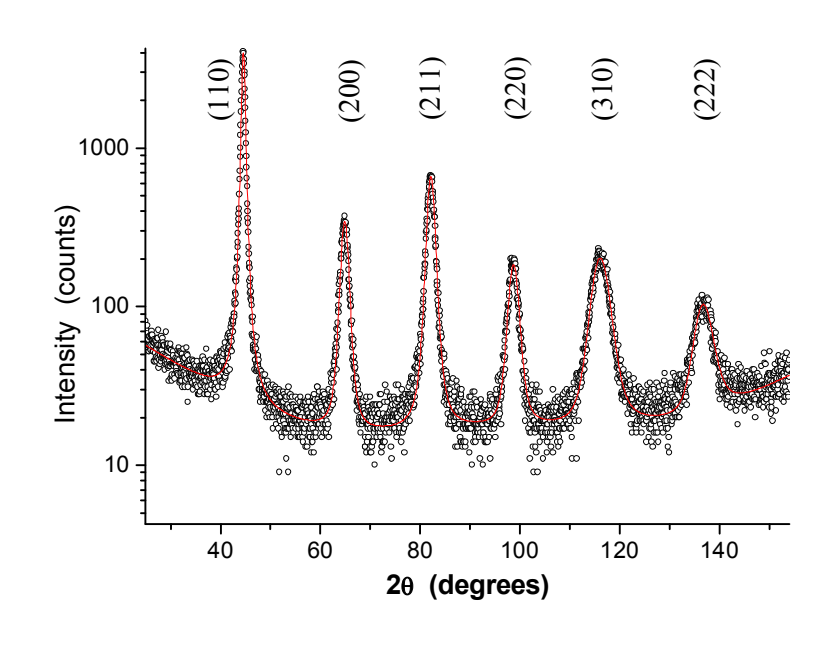

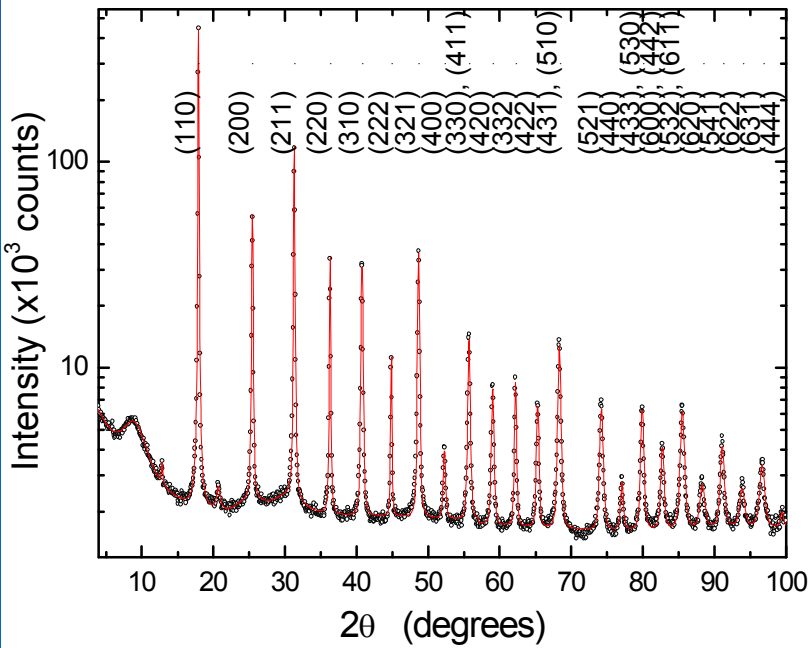

CuKα λ=0.15406 nm

ESRF ID31 λ=0.0632 nm

M. d'Incau,. Leoni & P. Scardi, J. Materials Research 22 (2007) 1744-1753.

SOME ADVANTAGES OF SRXRD

4) Tuning the energy according to adsorption edges. Resonant scattering, control of fluerescence emission and depth of analysis.

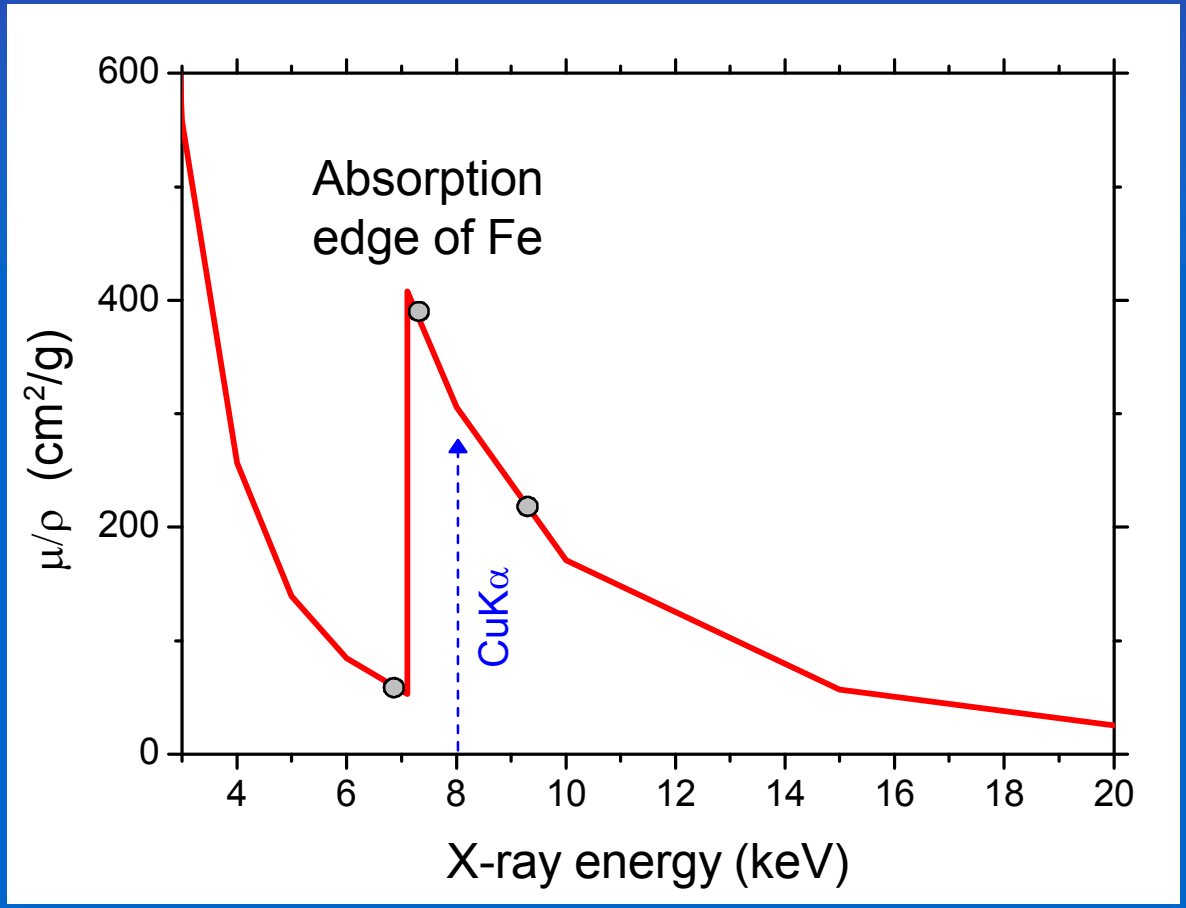

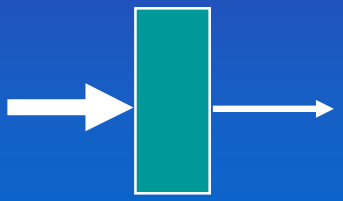

$$I = I_0 e^{-\left(\frac{\mu}{\rho}\right)\rho t}$$

X-RAY POWDER DIFFRACTION

Most frequent applications of powder diffraction

- Crystal structure determination
  (Powder diffraction structure solution and refinement)
- Phase Identification – pure crystalline phases or mixtures
  (Search-Match procedures)
- Quantitative Phase Analysis (QPA)
- Amorphous phase analysis (radial distribution function)
- Crystalline domain size/shape and lattice defect analysis
  (Line Profile Analysis - LPA)
- Determination of preferred orientations (Texture Analysis)
- Determination of residual stress field (Residual Stress Analysis)

STRUCTURE SOLUTION: WHY POWDER ?

Structure solution of heptamethylene-1,7-bis(diphenylphosphane oxide)

Structural formula

$Ph_2P(O)(CH_2)_7P(O)Ph_2$

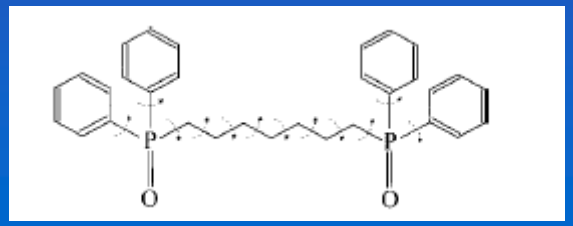

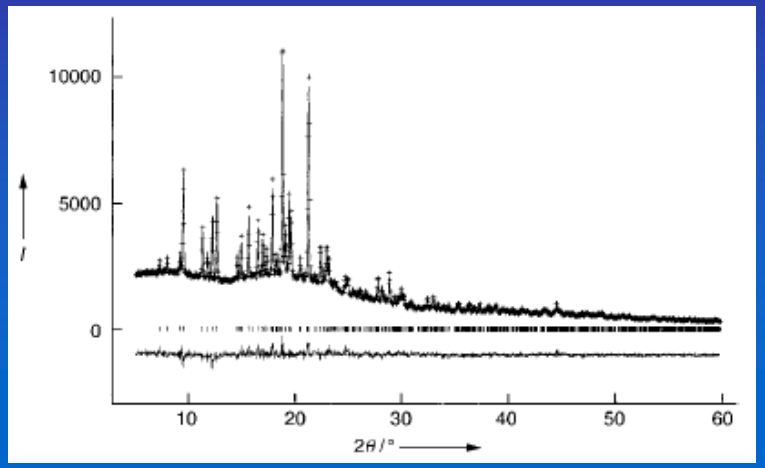

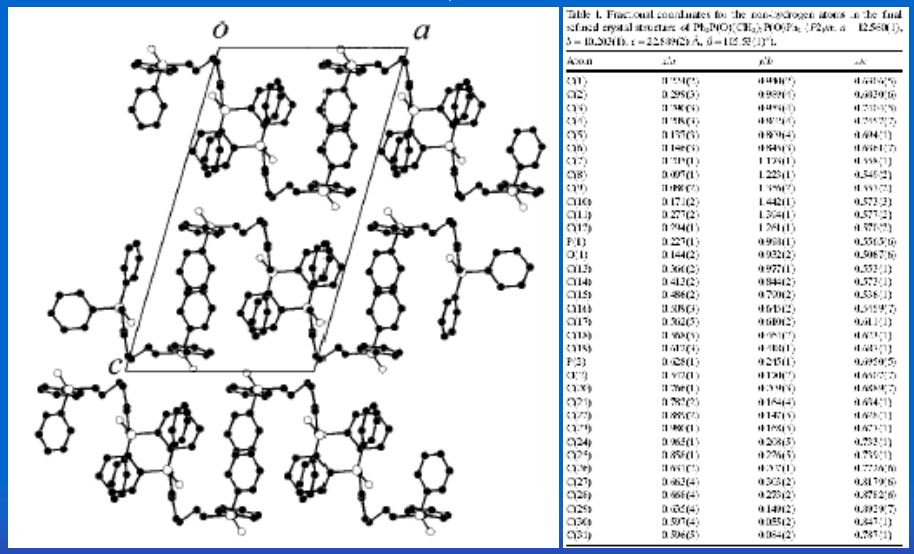

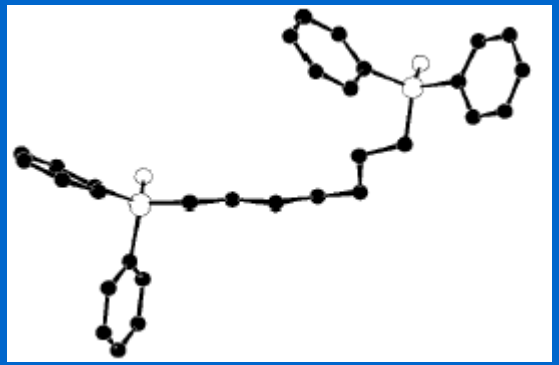

B.M. Kariuki, P. Calcagno, K. D. M. Harris, D. Philp and R.L. Johnston, Angew. Chem. Int. Ed. 1999, 38, No. 6, 831-835.

STRUCTURE SOLUTION & REFINEMENT: SRXRD

Structure solution/refinement of a complex triclinic organic compound ($C_{24}H_{16}O_7$)

K. D. Knudsen *et al.*, Angew. Chem. Int. Ed., 37 (1998) 2340

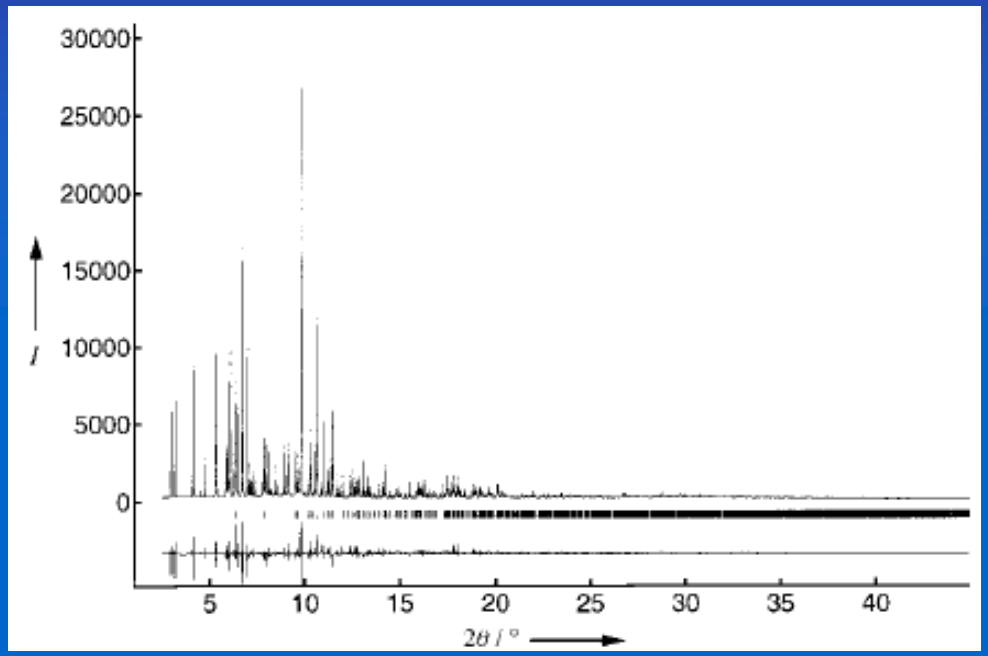

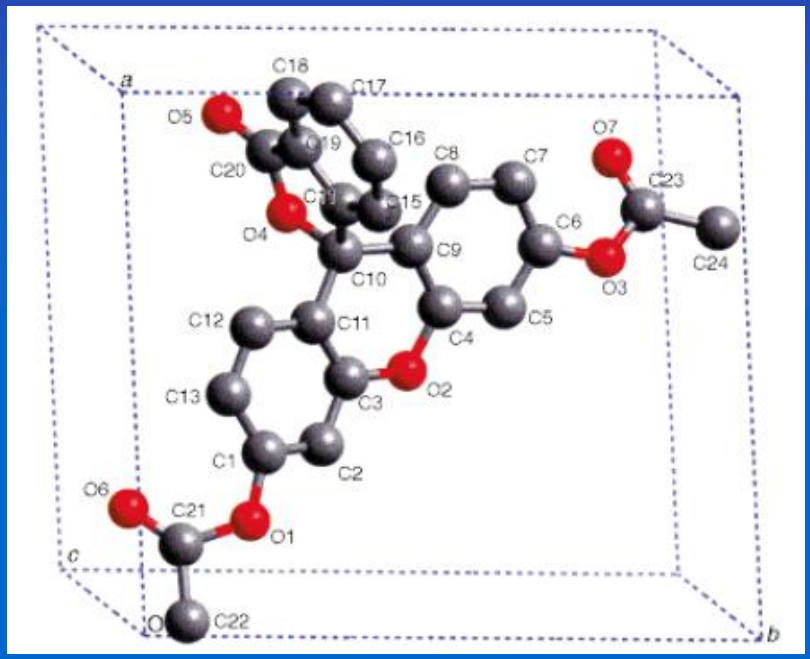

- Narrow peak profiles
- Large number of measurable peaks
- Accurate peak position/intensity
- X-ray energy tuning to adsorption edges

STRUCTURE SOLUTION & REFINEMENT: SRXRD

Site occupancy in battery electrode material $LaNi_{3.55}Mn_{0.4}Al_{0.3}Co_{0.75}$)

J.-M. Joubert *et al.*, J. Appl. Cryst. 31 (1998) 327

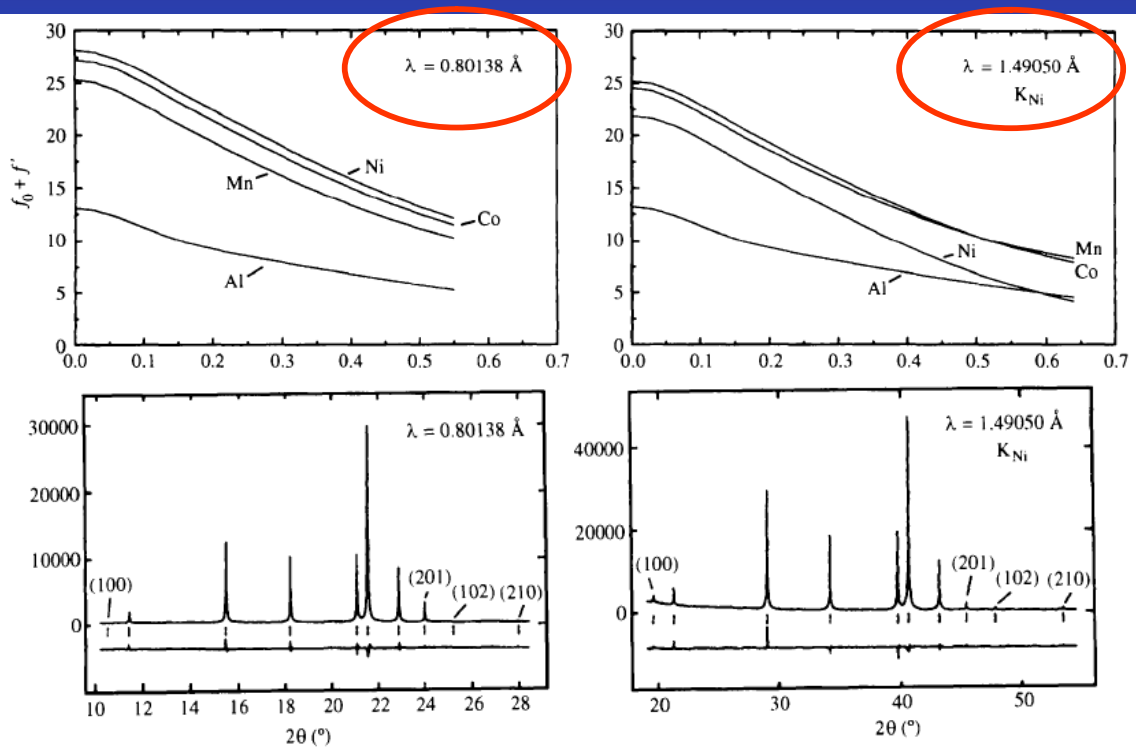

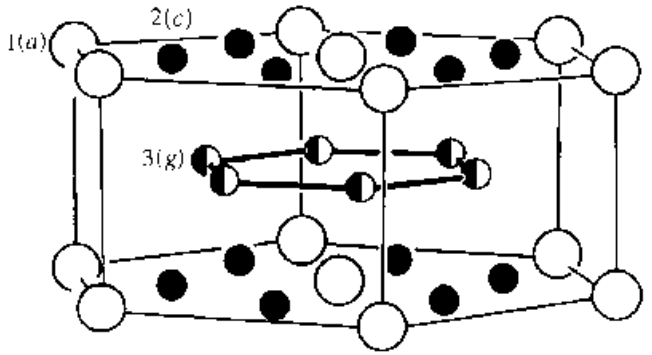

Fig. 1. The crystal structure of $LaNi_5$: the large spheres are La on site 1(*a*): the small spheres are Ni on sites 2(*c*) and 3(*g*).

Atom	Site	*x*	*y*	*z*	*B* (Å^2)	Occupancy (atoms site^{-1})
La	1(*a*)	0	0	0	2.06 (2)	1
Ni	2(*c*)	1/3	2/3	0	2.38 (2)	1.66 (2)
Mn						0.07 (1)
Al						0.032 (4)
Co						0.24 (1)
Ni	3(*g*)	1/2	0	1/2	1.97 (2)	1.89 (3)
Mn						0.33 (1)
Al						0.267 (6)
Co						0.51 (1)

- Narrow peak profiles
- Large number of measurable peaks
- Accurate peak position/intensity
- X-ray energy tuning to adsorption edges

STRUCTURE SOLUTION & REFINEMENT: SRXRD

Solving Larger Molecular Crystal Structures from Powder Diffraction Data by Exploiting Anisotropic Thermal Expansion, M. Brunelli et al., Angew. Chem. Int. Ed. 42, 2029, (2003)

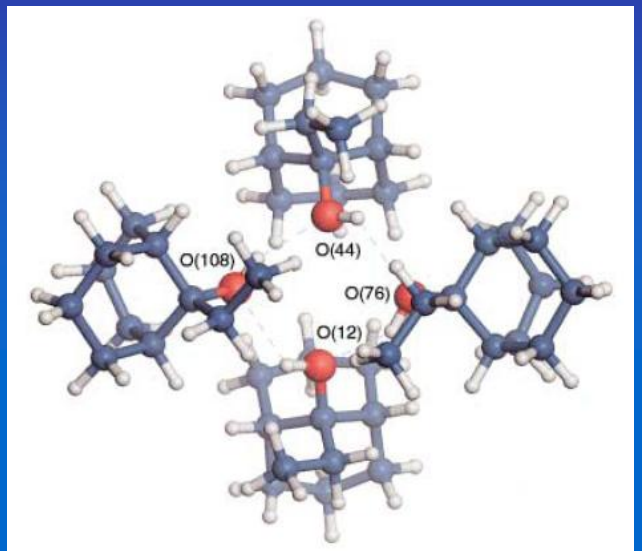

Figure 3. View of the arrangement of the four 9-ethylbicyclo[3.3.1]nona-9-ol molecules to form a hydrogen-bonded tetramer. The O–H···O hydrogen bonds are shown with dashed lines: O(12)-O(108) 2.825(4), O(44)-O(76) 2.761(4), O(76)-O(12) 2.804(4), O(108)-O(44) 2.869(4) Å. The crystallographic *c* direction is perpendicular to the plane of the Figure. O red, C blue, H gray.

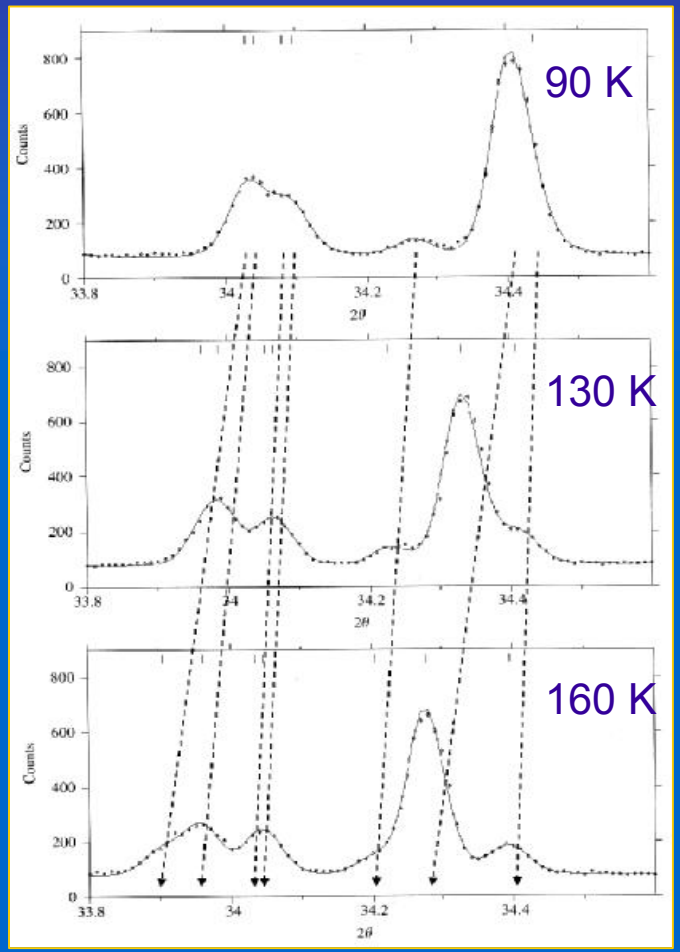

- Narrow peak profiles
- Large number of measurable peaks
- Accurate peak position/intensity
- X-ray energy tuning to adsorption edges
- Anisotropic thermal expansion

PHASE IDENTIFICATION

Phase identification is one of the first and most diffuse applications of powder diffraction, especially in industry for production, quality control and diagnostics, but also in research.

Each crystalline phase has its own pattern that can be used as a 'fingerprint'

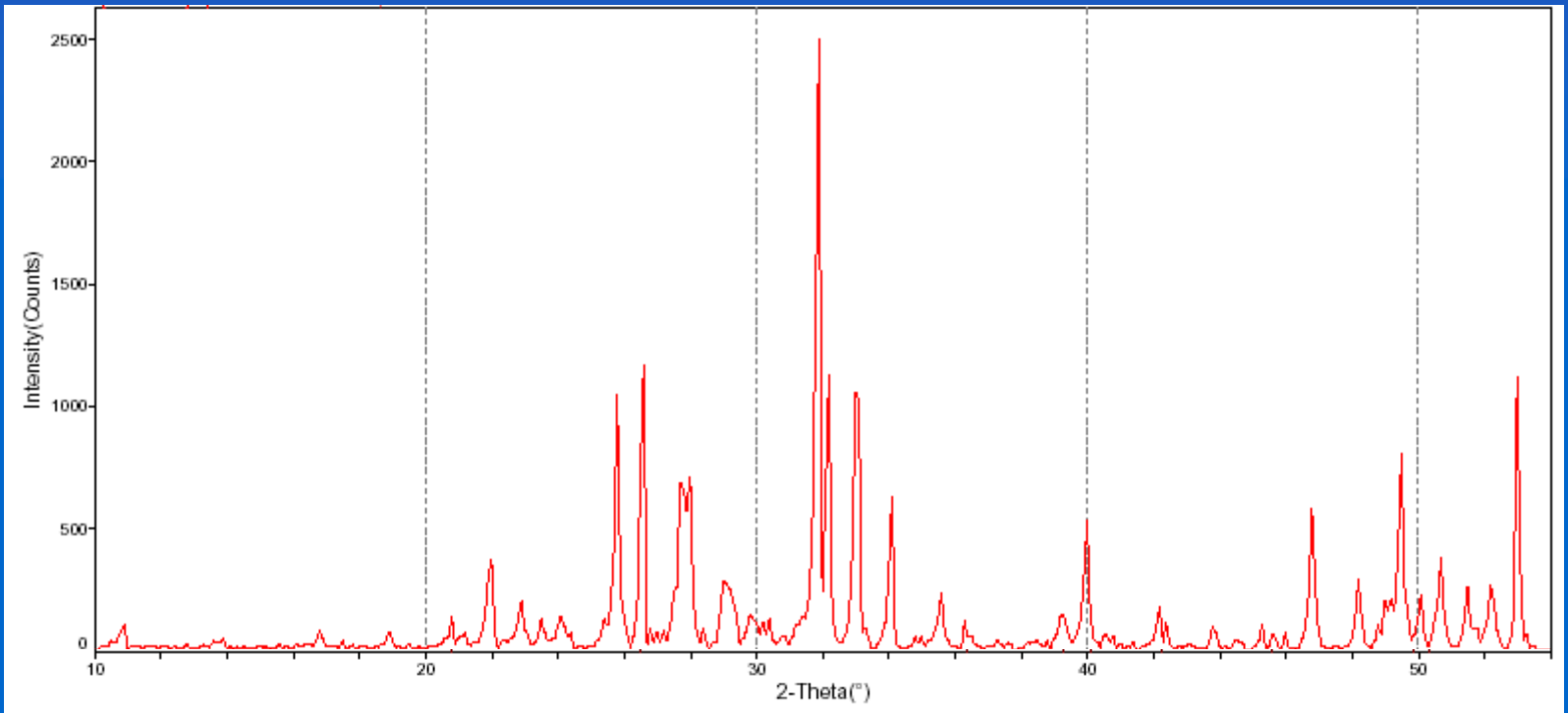

'Fingerprints' of unknown substances can be compared with those of known crystalline phases of a database → *Search-Match procedures*

PHASE IDENTIFICATION

The most powerful database is the PDF (Powder Diffraction File) by the ICDD (International Centre for Diffraction Data – www.icdd.com)

PDF-2

Peak pos/int

PDF-4

full structural information

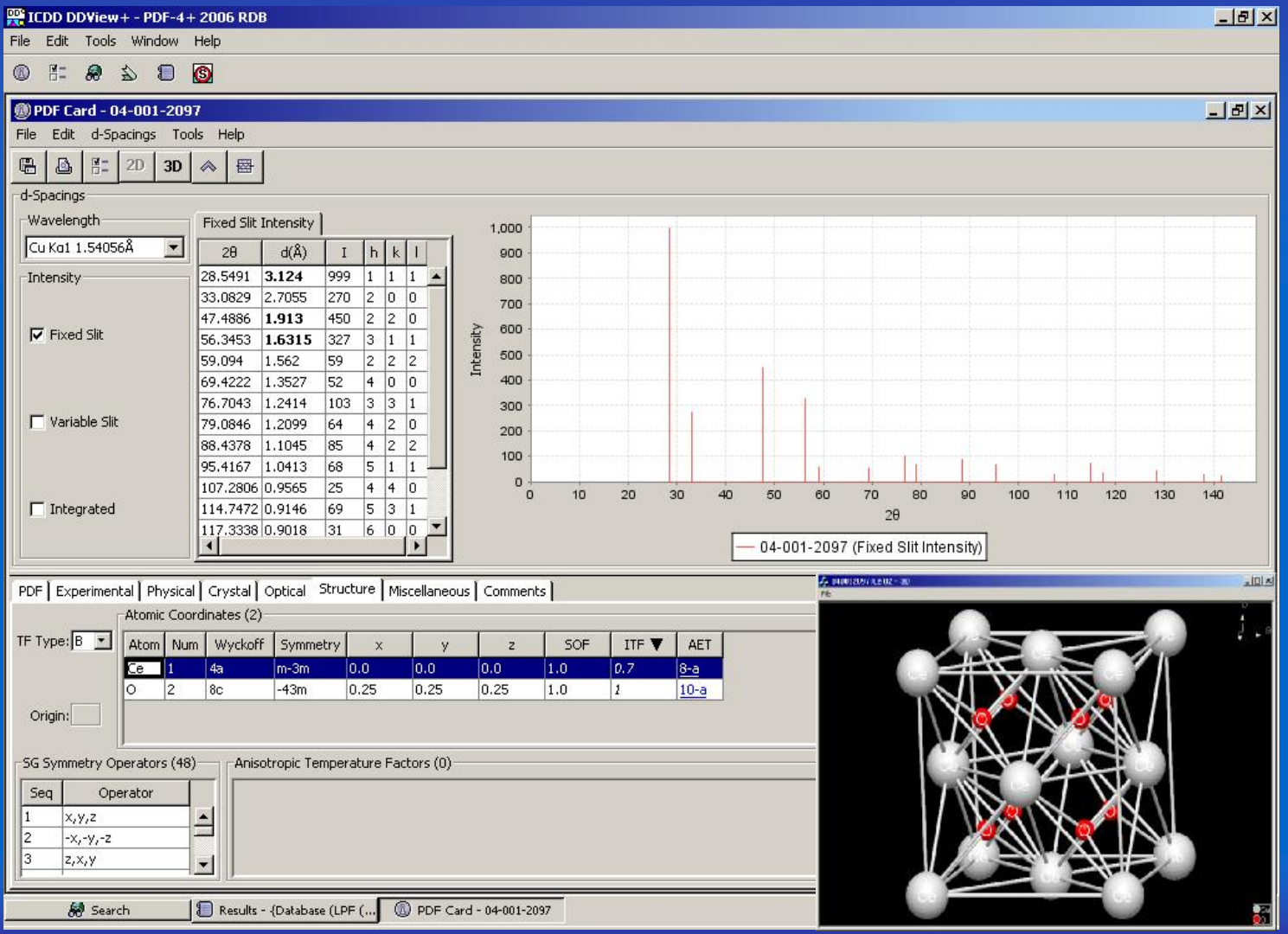

PHASE IDENTIFICATION

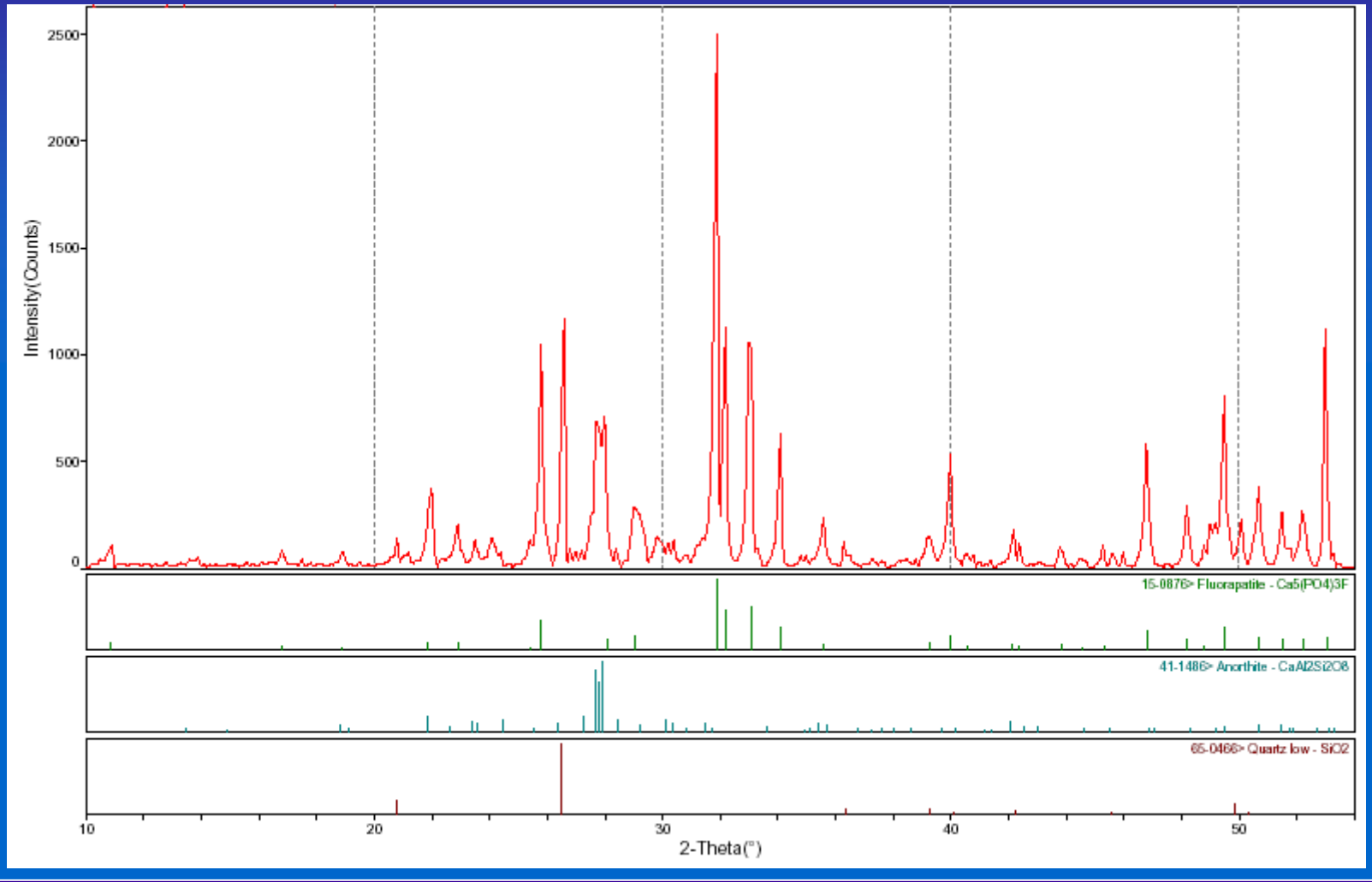

Automatic search-match procedures are based on peak position / intensity

MINOR PHASE IDENTIFICATION BY SRXRD

Iron oxide traces in ball milled α-Fe powder

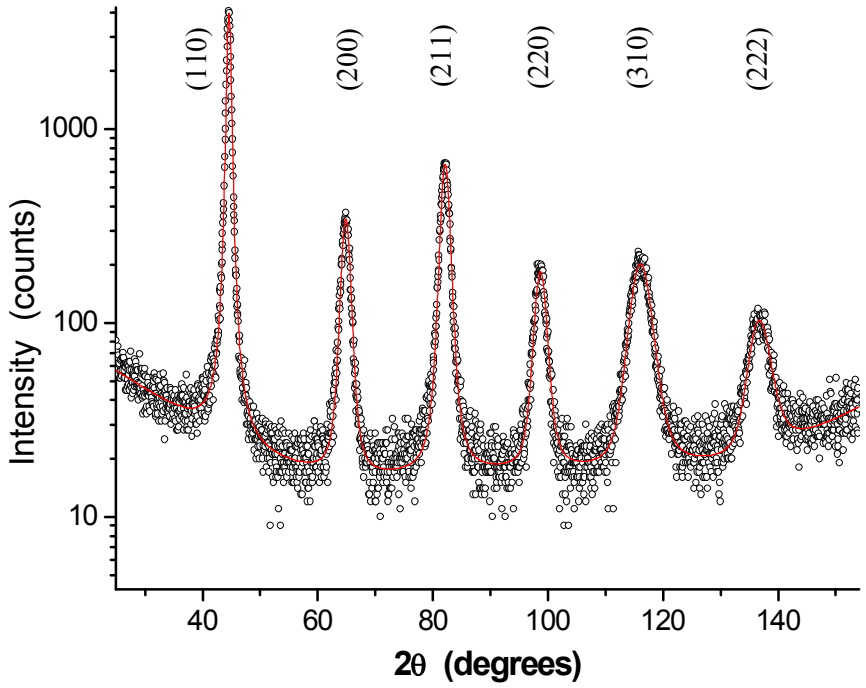

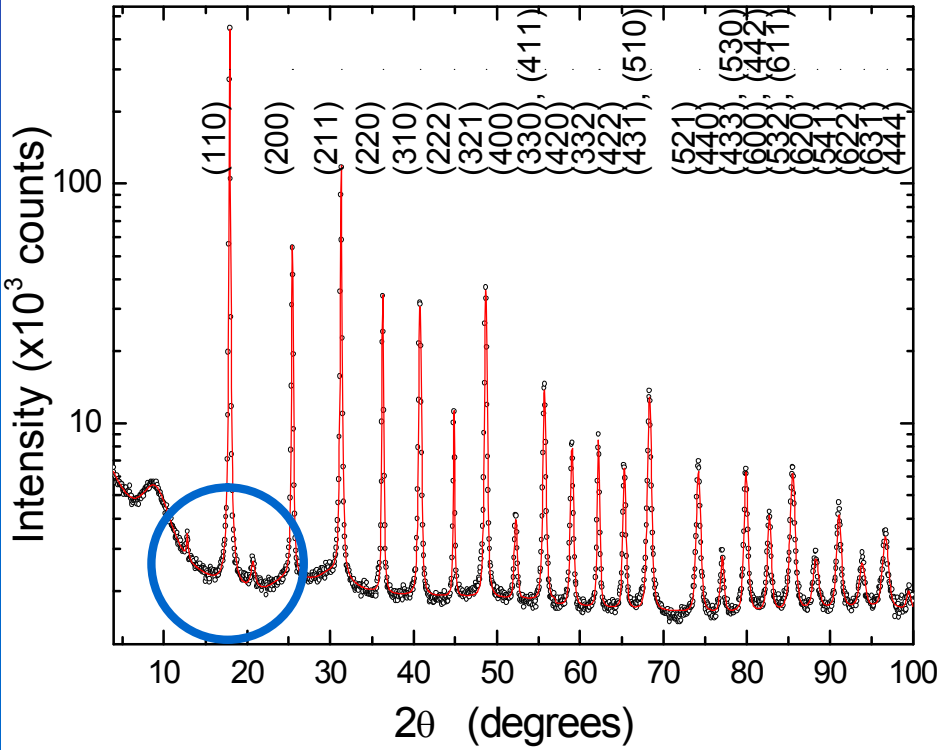

CuKα λ=0.15406 nm

ESRF ID31 λ=0.0632 nm

M. d'Incau,. Leoni & P. Scardi, J. Materials Research 22 (2007) 1744-1753.

QUANTITATIVE PHASE ANALYSIS (QPA)

The pattern of a phase mixture is the WEIGHTED sum of the patterns corresponding to the constituent phases. The weight depends of the specific scattering power and absorption of each phase in the mixture.

Several techniques exists for a quantitative determination of the phase content:

- QPA with **internal standard**
- QPA with "**virtual standard**" (RIR method)
- QPA via the **Rietveld method** (virtual standard)

THE RIETVELD METHOD

Intensity of the i-th point in the pattern

$$y_{ci} = \sum_j S_j \sum_k I_{k,j} \cdot \phi_{k,j}(2\theta) \cdot P_{k,j} + y_{bi}$$

Scale factor of j-th phase

Integrated Intensity k-th peak of j-th phase

Profile function

Preferred Orientation

Background term

Using the normalization condition: $\sum_k x_k = 1$ (not obvious !!)

it is possible to calculate the weight fraction x_j of the phase j in a polyphasic mixture as:

$$x_j = \frac{S_j \rho_j v_j}{\sum_l S_l \rho_l v_l}$$

→ J. Plasier

RIETVELD-BASED QPA

Example: mixture of mineral phases in a ligand

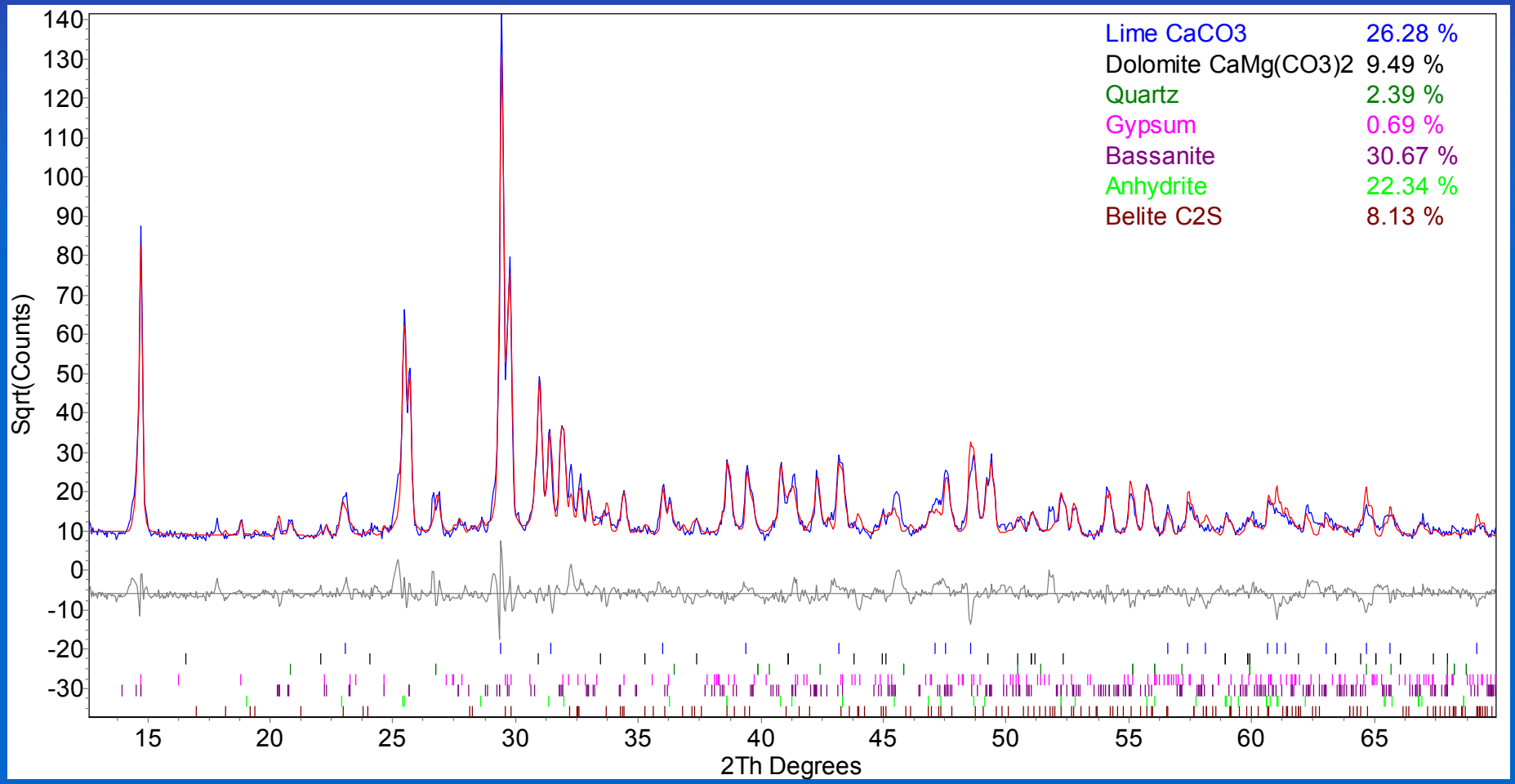

STRUCTURE SOLUTION IN MULTIPHASE SAMPLES

Structural and electronic properties of noncubic fullerides A'_4C_{60} (A'=Ba,Sr)

C.M. Brown *et al.*, Phys. Rev. Let. 83 (1999) 2258

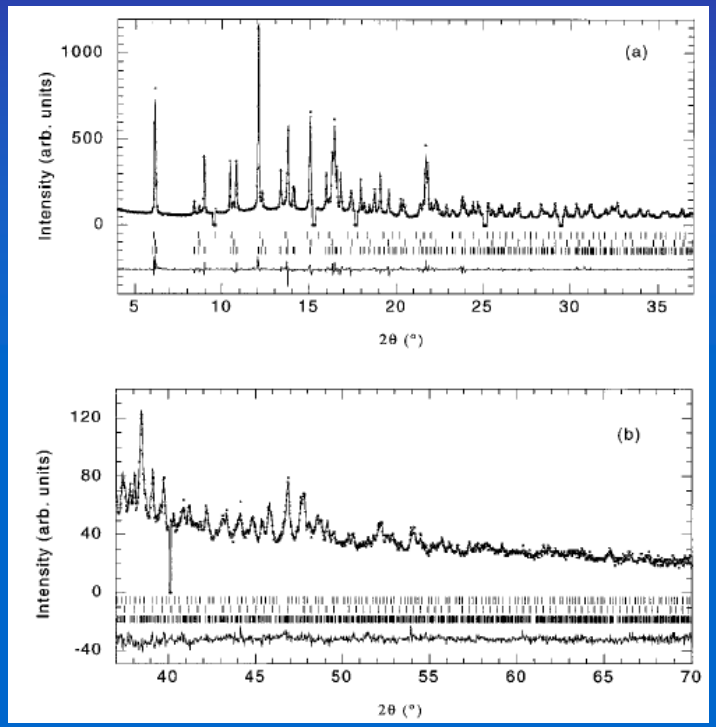

ESRF BM161 λ=0.084884 nm

FIG. 2. Final observed (points) and calculated (solid line) synchrotron x-ray powder diffraction profiles for Ba_4C_{60} at 295 K in the range 4° to 70° (λ = 0.848 84 Å). The lower panels show the difference profiles and the ticks mark the positions of the Bragg reflections of Ba_4C_{60} [majority phase: 86.1(2)%, lower most], Ba_6C_{60} [minority phase: 11.8(1)%, middle], and Ba_3C_{60} [minority phase: 2.1(1)% upper most]. Some sharp peaks originating from a nonfulleride phase were excluded from the refinement.

- Narrow peak profiles
- Large number of measurable peaks
- Accurate peak position/intensity
- X-ray energy tuning to adsorption edges

STRUCTURE SOLUTION IN MULTIPHASE SAMPLES

Structural and electronic properties of noncubic fullerides A'_4C_{60} (A'=Ba,Sr)

C.M. Brown *et al.*, Phys. Rev. Let. 83 (1999) 2258

TABLE I. Refined parameters for orthorhombic Ba_4C_{60} obtained from Rietveld refinement of the synchrotron x-ray powder diffraction data at 295 K (space group *Immm*, $R_{wp} = 5.3\%$, $R_{exp} = 2.6\%$). The cell constants are $a = 11.6101(2)$, $b = 11.2349(2)$, and $c = 10.8830(2)$ Å, and the weight fraction of the Ba_4C_{60} phase is 86.1(2)%. The weight fractions of the minority phases, Ba_6C_{60} and Ba_3C_{60} are 11.8(1)% and 2.1(1)%, respectively. The cell constants of cubic Ba_6C_{60} (space group $Im\bar{3}$) and Ba_3C_{60} (space group $Pm\bar{3}n$) are 11.1959(2) and 11.338(1) Å, respectively.

Atom	x/a	y/b	z/c	$B_{iso}/Å^2$ ($\beta_{11}, \beta_{22}, \beta_{33}$)
Ba(1)	0.5	0.2034(2)	0.0	1.9(1), 2.9(2), 0.9(1)
Ba(2)	0.2488(1)	0.5	0.0	2.7(1), 3.7(2), 0.6(1)
C(11)	0.3005(2)	0.0	0.0652(1)	0.16(8)
C(12)	0.0	−0.063 88(4)	0.3206(2)	0.16(8)
C(13)	0.10014(6)	−0.127 86(7)	0.2798(2)	0.16(8)
C(21)	0.2003(1)	−0.63 88(4)	0.2389(1)	0.16(8)
C(22)	0.12373(7)	−0.271 0(2)	0.106 82(6)	0.16(8)
C(23)	0.06187(4)	−0.310 5(2)	0.0	0.16(8)
C(31)	0.2240(2)	−0.207 0(1)	0.066 00(3)	0.16(8)
C(32)	0.06187(4)	−0.231 4(1)	0.213 7(1)	0.16(8)
C(33)	0.2622(2)	−0.103 45(6)	0.131 99(8)	0.16(8)

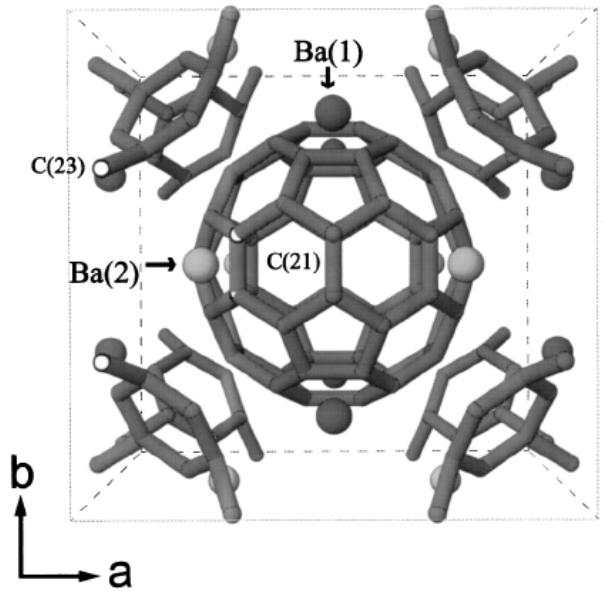

FIG. 3. Projection of the body centered orthorhombic structure of Ba_4C_{60} on the [110] basal plane. The two sets of crystallographically distinct barium ions, Ba(1) (*m*2*m* site) and Ba(2) (2*mm* site) are depicted as dark and light grey spheres, respectively. The hexagon C(21) and pentagon C(23) atoms which are in close contact to Ba(2) are depicted as white spheres.

- Narrow peak profiles
- Large number of measurable peaks
- Accurate peak position/intensity
- X-ray energy tuning to adsorption edges

AMORPHOUS PHASE ANALYSIS

The long-range order typical of crystalline structures is absent in amorphous materials. However, a certain degree of short-range order is always present.

Diffraction can be used to measure the ***radial distribution function***, i.e., the probability distribution to find an atom at a distance between r and $r+\delta r$ taken from a reference atom.

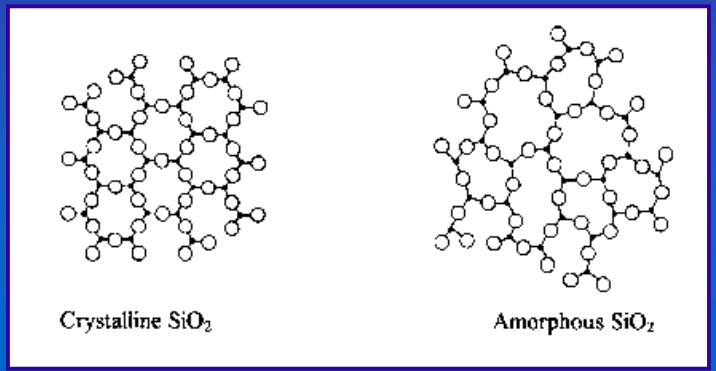

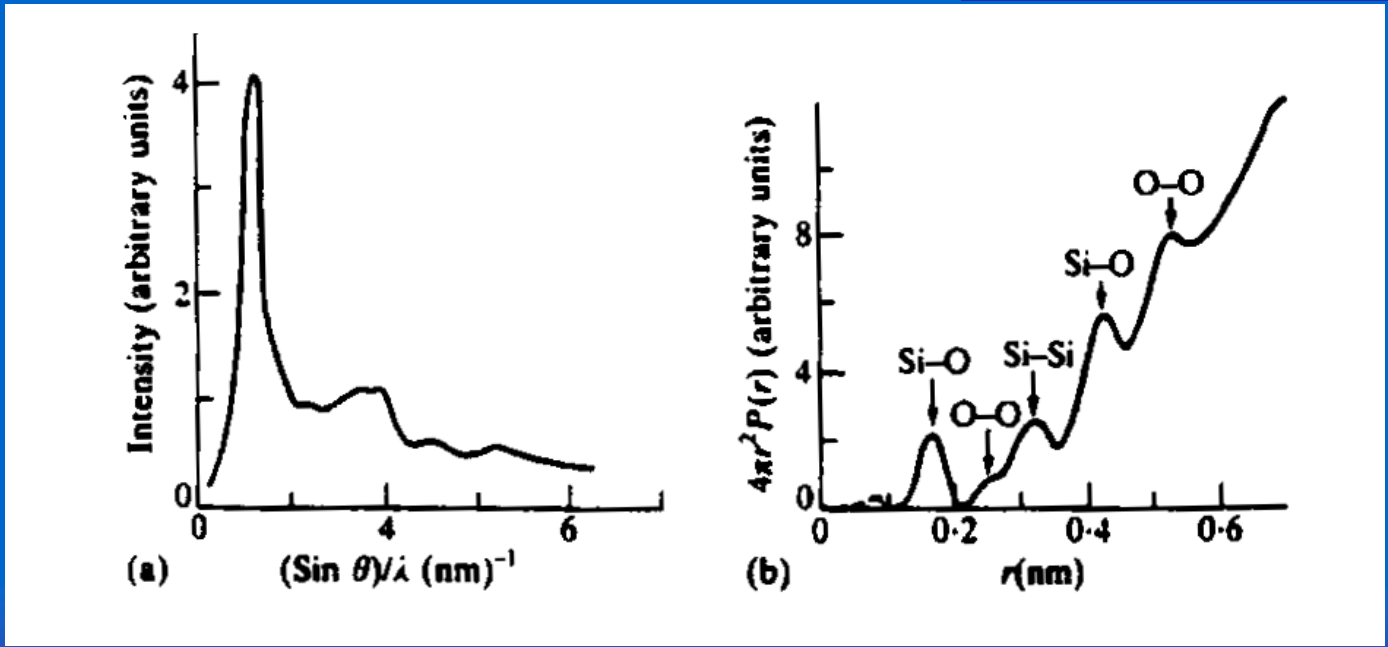

AMORPHOUS PHASE ANALYSIS

Mixture of (crystalline) corundum and amorphous silica

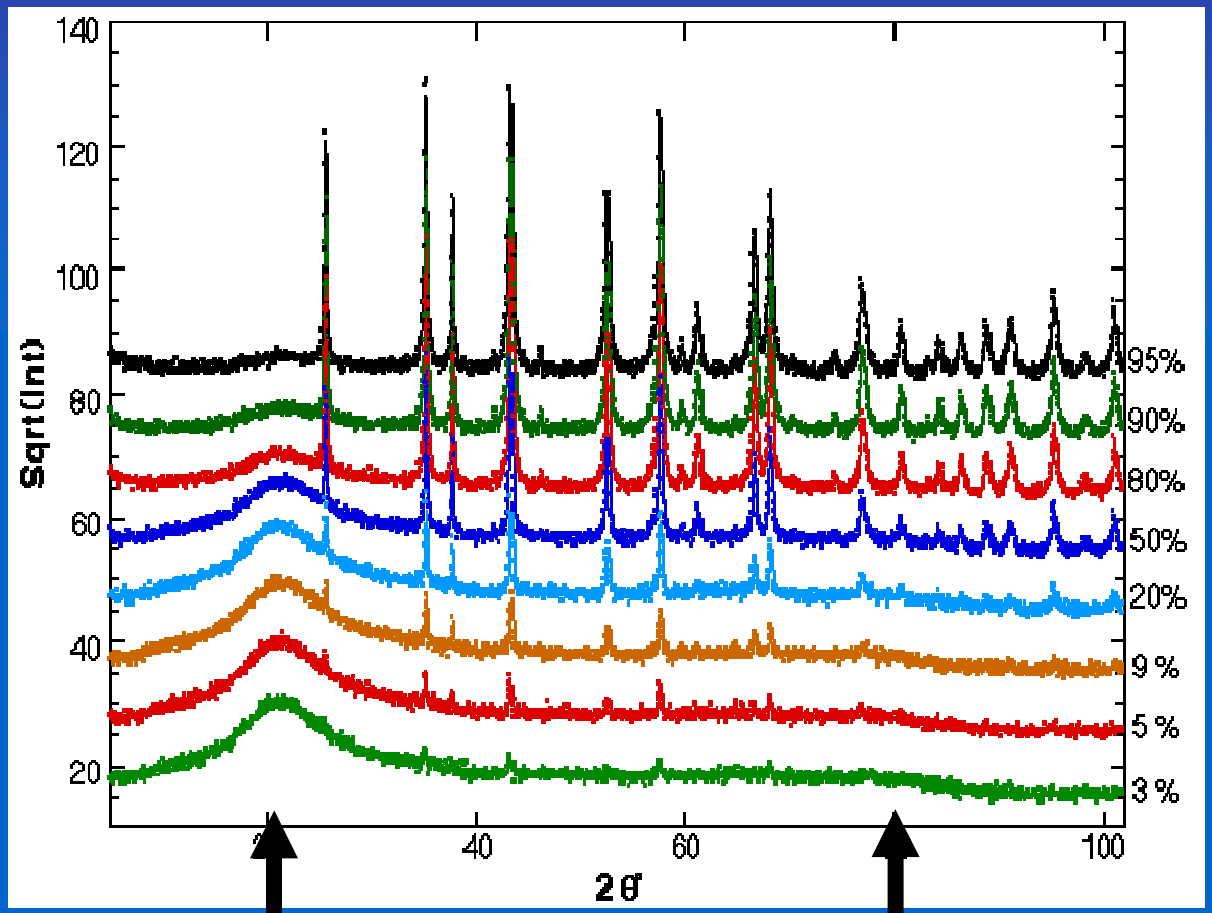

amorphous bands typical of the glass

Diffraction can provide:

- **fraction of amorphous phase** in mixtures
- **degree of crystallinity** (e.g. in glass-ceramics or in polymers)

PAIR DISTRIBUTION FUNCTION: USE OF SRXRD

Structure of nanocrystalline materials using atomic Pair Distribution Function (PDF) analysis: study of $LiMoS_2$.

V. Petkov *et al.*, Phys. Rev. B 65 (2002) 092105

$$PDF: \quad G(r) = 4\pi r\left[\rho(r) - \rho_0\right]$$

TABLE I. Structural parameters for MoS_2. Space group is $P6_3/mmc$. Mo is at $(\frac{1}{3}, \frac{2}{3}, \frac{1}{4})$ and S at $(\frac{1}{3}, \frac{2}{3}, z)$.

	PDF	Rietveld	Single crystal[a]
a (Å)	3.169(1)	3.168(1)	3.1604(2)
c (Å)	12.324(1)	12.322(1)	12.295(2)
z	0.623(1)	0.625(1)	0.629(1)

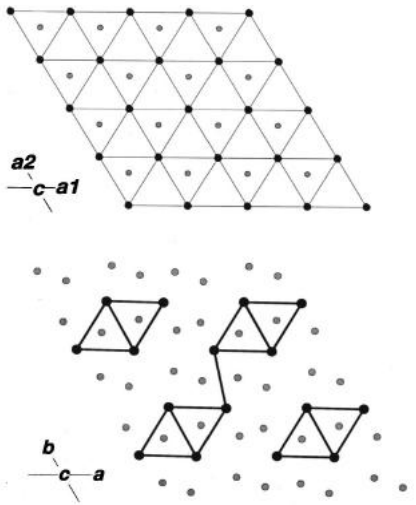

FIG. 4. Projection down the c axis of the crystal structures of hexagonal MoS_2 (up) and triclinic $LiMoS_2$ (down). The large black circles are Mo atoms and the small gray circles are the S atoms. Li atoms are not shown for the sake of clarity.

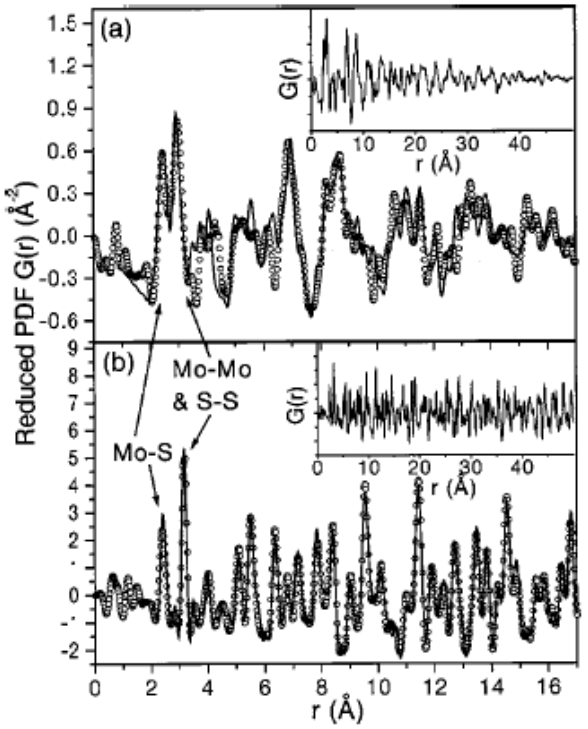

FIG. 2. Experimental (dots) and fitted (solid line) PDF's for $LiMoS_2$ (a) and MoS_2 (b). Note the different scale between (a) and (b). The first two peaks in the PDF's are labeled with the corresponding atomic pairs. The experimental data are shown in an expanded scale in the insets.

LINE PROFILE ANALYSIS

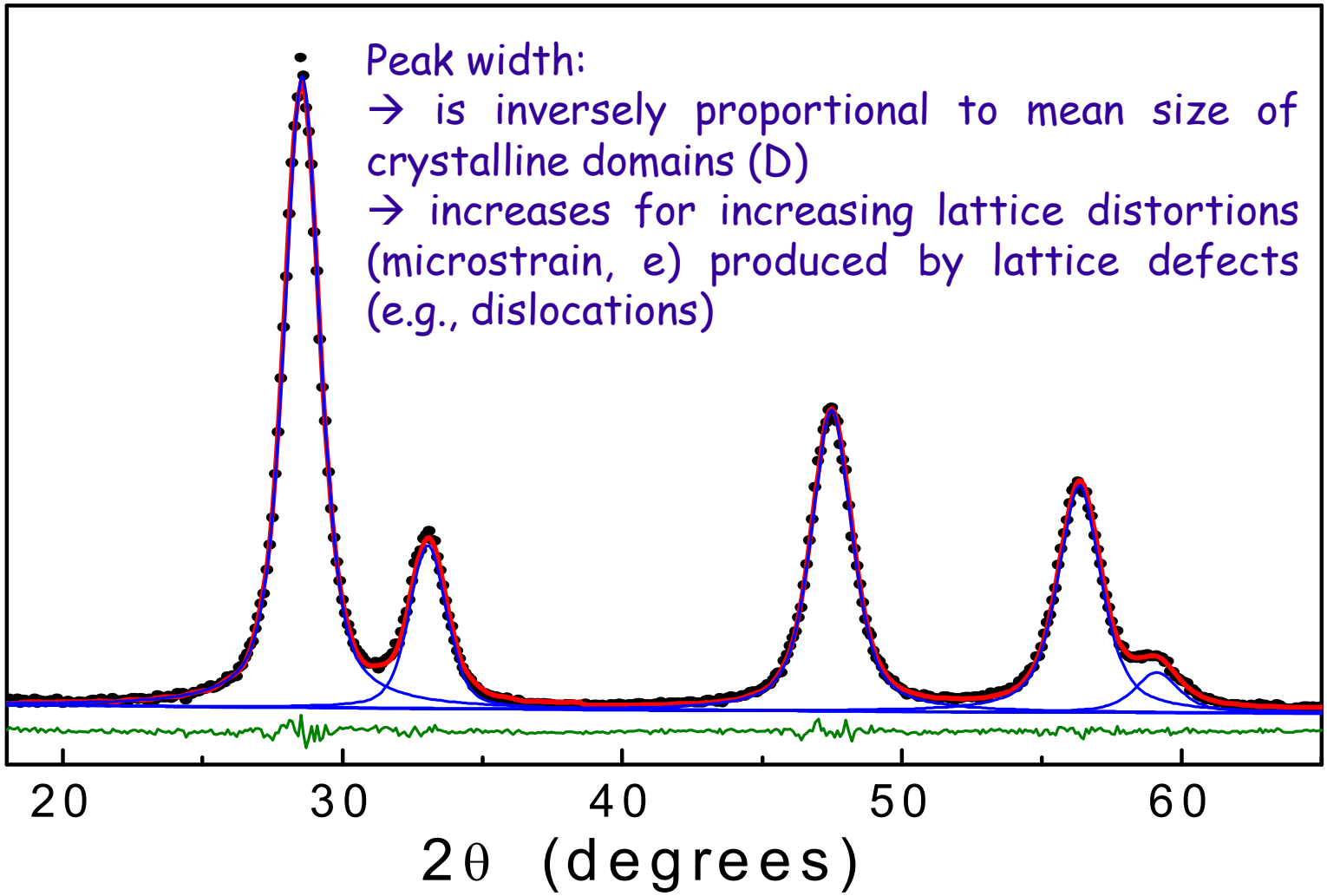

→ LPA: second part of this lecture

TEXTURE ANALYSIS

A 'true' powder has randomly oriented crystalline domains.
The diffracted intensity does not depend on the probing direction.

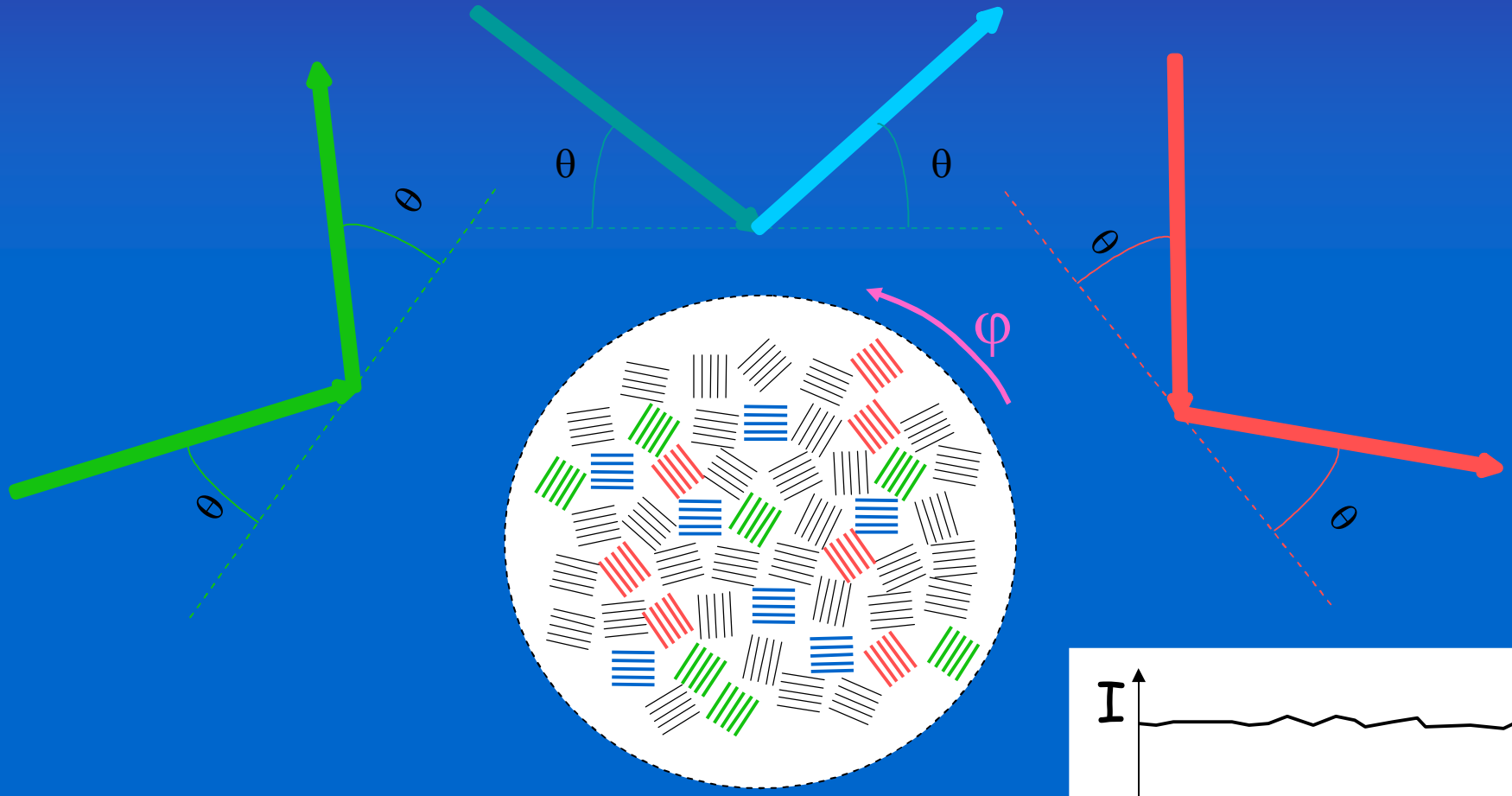

for any *hkl*

random orientation

TEXTURE ANALYSIS

If the grain (crystal) orientation is not random, the diffracted signal depends on the incident angle.

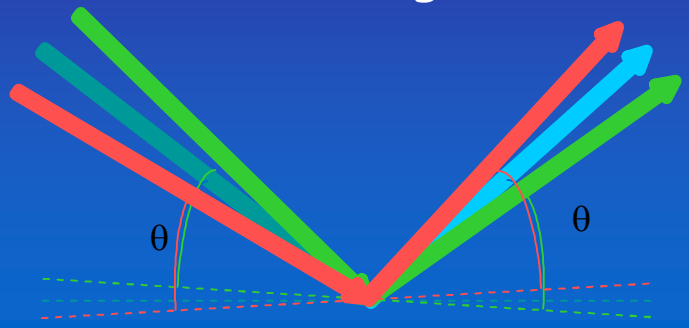

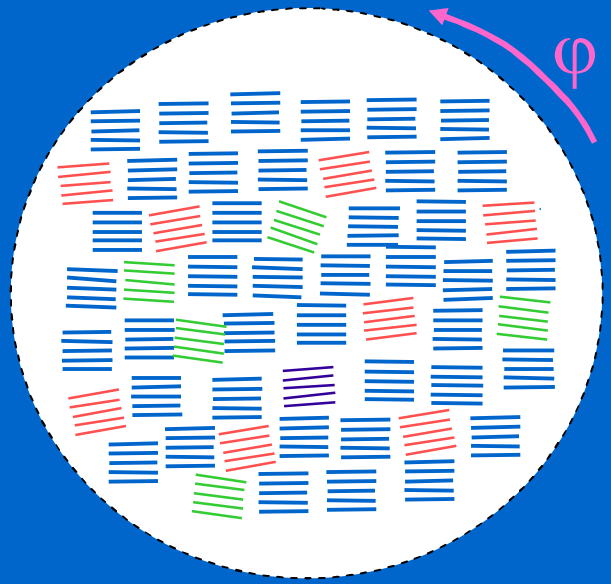

preferred orientation

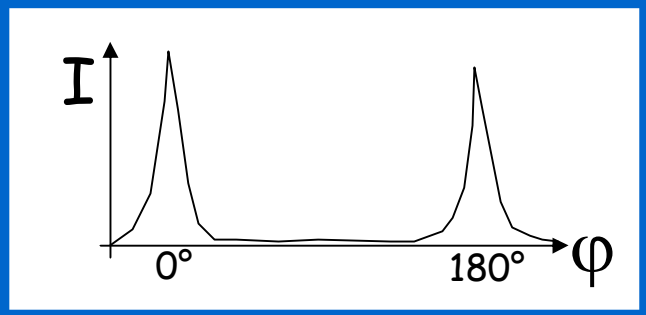

TEXTURE ANALYSIS

The information can be reported on suitable maps: pole figures. The stereographic projection is adopted

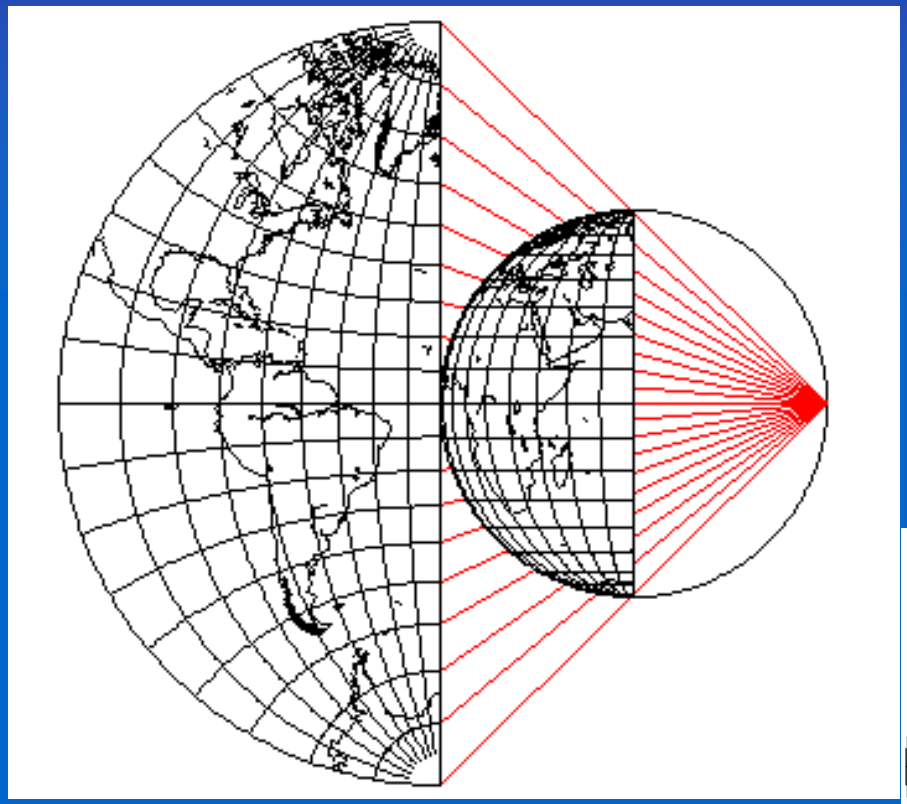

Two angles are used in the projection

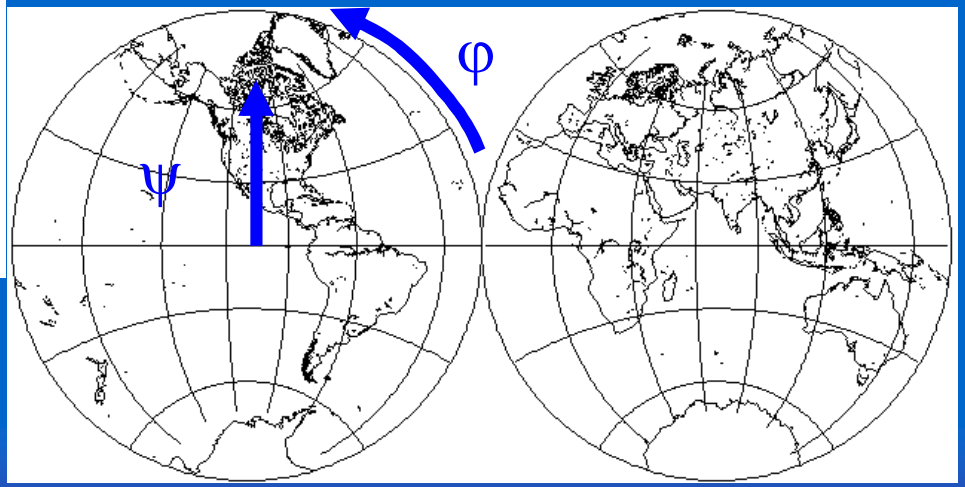

TEXTURE ANALYSIS

Eulerian cradle for stress/texture measurement: laboratory instrum.

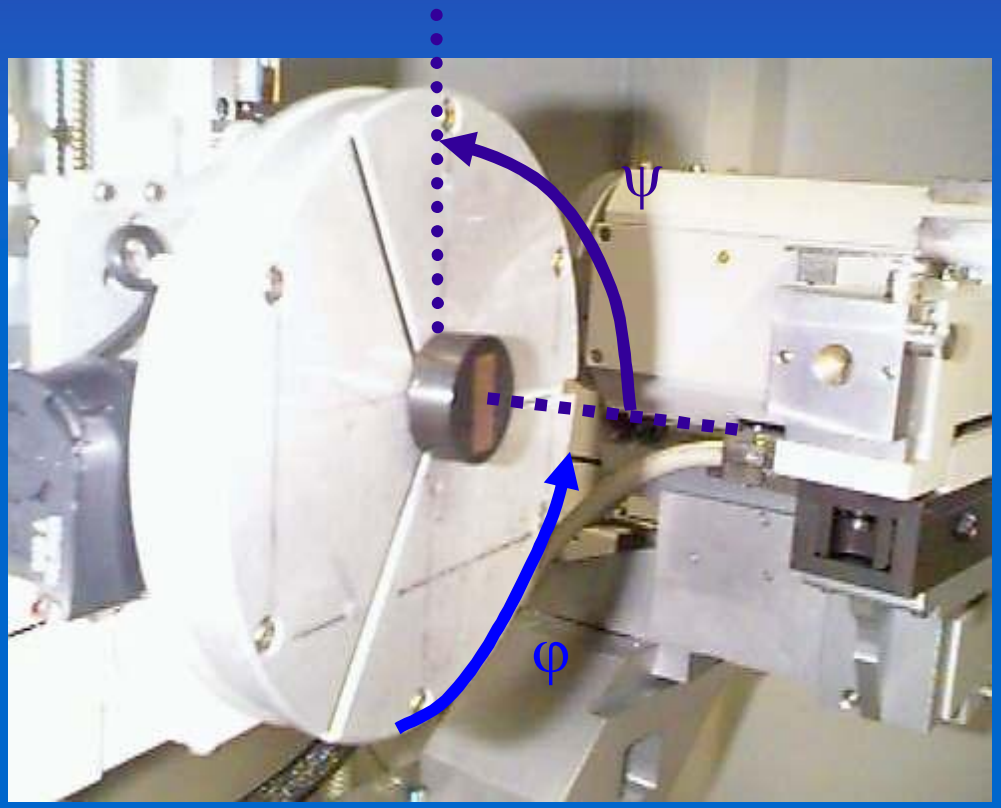

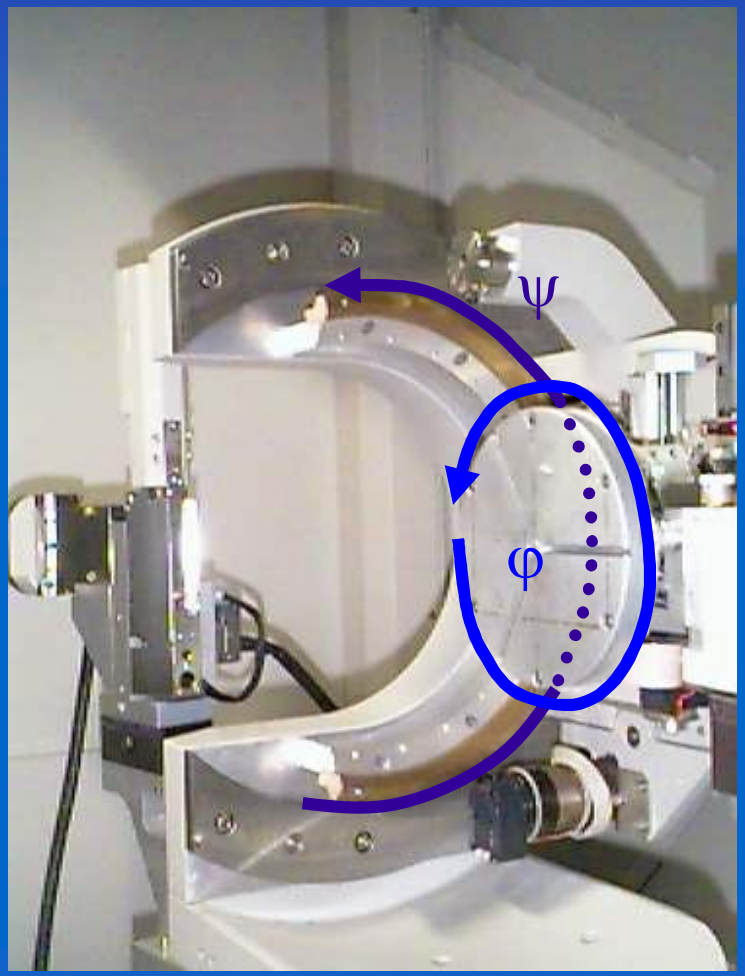

TEXTURE & STRESS ANALYSIS BY SRXRD

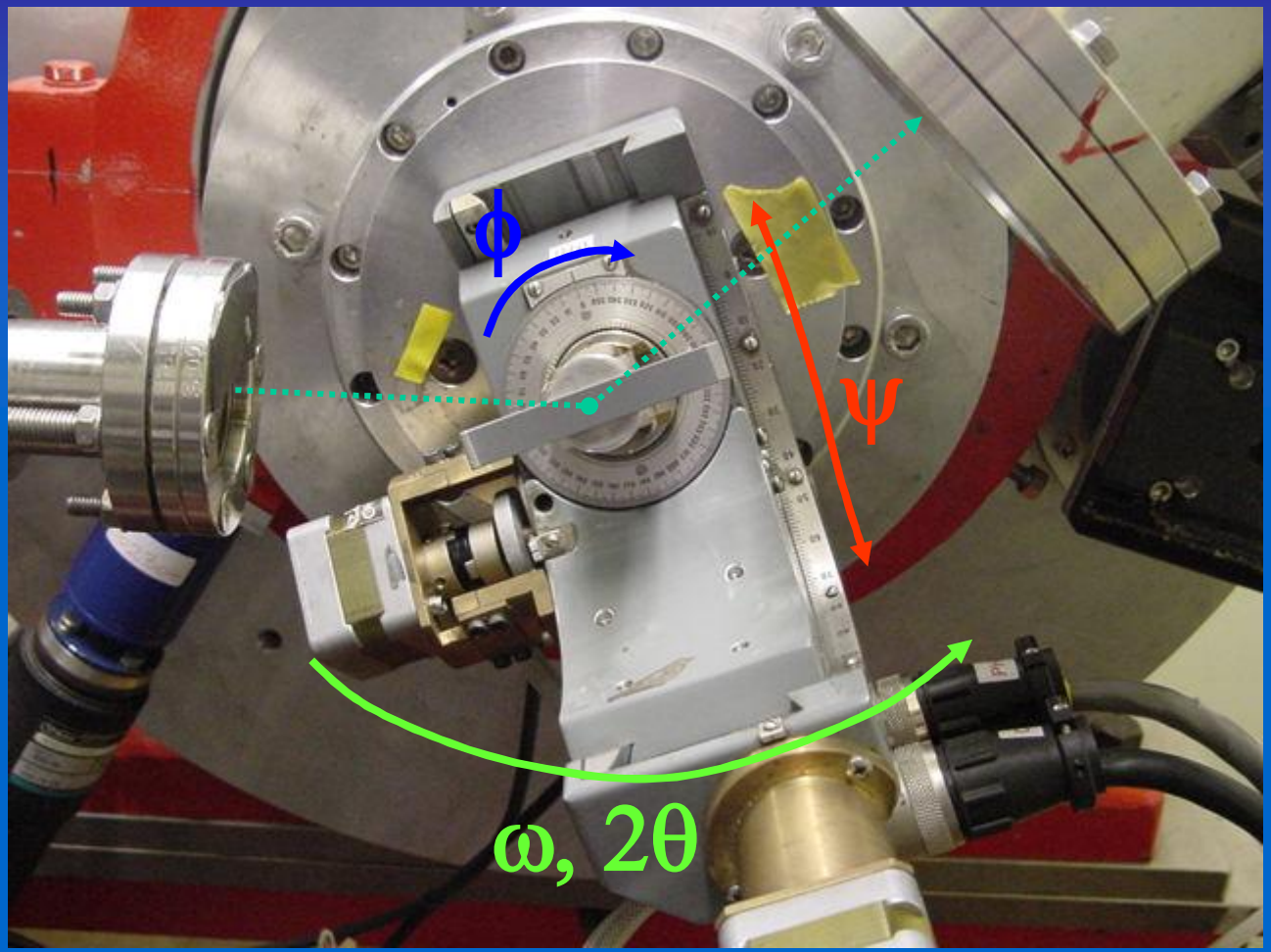

Eulerian cradle for stress/texture measurement: Daresbury beamline 2.3

TEXTURE ANALYSIS

Crystallographic texture: pole figures

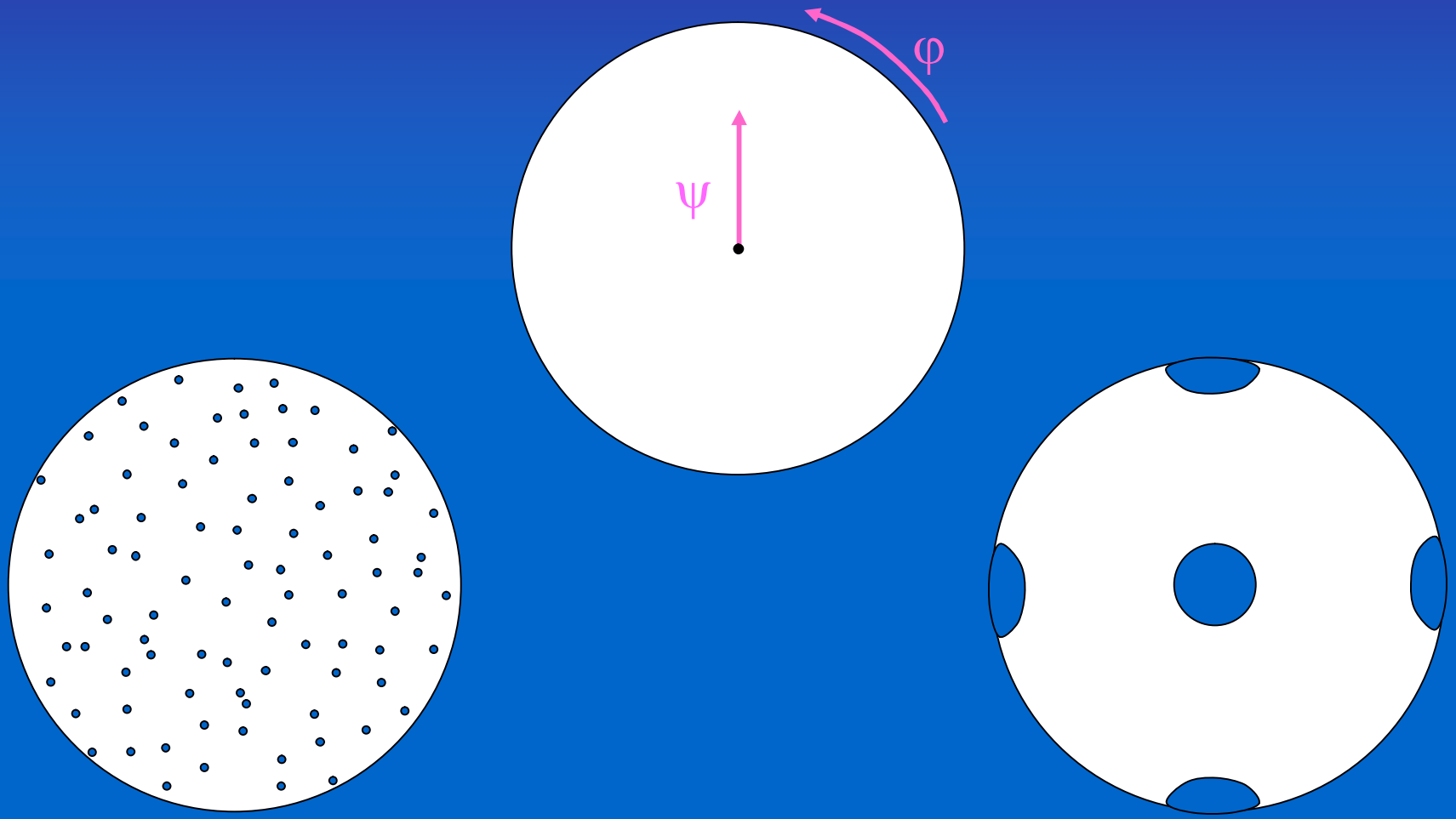

random orientation

preferred orientation

TEXTURE ANALYSIS

In general, texture can be quite complex. Several pole figures, for different (hkl), may be required to understand the orientation

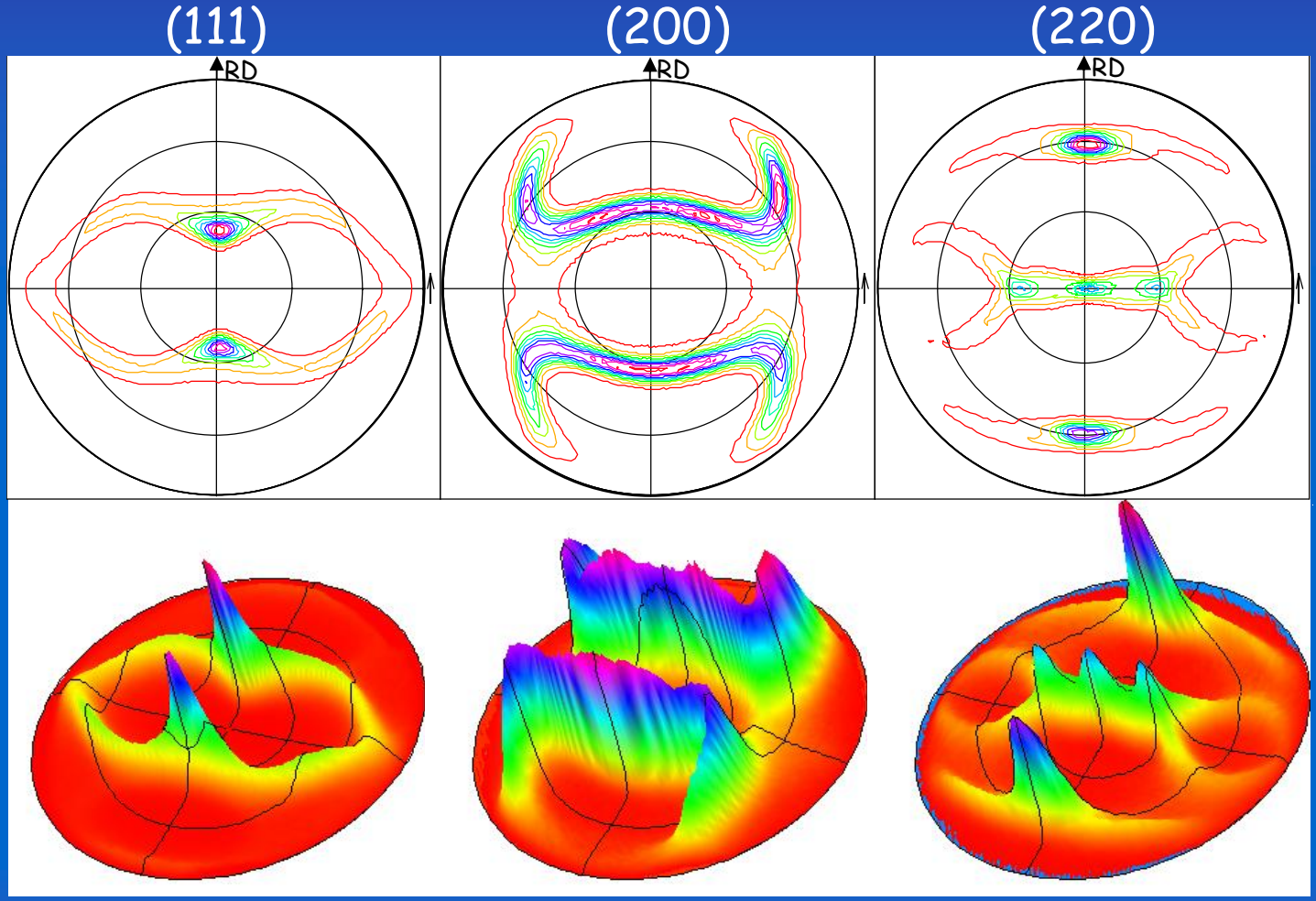

Cold-rolled Ni for high-Tc superconducting wires

RESIDUAL STRESS ANALYSIS

Why residual stresses?

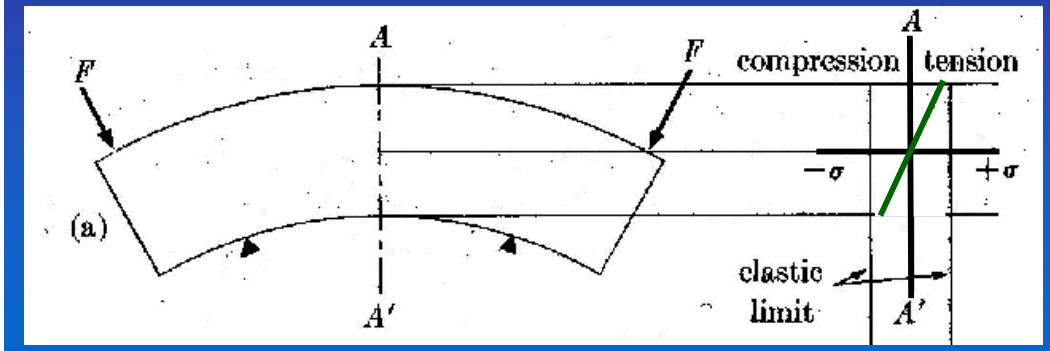

Example: residual stress by plastic flow in bending:

(a) loaded **below** elastic limit

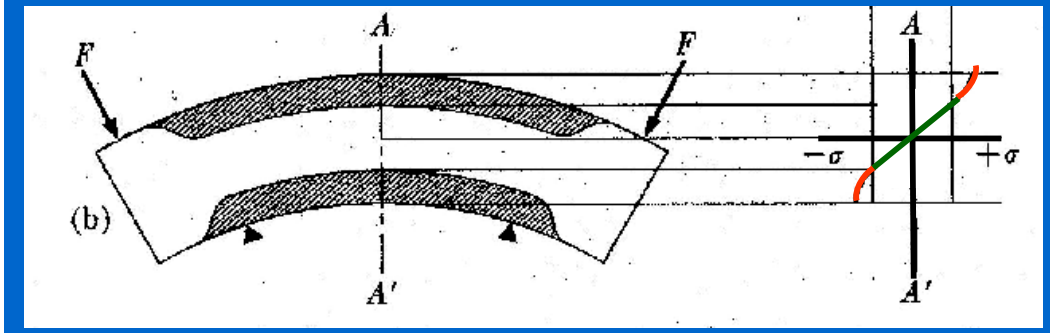

(b) loaded **above** elastic limit

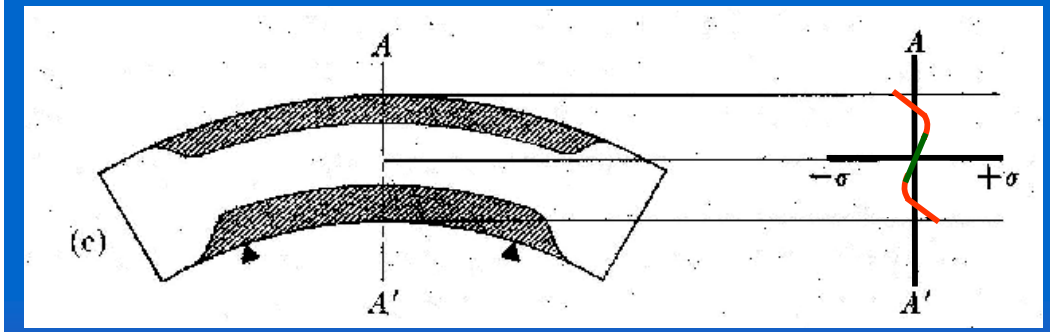

(c) unloaded

Shaded regions have been plastically deformed

Source: B.D. Cullity "Elements of X-ray diffraction" II Edition. Addison-Wesley. Reading (1978)

RESIDUAL STRESS ANALYSIS

Crystalline domains can be used as strain gauges

grain deformation

$$\varepsilon = \frac{\Delta l}{l}$$

lattice deformation

$$\varepsilon = \frac{\Delta d}{d}$$

The deformation is measured along different directions, by tilting the sample.
The in-plane strain is obtained by measuring *d* along off-plane directions.

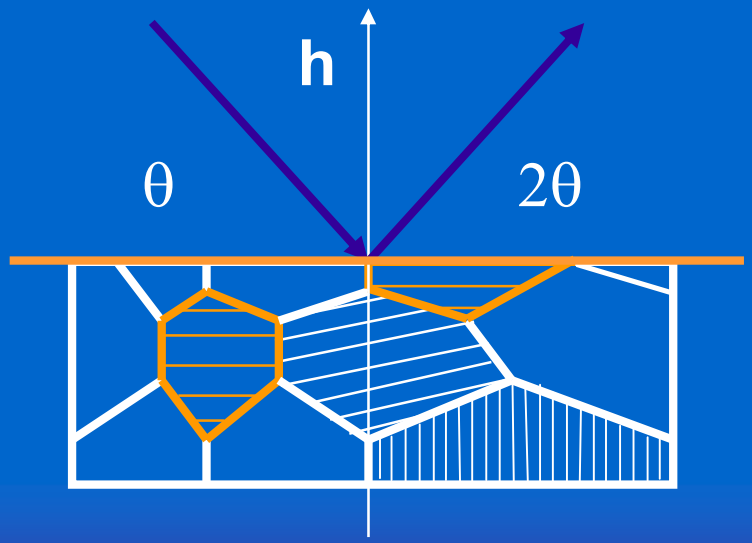

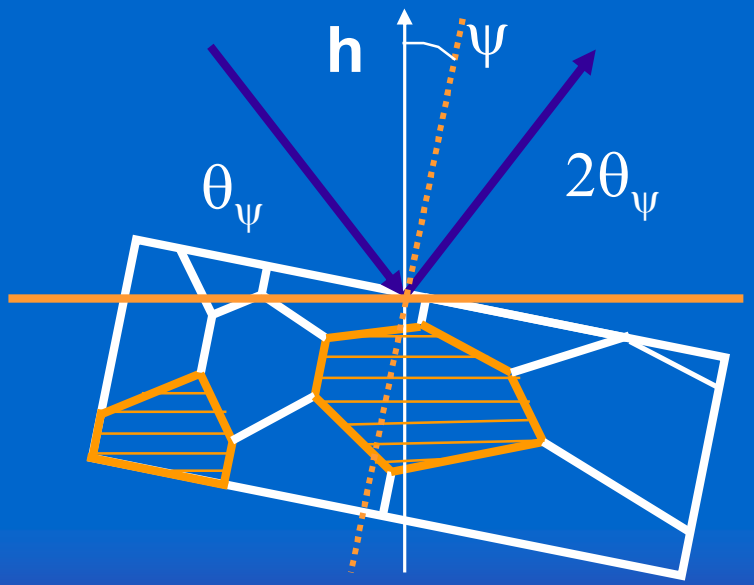

RESIDUAL STRESS ANALYSIS

If the stress field is plane and rotationally symmetric:

$\sigma_{11}=\sigma_{22}=\sigma_{||}$, $\sigma_{12}=\sigma_{13}=\sigma_{23}=\sigma_{33}=0$

and if no gradient and no texture are present, then:

$$< \varepsilon_{\psi}^{hkl} >= \left(2S_1^{hkl} + \tfrac{1}{2} S_2^{hkl} \sin^2 \psi \right) \sigma_{\psi}^{S}$$

"sin²ψ formula"

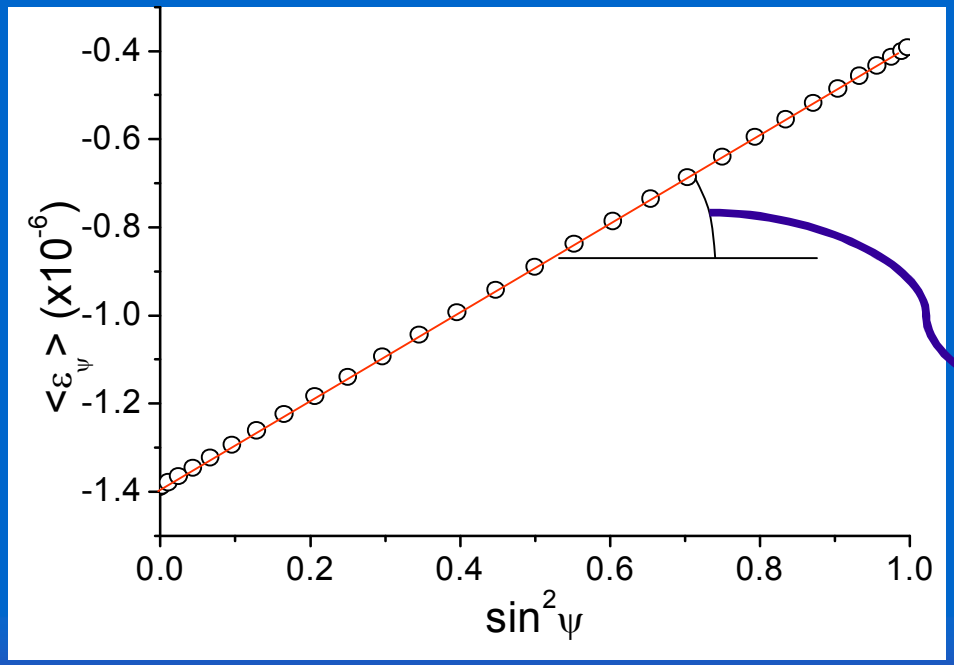

S_1^{hkl}, $\tfrac{1}{2}S_2^{hkl}$

X-ray elastic constants (XECs)

slope related to the average *in-plane* stress

RESIDUAL STRESS GRADIENT BY SRXRD

Residual stress in diamond coated components: multiple wavelength XRD

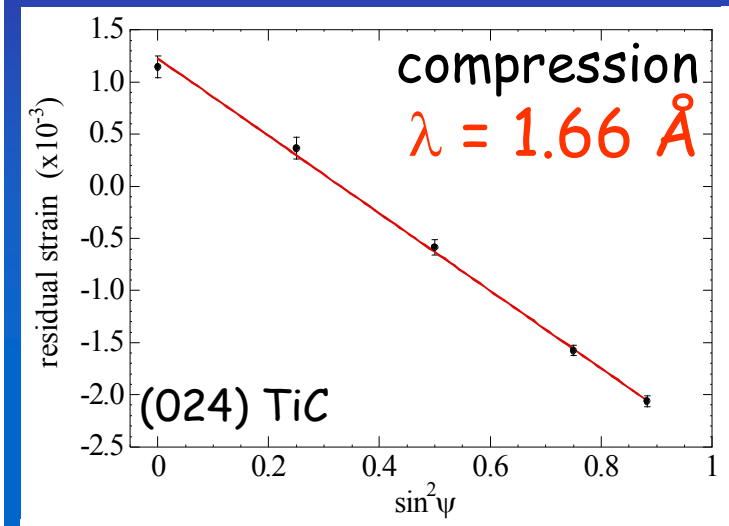

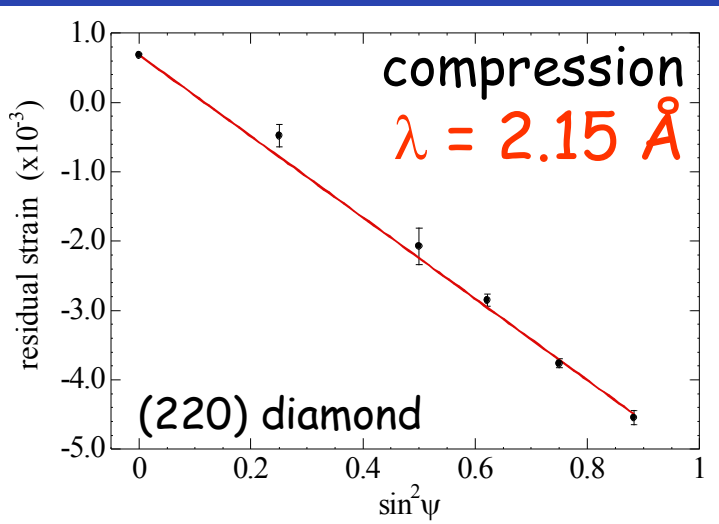

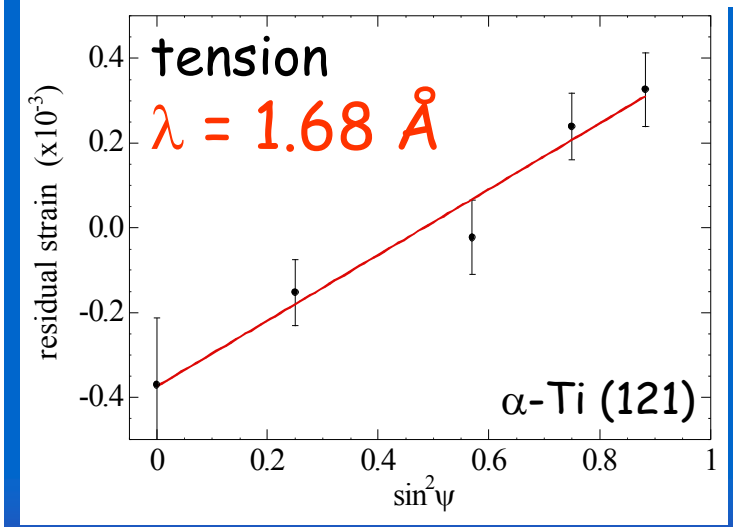

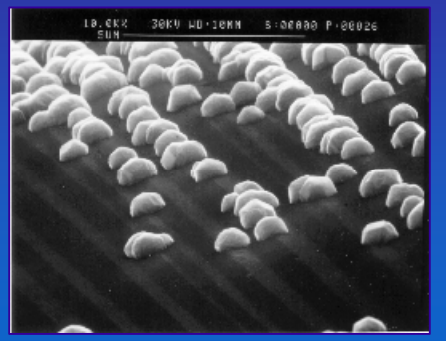

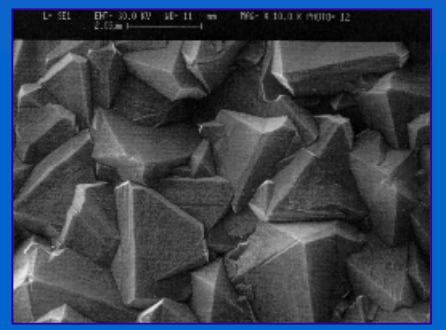

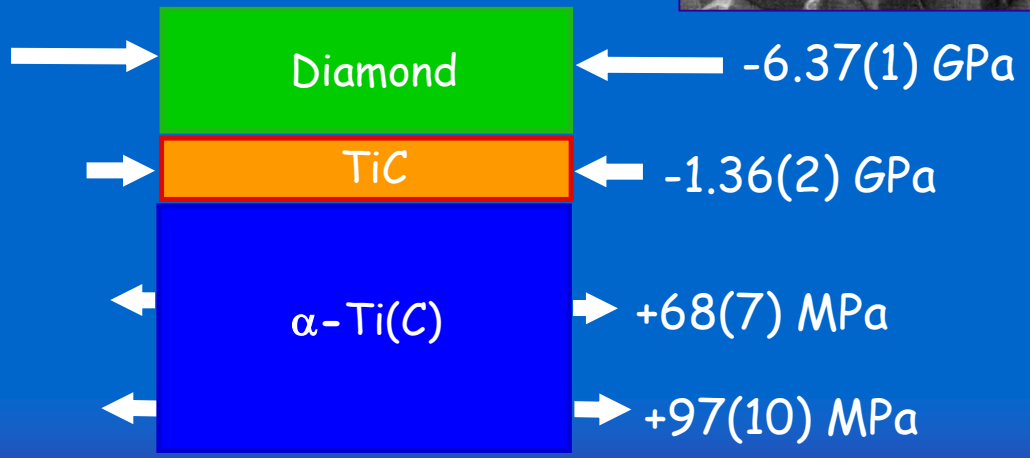

RESIDUAL STRESS GRADIENT BY SRXRD

Possible geometries for through-thickness stress mapping

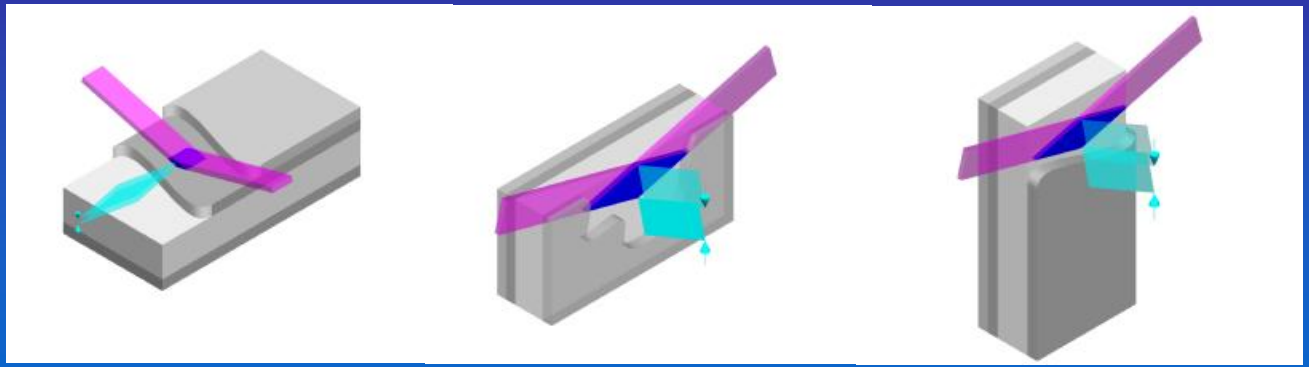

Residual stress profile in a Alumina-Zirconia-Mullite ceramic laminates

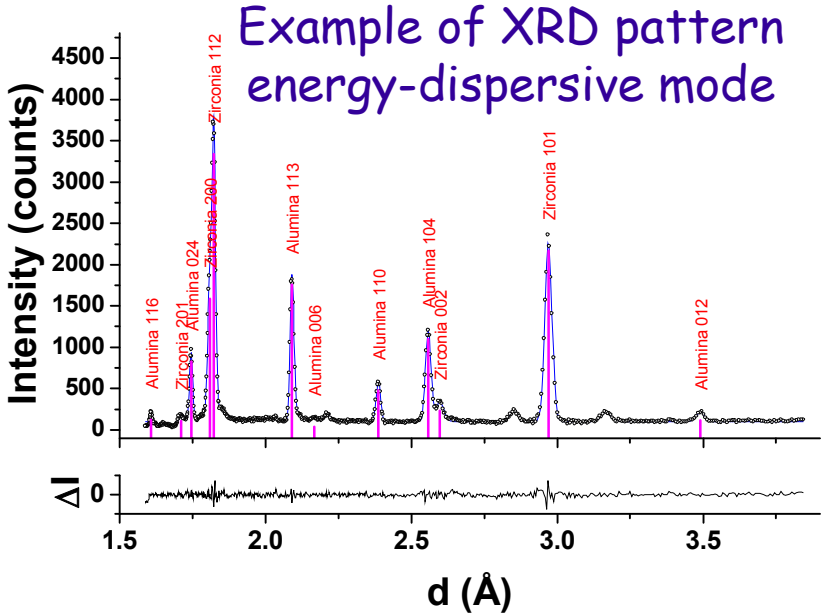

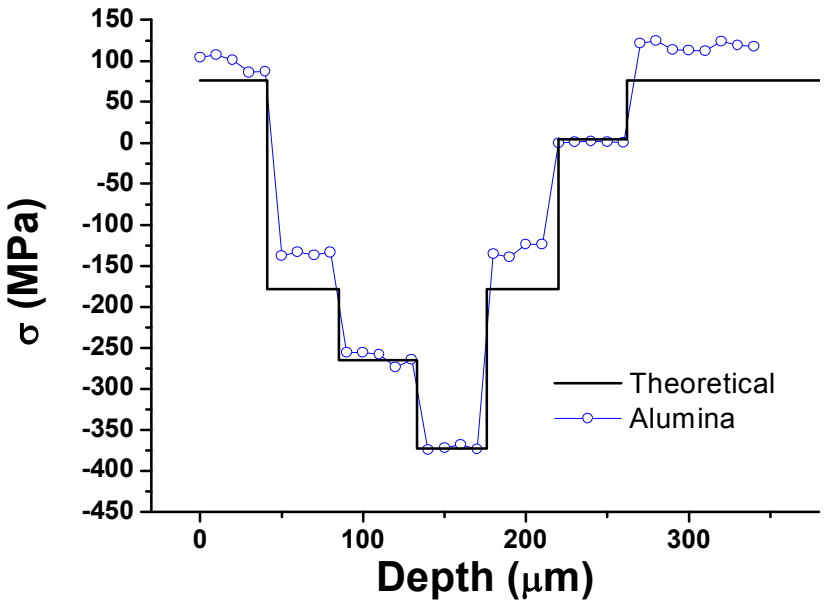

PART 1: REFERENCES

[1] B.D. Cullity, *Elements of X-ray Diffraction*, Addison-Wesley, Reading MA, 1978.

[2] R. Jenkins & R. L. Snyder, *Introduction to X-ray Powder Diffractometry*, Wiley, New York, 1996

[3] H.P. Klug & L.E. Alexander, *X-ray Diffraction procedures*, Wiley, New York, 1974.

[4] B.E. Warren, *X-ray Diffraction*, Addison-Wesley, Reading, MA, 1969.

[5] R.A.Young (Ed.), *The Rietveld method*, Oxford University Press, Oxford, 1993.

[6] R.E. Dinnebier and S.J.L. Billinge (Eds.), Powder Diffraction: Theory and Practice, The Royal Society of Chemistry, Cambridge, 2008.

[7] International Tables for X-ray Crystallography, 3rd series. Kluwer Academic Publishers, Dordrecht, Boston, London. Vol.A (1983), Vol.B (1993), Vol.C (1992), "Brief Teaching Edition of Volume A" (1985).

[8] P.P. Ewald, *Fifty years of X-ray Diffraction*, Reprinted in pdf format for the IUCr XVIII Congress, Glasgow, Scotland. Copyright © 1962, 1999 International Union of Crystallography, Chester, UK.

[9] International Union of Crystallography: http://www.iucr.org

[10] International Centre for Diffraction Data, Newtown Square, PA, USA. http://www.icdd.com

PRESENTATION OUTLINE

PART 1

- Basic elements of crystallography and X-ray diffraction (XRD) theory
- Some advantages and peculiarities of synchrotron radiation XRD (SRXRD)

PART 2

- SRXRD from nanocrystalline and highly deformed materials

NANOCRYSTALLINE & HEAVILY DEFORMED MATERIALS

Two typical cases of study

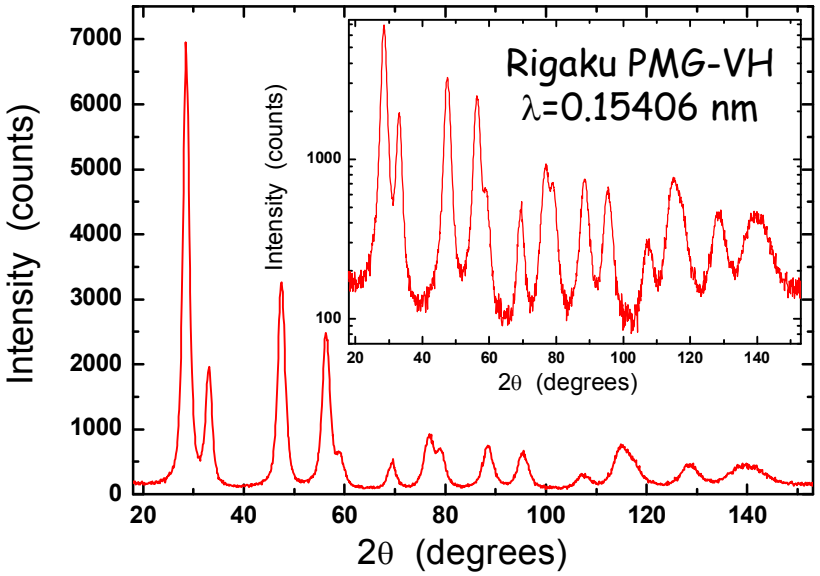

Cerium oxide powder from xerogel

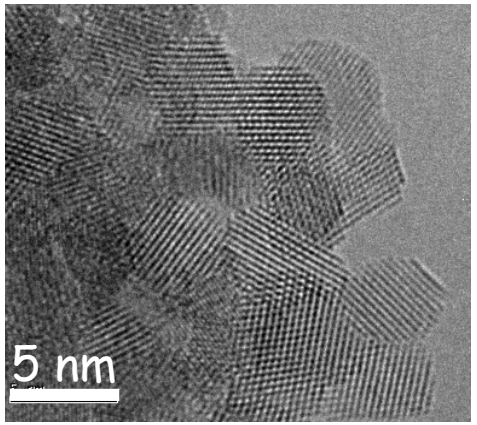

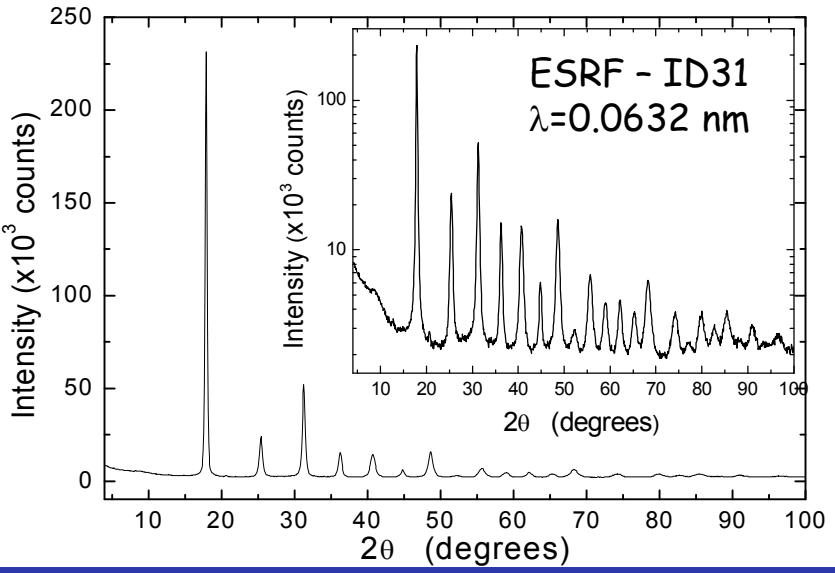

Ball milled Fe-1.5%Mo

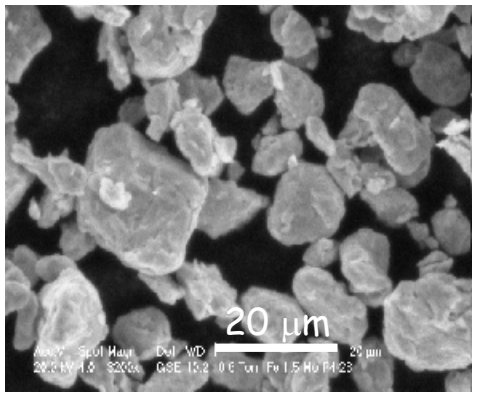

DIFFRACTION PATTERN FROM A POLYCRYSTALLINE

According to Bragg's law, peaks are δ-functions (infinitely narrow)

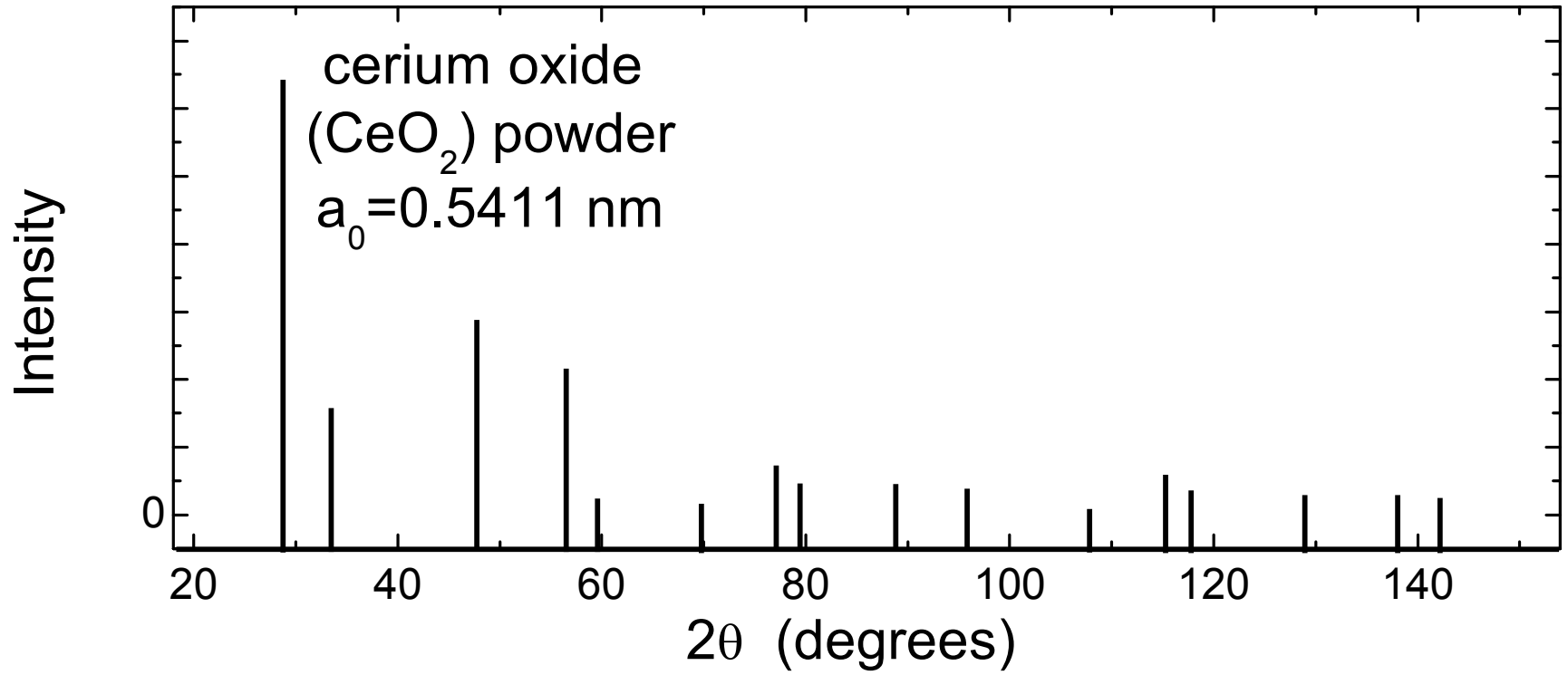

DIFFRACTION PATTERN FROM A POLYCRYSTALLINE

Actually, Bragg peaks from real (nanocrystalline) materials are broadened

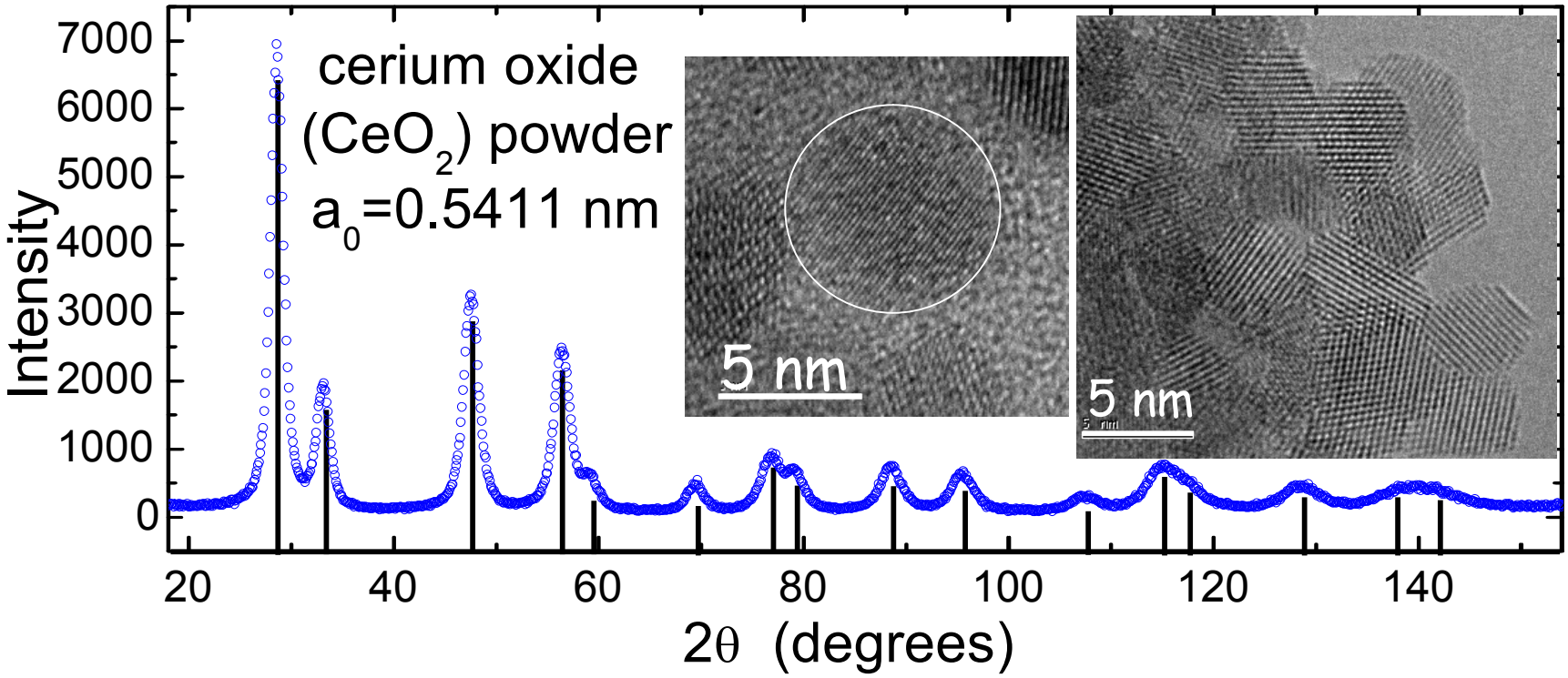

DIFFRACTION PATTERN FROM A POLYCRYSTALLINE

Integral Breadth (area/intensity) as a measurement of peak broadening

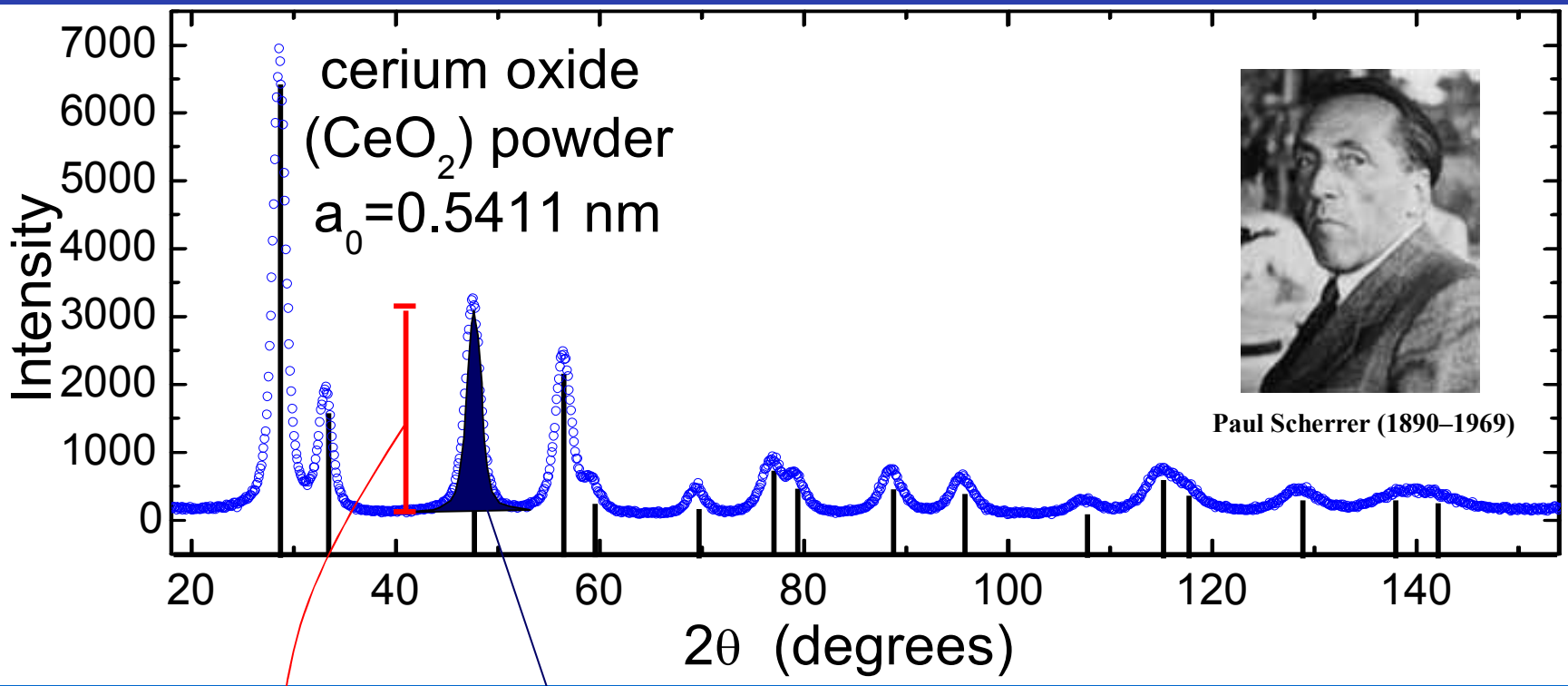

Paul Scherrer (1890–1969)

Integral Breadth

$$\beta = \frac{\int I(2\theta)\, d2\theta}{I(2\theta_B)} = \frac{\lambda}{L\cos\theta}$$

Scherrer formula (1918)

L : *effective* crystalline domain size (L ≈ 1 - 200 nm)

STRAIN BROADENING: DISLOCATIONS

Lattice defects may also cause line broadening: e.g., dislocations

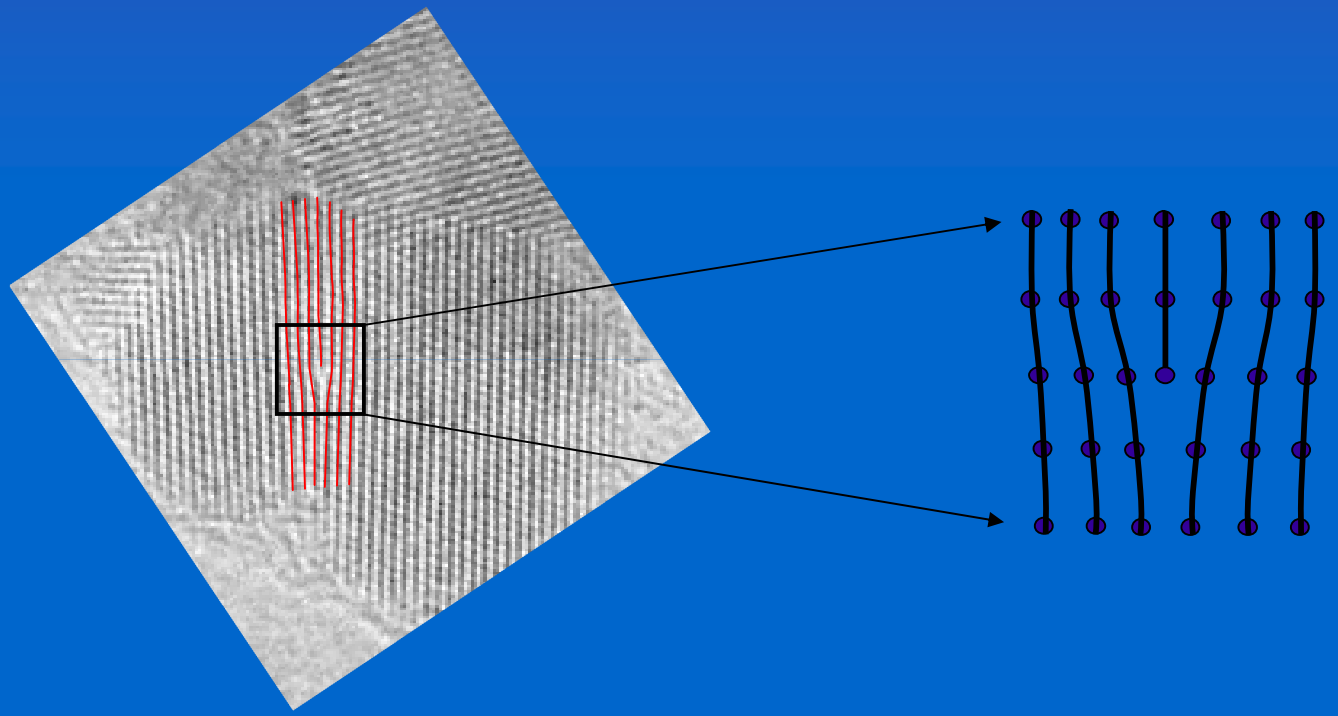

Edge dislocation in a crystalline nanograin

STRAIN BROADENING: DISLOCATIONS

Lattice defects may also cause line broadening: e.g., dislocations

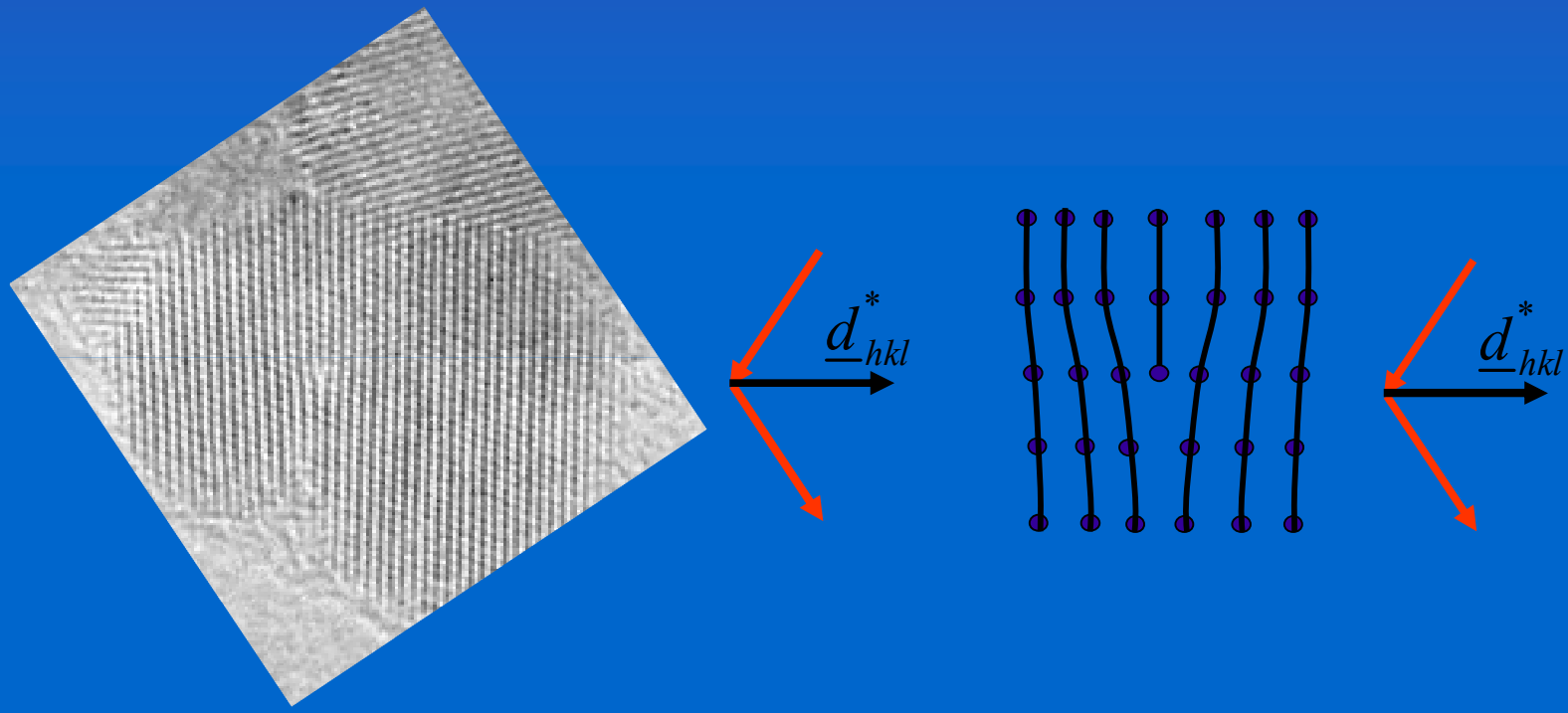

Dislocation "visibility" depends on the viewing direction (d^*_{hkl})
→ line broadening anisotropy

STRAIN BROADENING: DISLOCATIONS

Lattice defects may also cause line broadening: e.g., dislocations

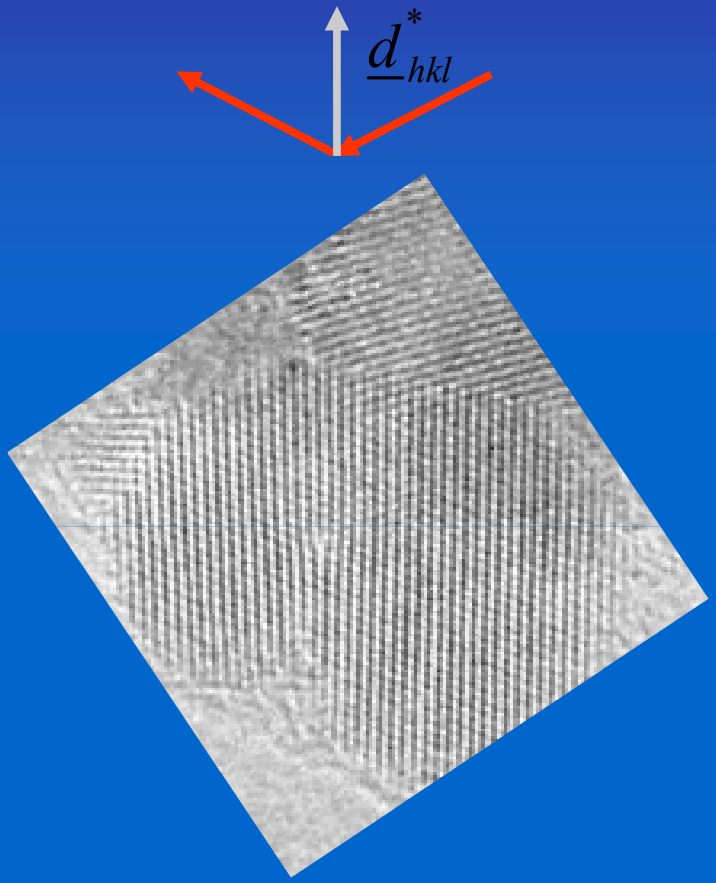

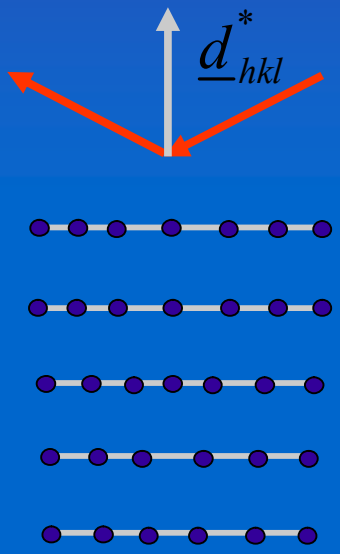

'invisible'

Dislocation "visibility" depends on the viewing direction (d^*_{hkl})
→ line broadening anisotropy

MICROSTRAIN EFFECT IN POWDER DIFFRACTION

Heuristic approach: differentiate Bragg's law (with λ = constant):

$$0 = 2\Delta d \sin(\theta) + 2d \cos(\theta)\Delta(\theta)$$

Introducing the strain: $\varepsilon = \Delta d / d$

$$\Delta(2\theta) = -2\tan(\theta)\frac{\Delta d}{d} = -2\varepsilon \tan(\theta)$$

MICROSTRAIN EFFECT IN POWDER DIFFRACTION

A uniform strain, gives a *shift* in diffraction peak position:

$$\Delta(2\theta) = -2\varepsilon \tan(\theta)$$

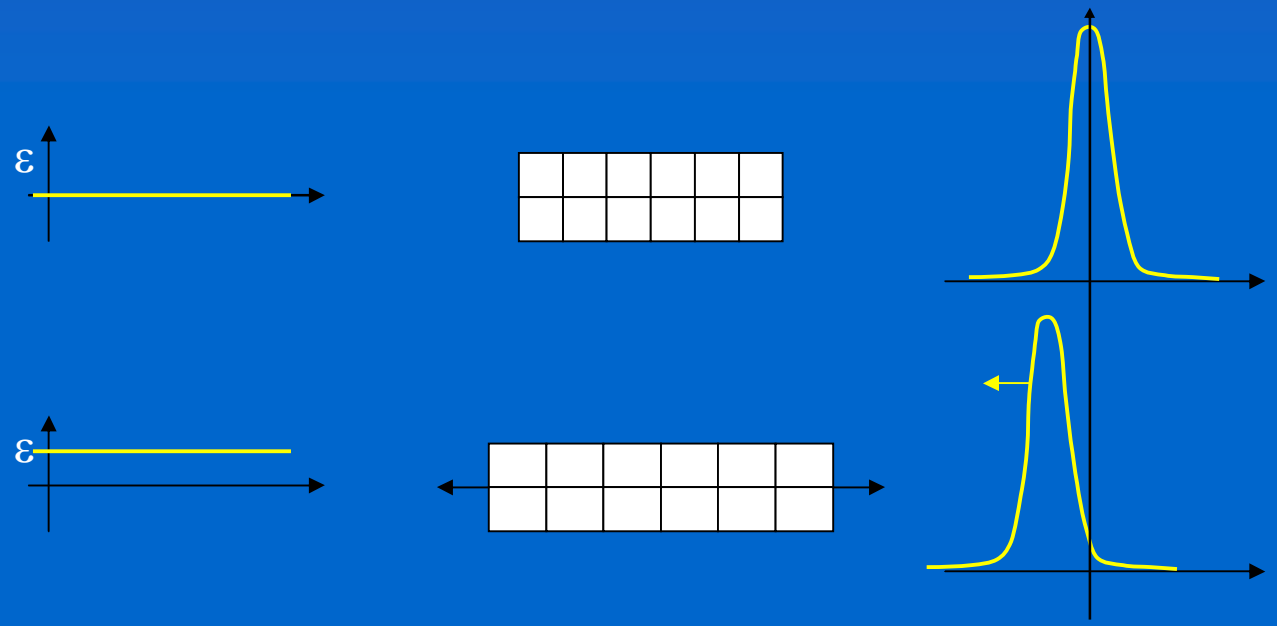

⟹ *Residual strain/stress analysis*

MICROSTRAIN EFFECT IN POWDER DIFFRACTION

Non-uniform strain gives a distribution $p_L(\varepsilon)$. Mean strain can be zero (e.g. in a powder), even if a **microstrain** (r.m.s. strain) is present:

$$\left\langle \varepsilon^2 \right\rangle^{1/2} = \left\langle \left(\Delta d/d \right)^2 \right\rangle^{1/2}$$

$$\Delta(2\theta) = -2\varepsilon \tan(\theta) \quad \Longrightarrow \quad \beta(2\theta) \approx 2\left\langle \varepsilon^2 \right\rangle^{1/2} \tan\theta$$

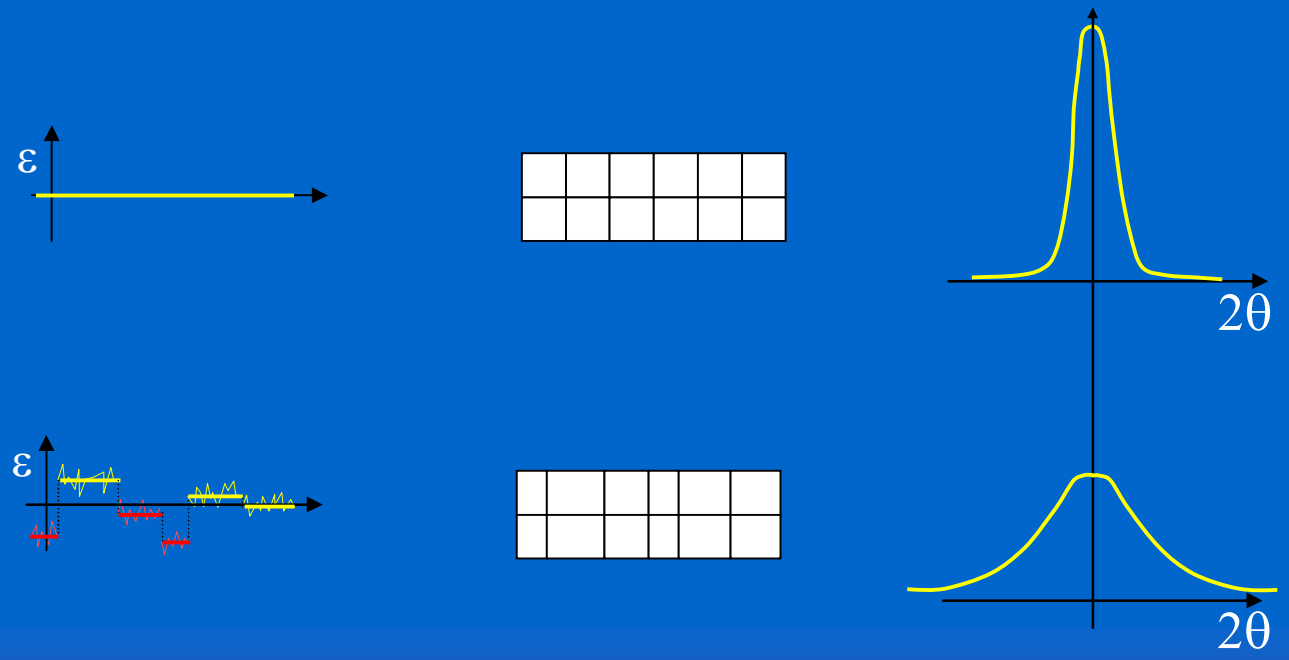

SIZE - STRAIN EFFECT IN POWDER DIFFRACTION

Combined effects - domain size and lattice distortions

$$\beta(2\theta) \approx \frac{\lambda}{L\cos\theta} + 2\left\langle \varepsilon^2 \right\rangle^{1/2} \tan\theta$$

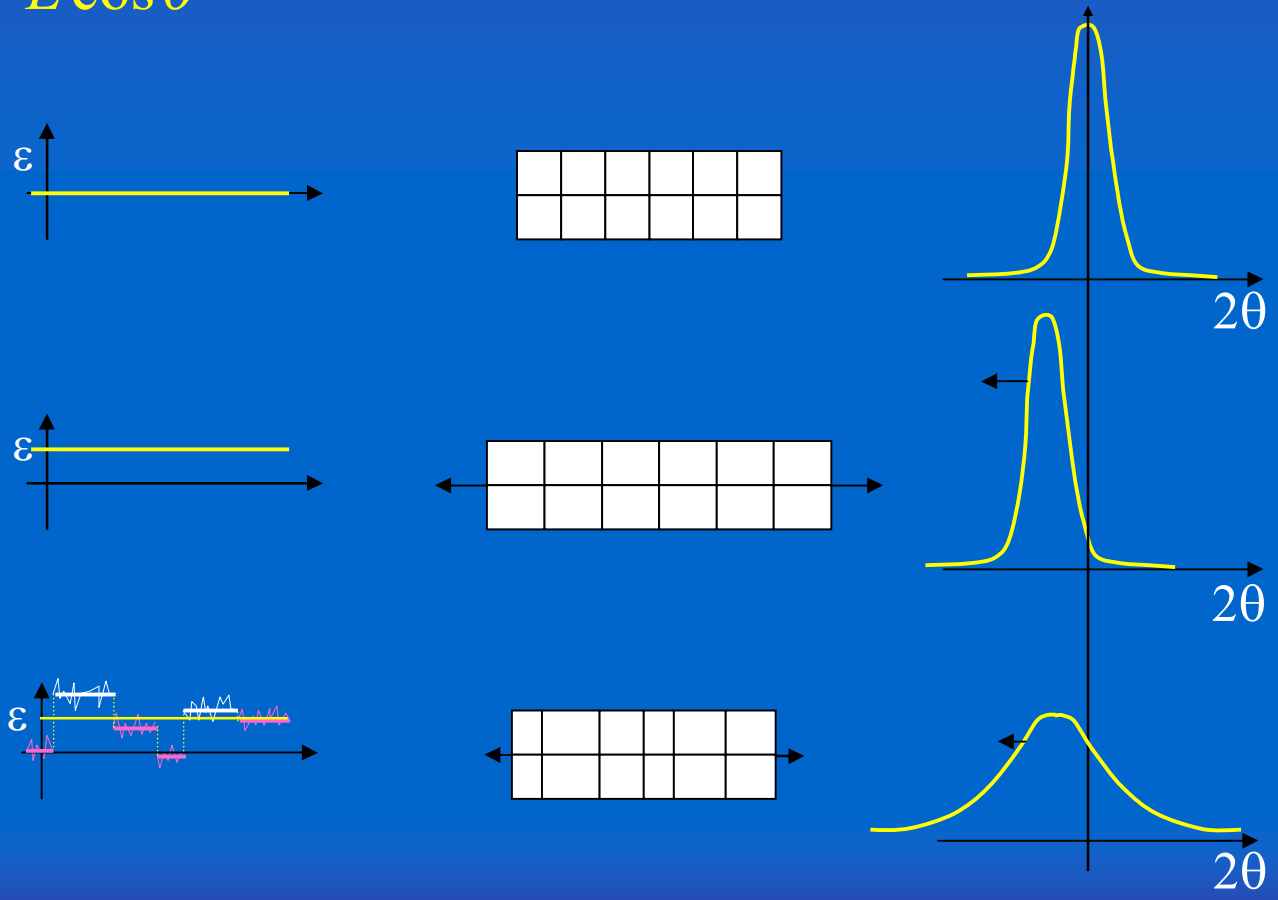

INTEGRAL BREADTH METHODS

Combined effects - domain size and lattice distortions

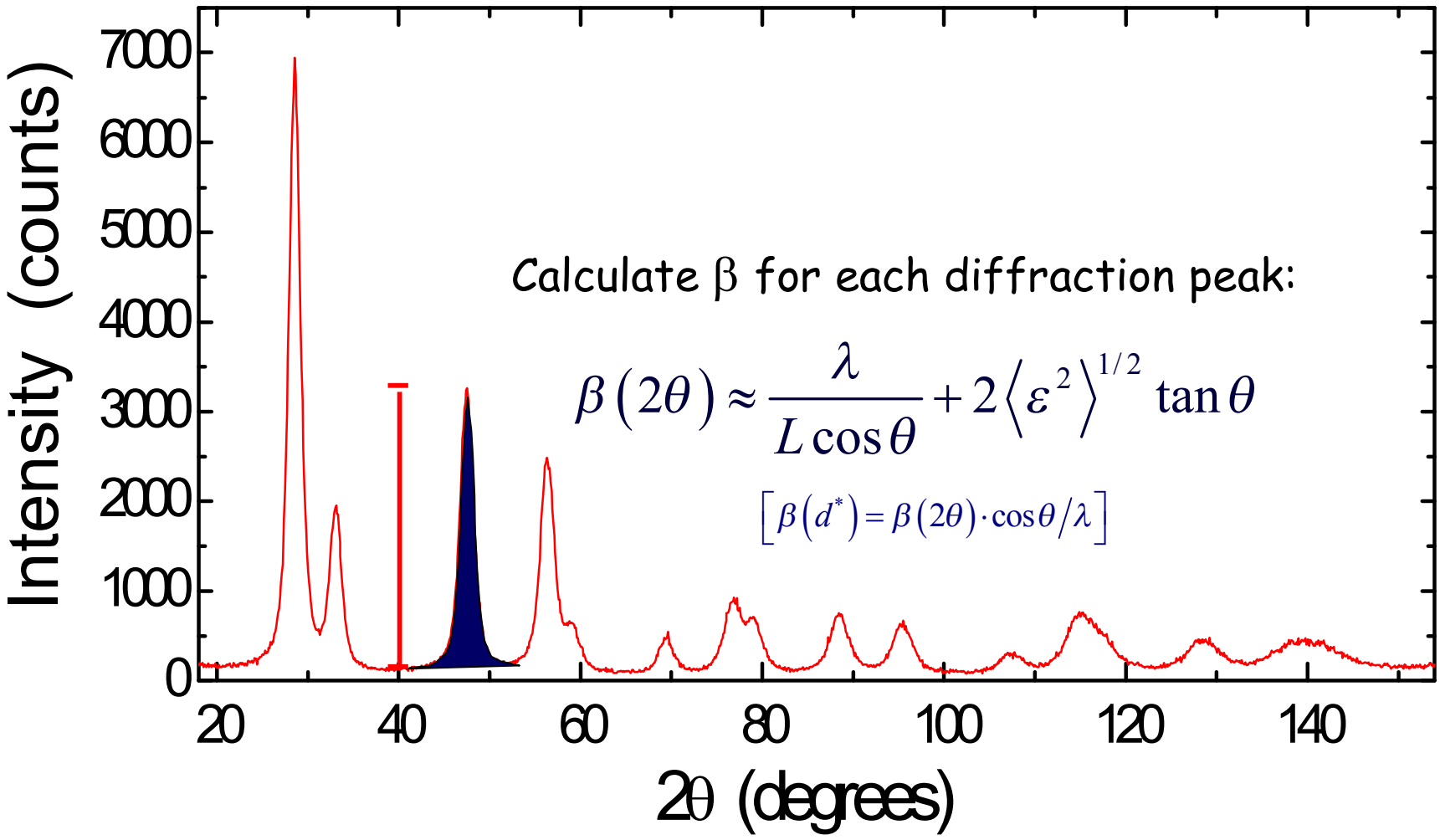

INTEGRAL BREADTH METHODS

Combined effects - domain size and lattice distortions

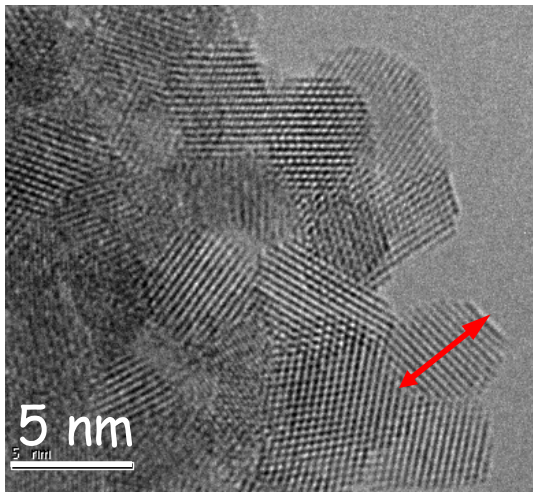

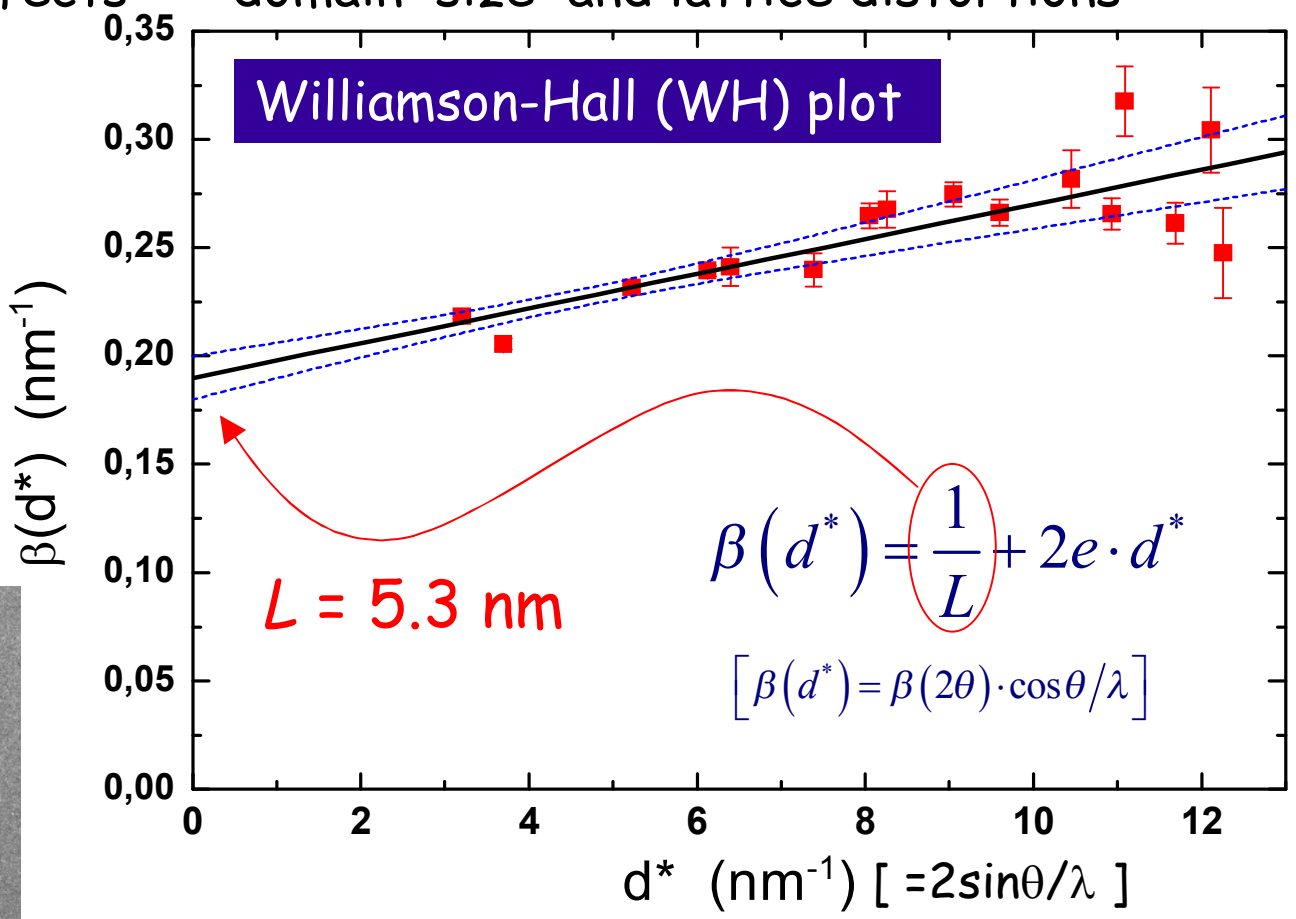

LIMITATIONS OF TRADITIONAL METHODS OF LINE PROFILE ANALYSIS

INTEGRAL BREADTH METHODS: LIMITATIONS

Peak profiles tend to overlap: difficult to obtain integral breadths

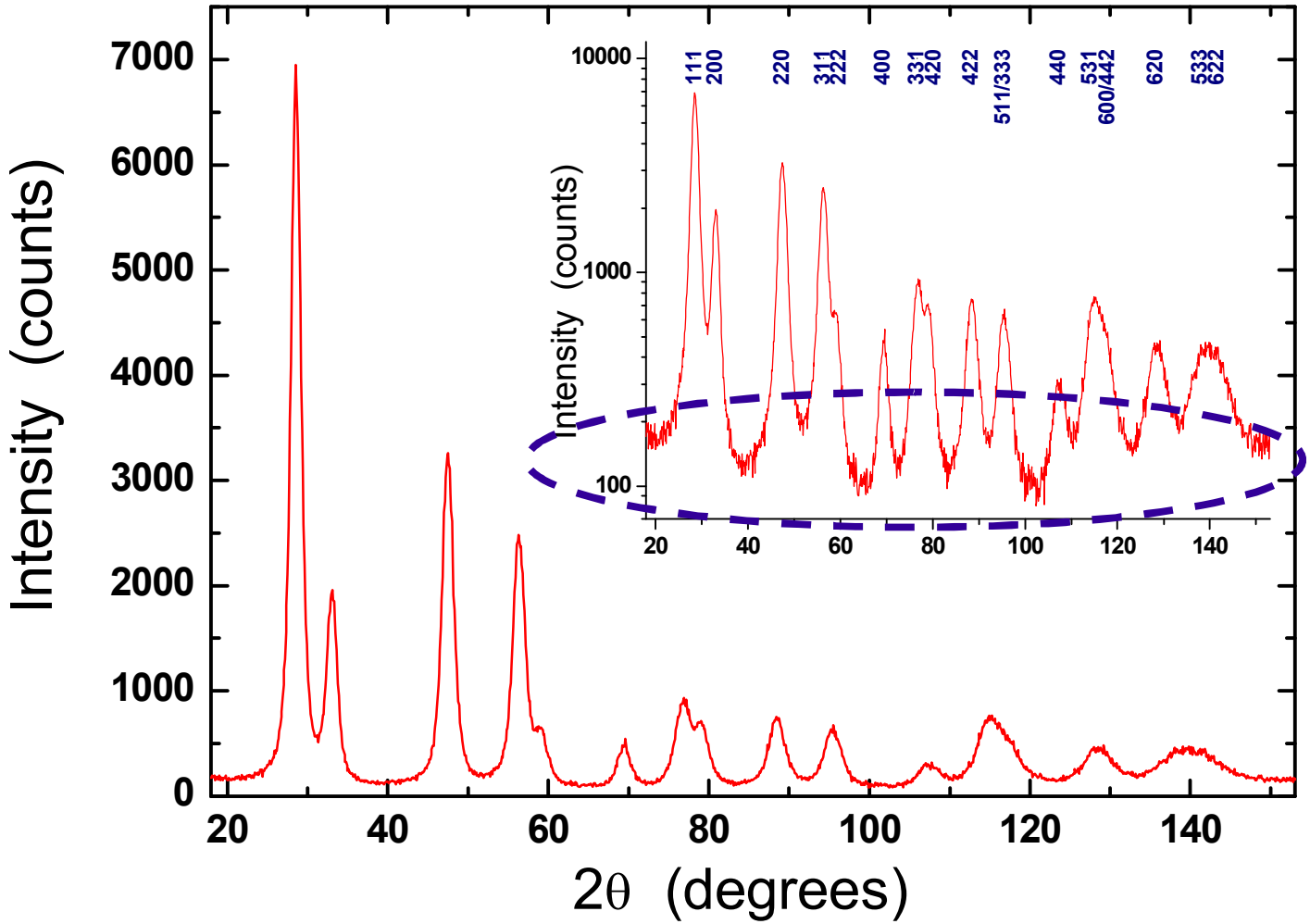

PROFILE FITTING AND LINE PROFILE ANALISYS

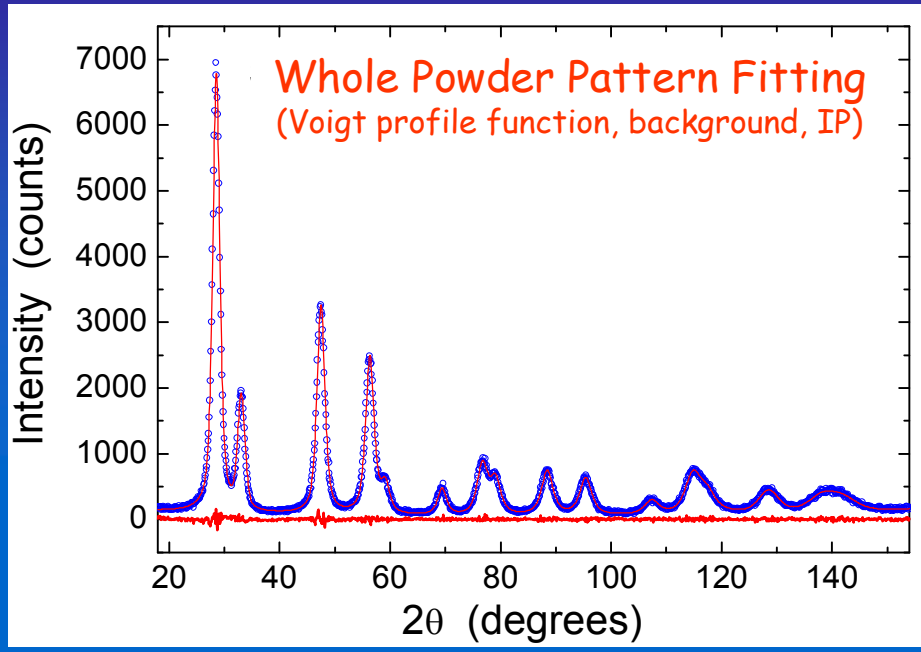

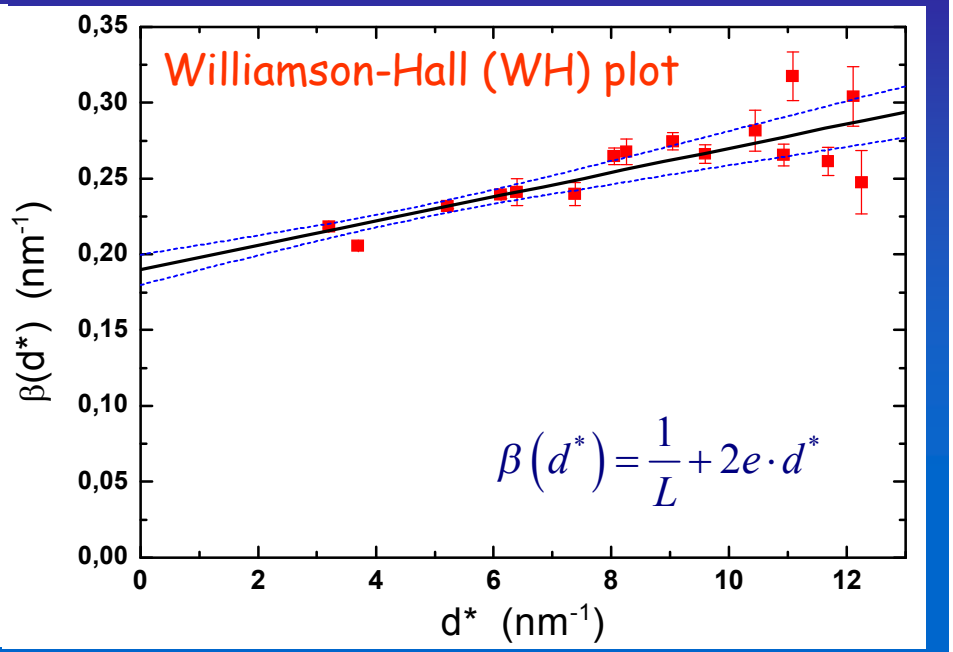

MARQX software: Y.H. Dong & P. Scardi J. Appl. Cryst. 33 (2000) 184

Modern approach to LPA relies on peak profile fitting for

- Pattern decomposition
- Background separation
- Deconvolution / convolution with instrumental profile component

Although simple and flexible profile fitting is substantially arbitrary and controversial: no reason for adopting a given analytical shape !!!

INTEGRAL BREADTH METHODS: LIMITATIONS

What is the meaning of *L*,
the 'size' value given by the Scherrer formula ??

$$\beta(2\theta) = \frac{\lambda}{L\cos\theta}$$

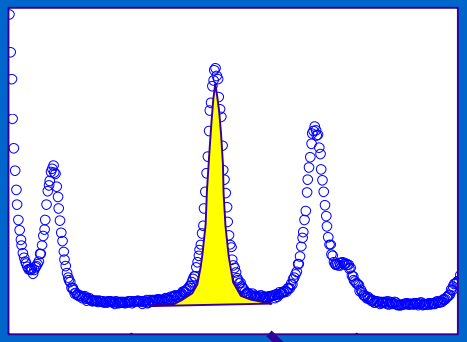

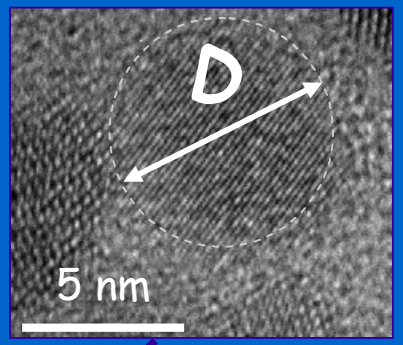

$L \neq D$

INTEGRAL BREADTH METHODS: LIMITATIONS

In most cases nano powders have a distribution of sizes (and shapes)

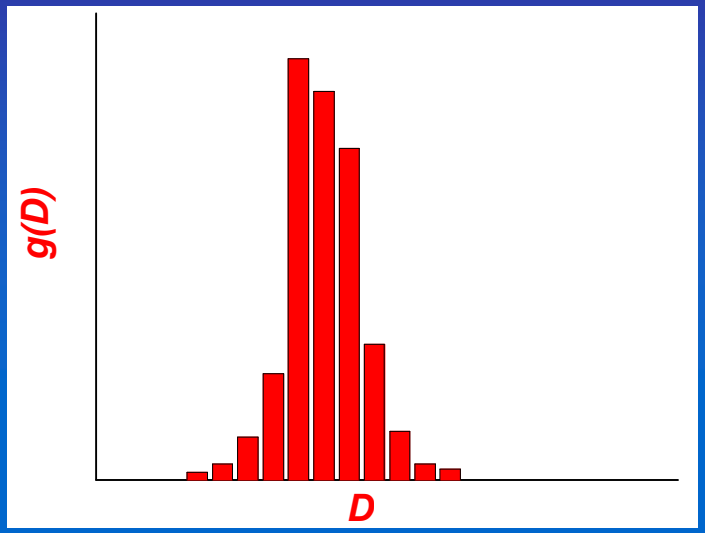

Distribution 'moments'

$$M_i = \int D^i g(D) dD$$

$M_1 \rightarrow$ *mean*

$M_2 - M_1^2 \rightarrow$ *variance*

$$L \rightarrow \langle L \rangle_V = \frac{1}{K_\beta} \frac{M_4}{M_3}$$

K_β, a shape factor, generally function of *hkl* (4/3 for spheres)

INTEGRAL BREADTH METHODS: LIMITATIONS

$$L \rightarrow \langle L \rangle_V = \frac{1}{K_\beta}\frac{M_4}{M_3} \neq D$$

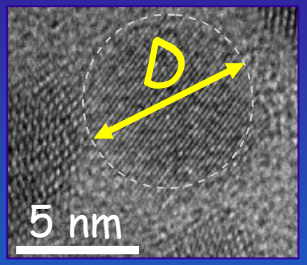

Example: lognormal distributions of spheres, g(D) (mean μ, variance σ)

For little asymmetrical or narrow distributions

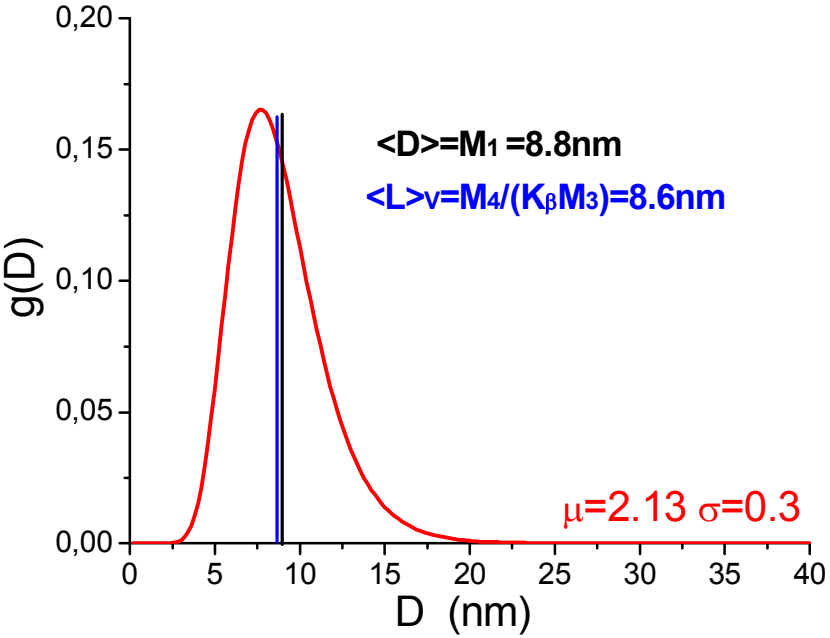

For broad, asymmetrical distributions

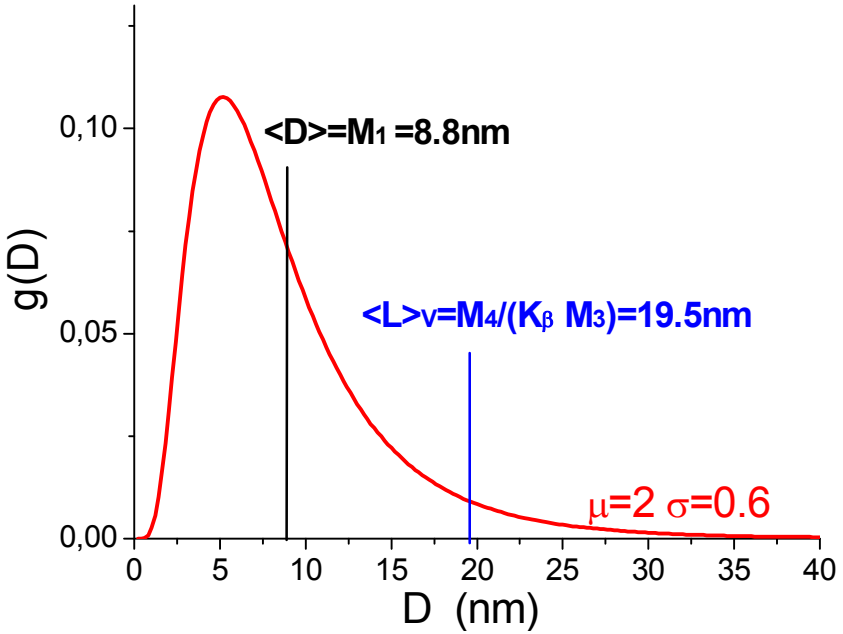

INTEGRAL BREADTH METHODS: MAIN LIMITATIONS

- Peak overlapping → requires profile fitting with *arbitrary* profile functions
- Effective domain size, *L* → real information is the *size distribution*
- Microstrain e is not a constant → *microstrain distribution*

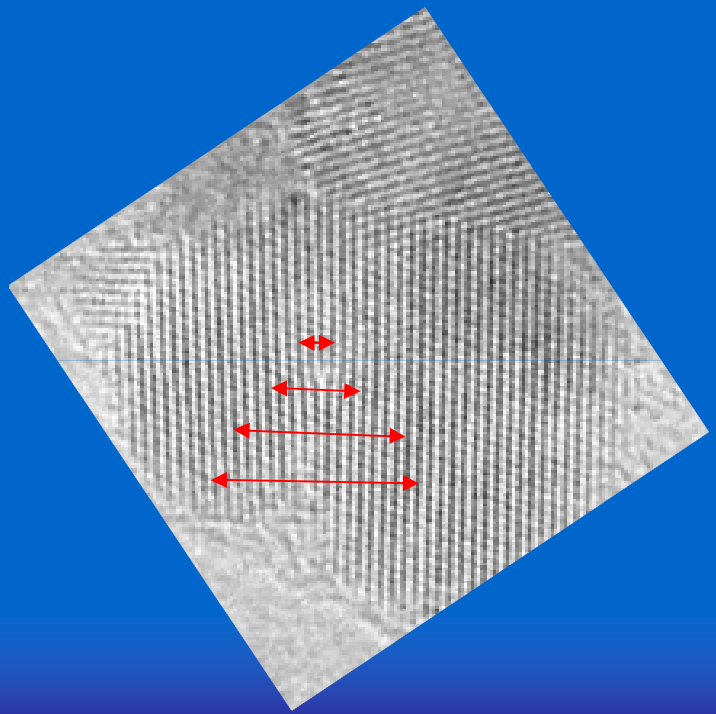

INTEGRAL BREADTH METHODS: MAIN LIMITATIONS

- Peak overlapping → profile fitting with *arbitrary* profile functions
- Effective domain size, *L* → real information is the *size distribution*
- Microstrain e is not a constant → *microstrain distribution*
- Line broadening effects ***do not*** simply "add" as in the Williamson-Hall formula

$$\beta\left(d^*\right) = \underbrace{\frac{1}{L}}_{\text{'size'}} + \underbrace{2e \cdot d^*}_{\text{'strain'}}$$

WHOLE POWDER PATTERN MODELLING - WPPM

Modelling of the experimental pattern based on **physical models** of the microstructure and lattice defects:

Diffraction Pattern ⟷ **WPPM** (*Physical Model*) ⟷ Microstructural Parameters

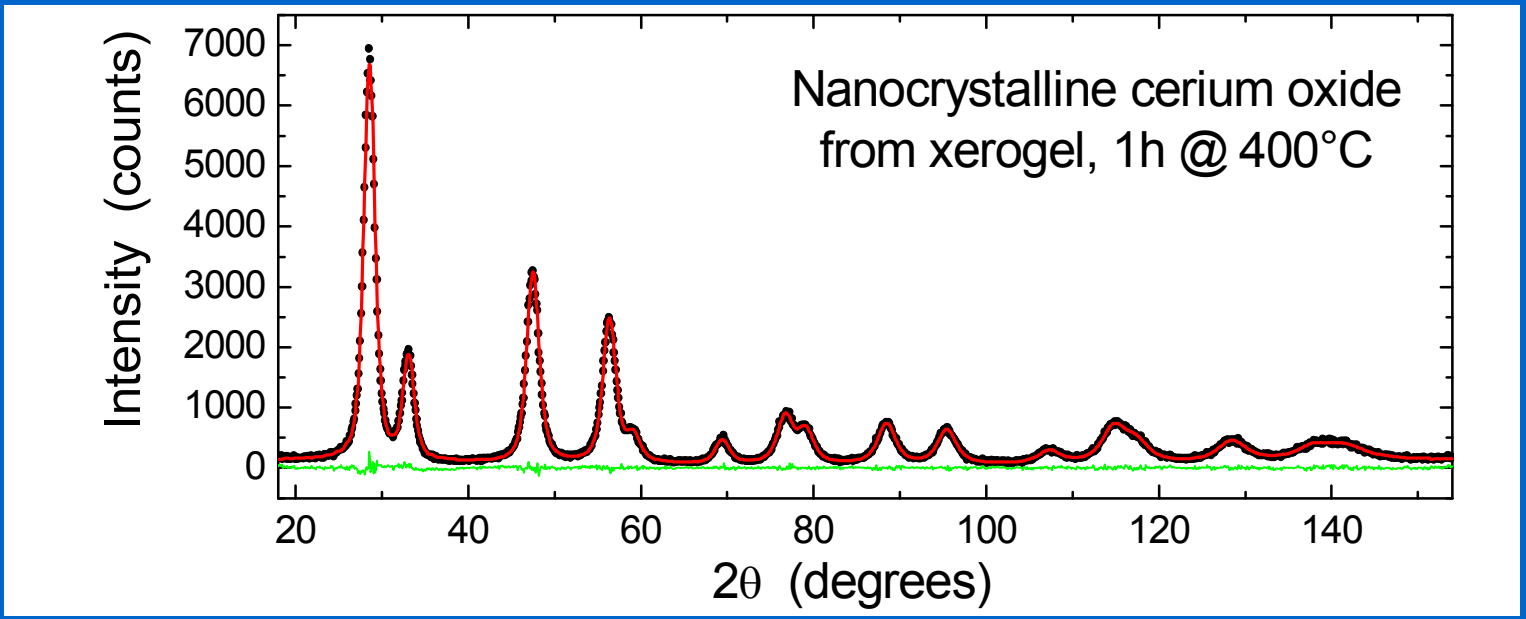

M. Leoni, R. Di Maggio, S. Polizzi & P. Scardi, J. Am. Ceram. Soc. 87 (2004) 1133.
P.Scardi & M. Leoni, Acta Cryst. A 57 (2001) 604. P.Scardi & M. Leoni, Acta Cryst. A 58 (2002) 190

WHOLE POWDER PATTERN MODELLING

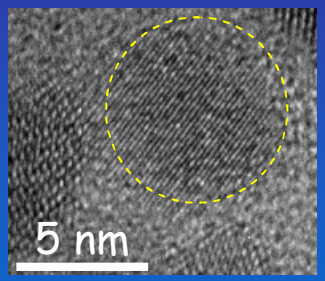

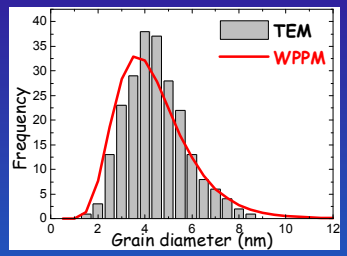

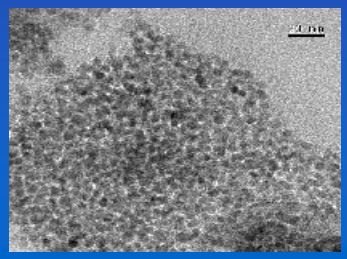

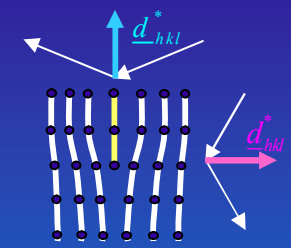

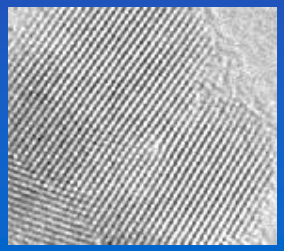

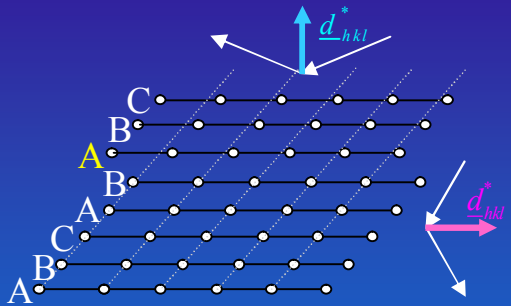

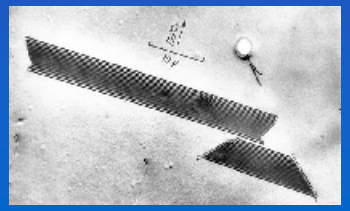

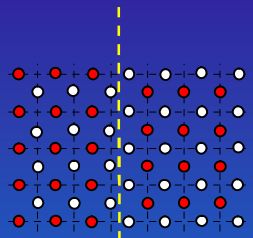

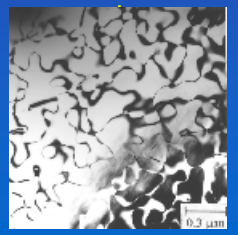

(...)

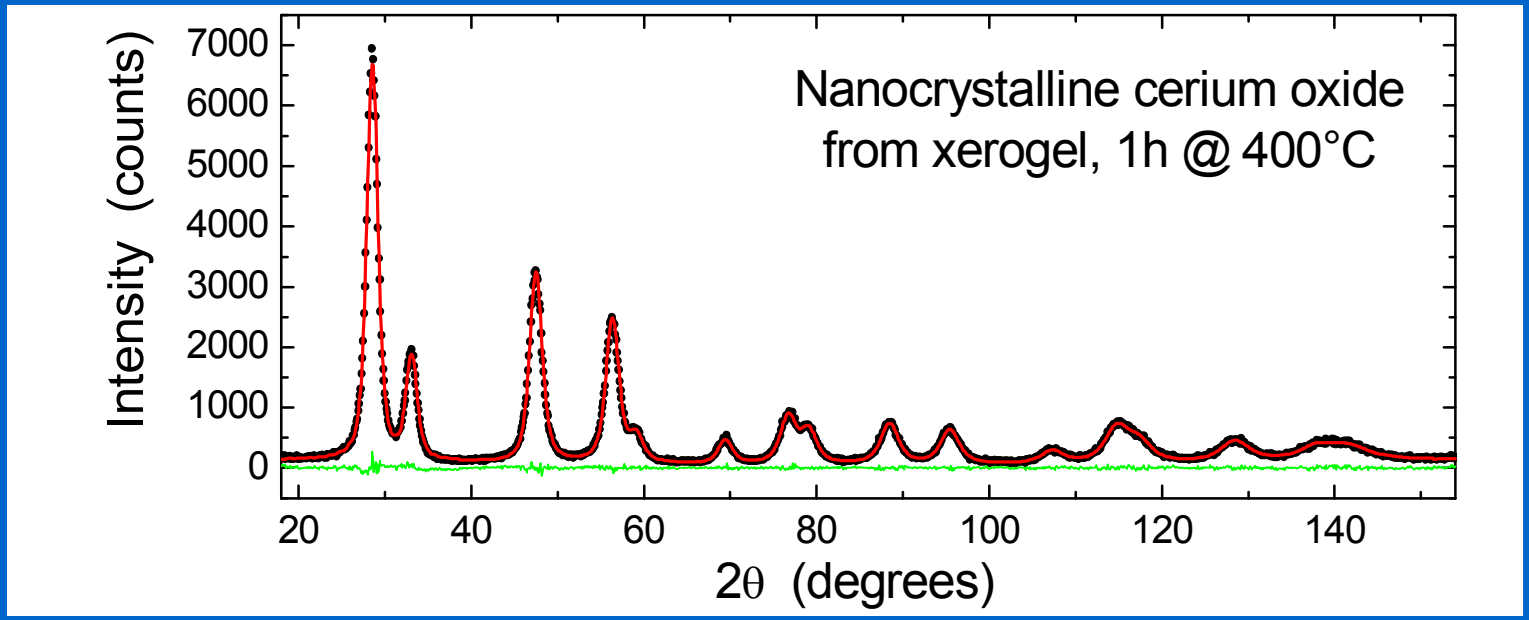

M. Leoni, R. Di Maggio, S. Polizzi & P. Scardi, J. Am. Ceram. Soc. 87 (2004) 1133.
P.Scardi & M. Leoni, Acta Cryst. A 57 (2001) 604. P.Scardi & M. Leoni, Acta Cryst. A 58 (2002) 190

WHOLE POWDER PATTERN MODELLING

Modelling of the experimental pattern based on
physical models of the microstructure and lattice defects:

How does it work ??

DIFFRACTION LINE PROFILE: CONVOLUTION OF EFFECTS

The diffraction peak is a **convolution** (⊗) of *profile components* :

instrumental profile (IP), domain size (S), microstrain (D), faulting (F), anti-phase domain boundaries (APB), stoichiometry fluctuations (C), grain surface relaxation (GSR), etc.

$$I(s) = \underbrace{I^{IP}(s)}_{h} \otimes \underbrace{I^{S}(s) \otimes I^{D}(s) \otimes I^{F}(s) \otimes I^{APB}(s) \otimes I^{C}(s) \otimes I^{GRS}(s) \ldots}_{f}$$

$h = g \otimes f$

Instrument — Specimen-related

What is the difference between *convolution* and *sum* of effects ??

DIFFRACTION LINE PROFILE: CONVOLUTION OF EFFECTS

Example: consider instrument (IP) and domain size (S):

$$I(s) = I^{IP}(s) \otimes I^{S}(s)$$

$$I(s) = \int I^{IP}(t) I^{S}(s-t)\, dt$$

g profile, slit (box) function; f profile, bell-shape function (e.g. gaussian)

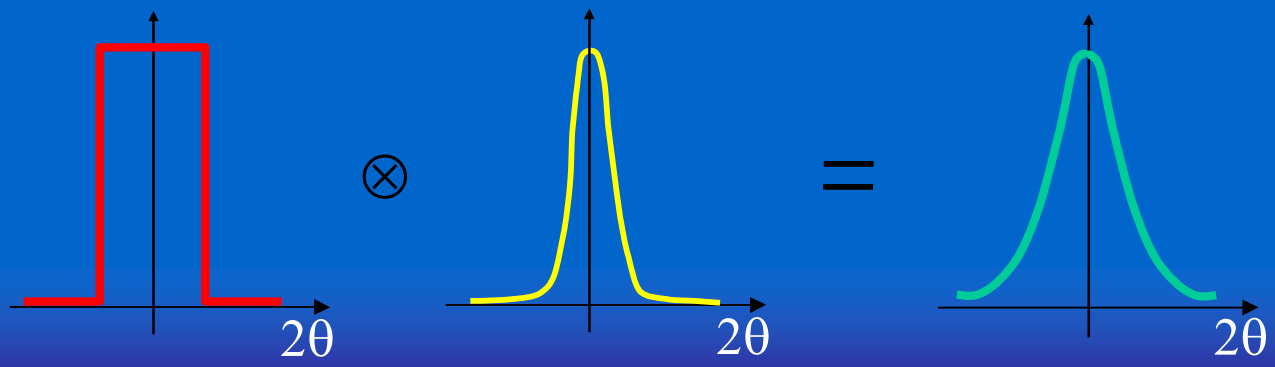

WPPM : HOW DOES IT WORK ??

The diffraction profile results from a convolution of effects:

$$I(s) = I^{IP}(s) \otimes I^{S}(s) \otimes I^{D}(s) \otimes I^{F}(s) \otimes I^{APB}(s) \otimes I^{C}(s) \otimes I^{GRS}(s) \ldots$$

the Fourier Transform of I(s) is the product of the FTs of the single profile components

$$I(s) \propto \cdot \int_{-\infty}^{\infty} C(L) e^{2\pi i L \cdot s_{hkl}} \, dL$$

$$C = \prod_i A_i = \underbrace{T^{IP}_{pV}}_{\text{instr. profile}} \cdot \underbrace{A^{S}_{\{hkl\}}}_{\text{domain size/shape}} \cdot \underbrace{A^{D}_{\{hkl\}} \cdot (A^{F}_{hkl} + iB^{F}_{hkl}) \cdot A^{APB}_{\{hkl\}} \cdot \ldots}_{\text{lattice defects / strain}}$$

P. Scardi & M. Leoni J. Appl. Cryst. 39 (2006) 24 - P. Scardi & M. Leoni, Acta Cryst. A58 (2002) 190

$A_i(L)$ EXPRESSIONS (ANALYTICAL OR NUMERICAL FORM)

$$T_{pV}^{IP}(L) = (1-k)\cdot\exp\left(-\pi^2\cdot\sigma_s^2 L^2/\ln 2\right) + k\exp\left(-2\pi\cdot\sigma_s L\right)$$

Instrumental profile

Domain size effect: μ, σ

$$A^S(L) = \sum_{n=0}^{3} H_n^c \cdot Erfc\left[\frac{\ln\left(L\cdot K^c\right) - \mu - (3-n)\sigma^2}{\sigma\sqrt{2}}\right]\frac{M_{l,3-n}}{2M_{l,3}}\cdot L^n$$

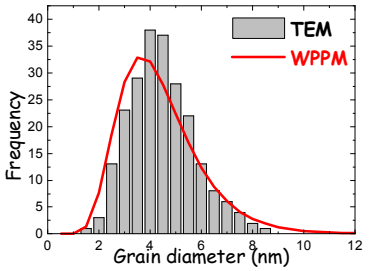

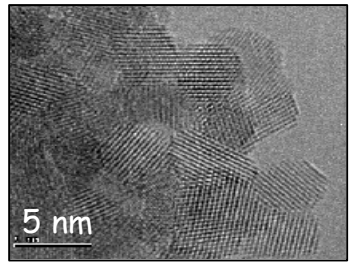

Dislocation (strain) effect: ρ, **Re**, $(\bar{C}_{hkl})$

$$A_{\{hkl\}}^D(L) = \exp\left[-\frac{1}{2}\pi|b|^2\,\bar{C}_{hkl}\,\rho\,d_{\{hkl\}}^{*2}\cdot L^2 f^*\left(L/R_e\right)\right]$$

$$\bar{C}_{hkl} = A + B\cdot\frac{h^2k^2 + k^2l^2 + l^2h^2}{\left(h^2+k^2+l^2\right)^2} = A + B\cdot H$$

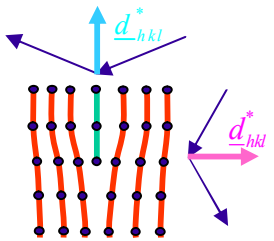

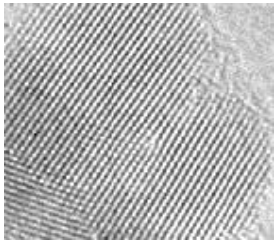

Faulting: α (def.), β (twin)

$$A_{hkl}^F(L) = \left(1-3\alpha-2\beta+3\alpha^2\right)^{\left|\frac{1}{2}Ld^*_{\{hkl\}}\cdot\frac{L_o}{h_o^2}\sigma_{L_o}\right|}$$

$$B_{hkl}^F(L) = -\sigma_{L_o}\cdot\frac{L}{|L|}\cdot\frac{L_o}{|L_o|}\cdot\beta\Big/\left(3-6\beta-12\alpha-\beta^2+12\alpha^2\right)^{1/2}$$

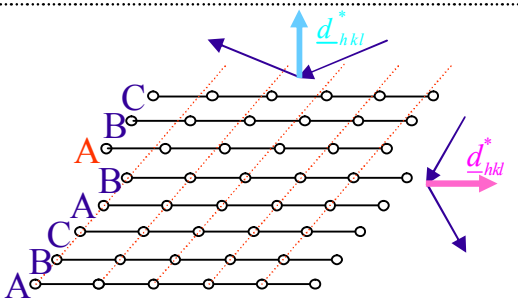

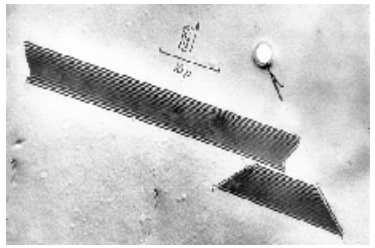

Anti-Phase Domains: γ

$$A_{\{hkl\}}^{APB}(L) = \exp\left[-\frac{-2\gamma\left(|h|+|k|\right)\cdot L}{d_{hkl}\left(h^2+k^2+l^2\right)}\right]$$

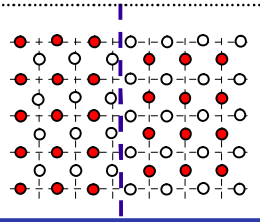

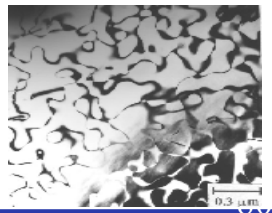

WHOLE POWDER PATTERN MODELLING

- Diffraction profiles are modelled directly in terms of relatively few microstructural parameters: μ, σ - ρ, R_e - α, β - γ ...
- No arbitrary profile functions (Voigt, pseudo-Voigt, Pearson VII, etc.)

WPPM : based on physical models of microstructure and lattice defects

More Theory: see REFERENCES

WPPM

APPLICATIONS

WPPM APPLICATIONS: NANOCRYSTALLINE CERIA

Nanocrystalline cerium oxide: growth kinetics of a xerogel

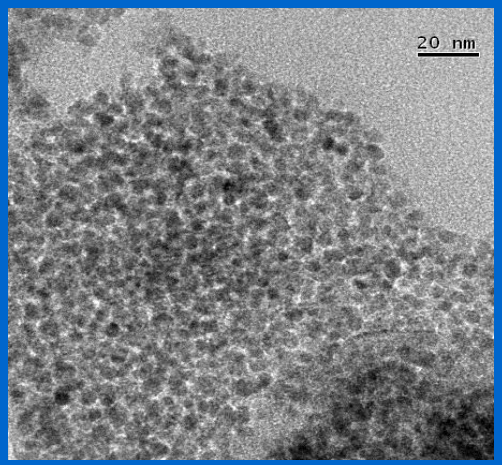

WPPM APPLICATIONS: NANOCRYSTALLINE CERIA

Xerogel obtained by vacuum-drying: broad diffraction lines of nanocrystalline fcc phase

0.8 hour

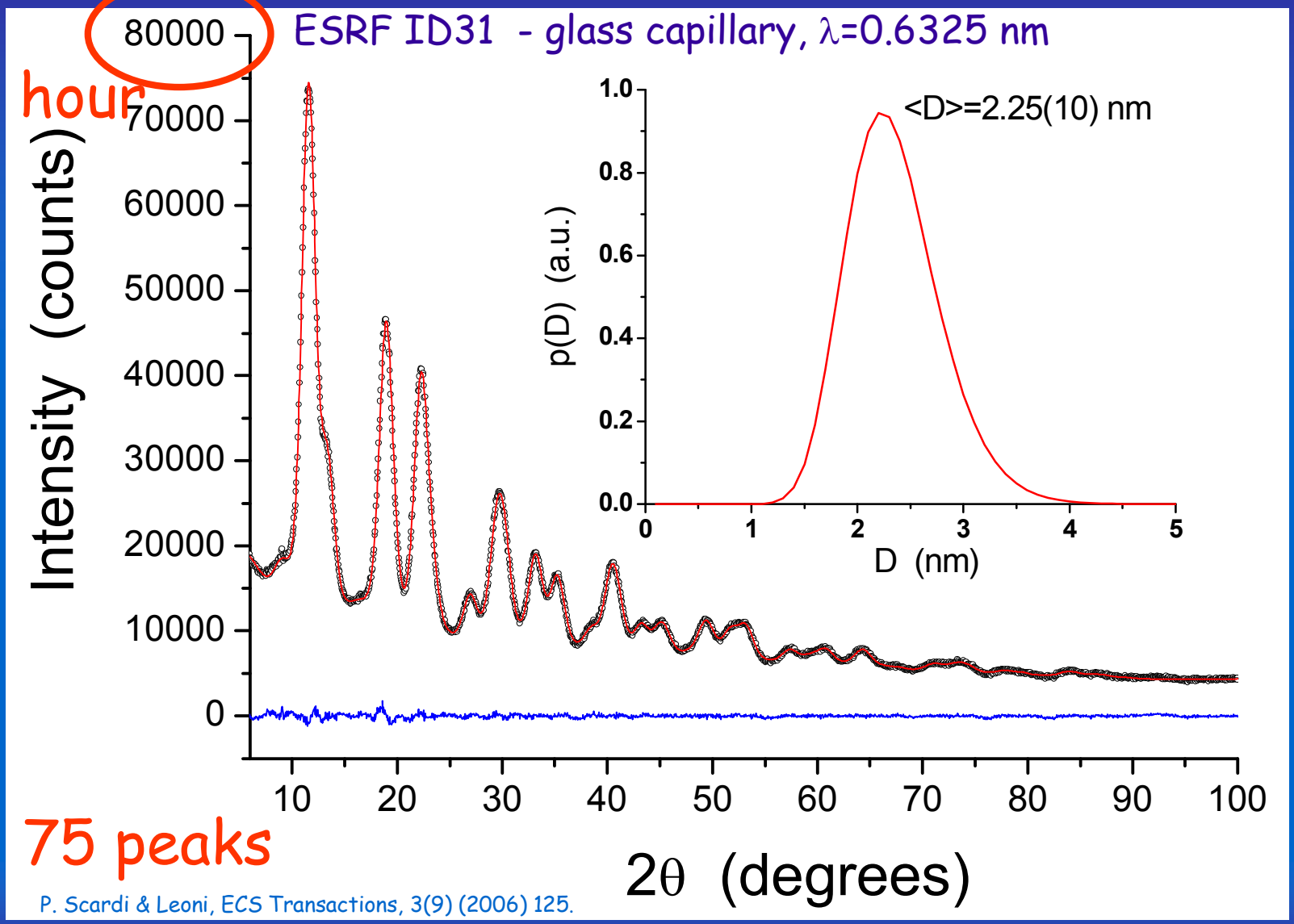

75 peaks

P. Scardi & Leoni, ECS Transactions, 3(9) (2006) 125.

WPPM APPLICATIONS: NANOCRYSTALLINE CERIA

Evolution of line profiles during isothermal treatment: 300°C, 350°C, 400°C

High temperature blower on ID31 at ESRF

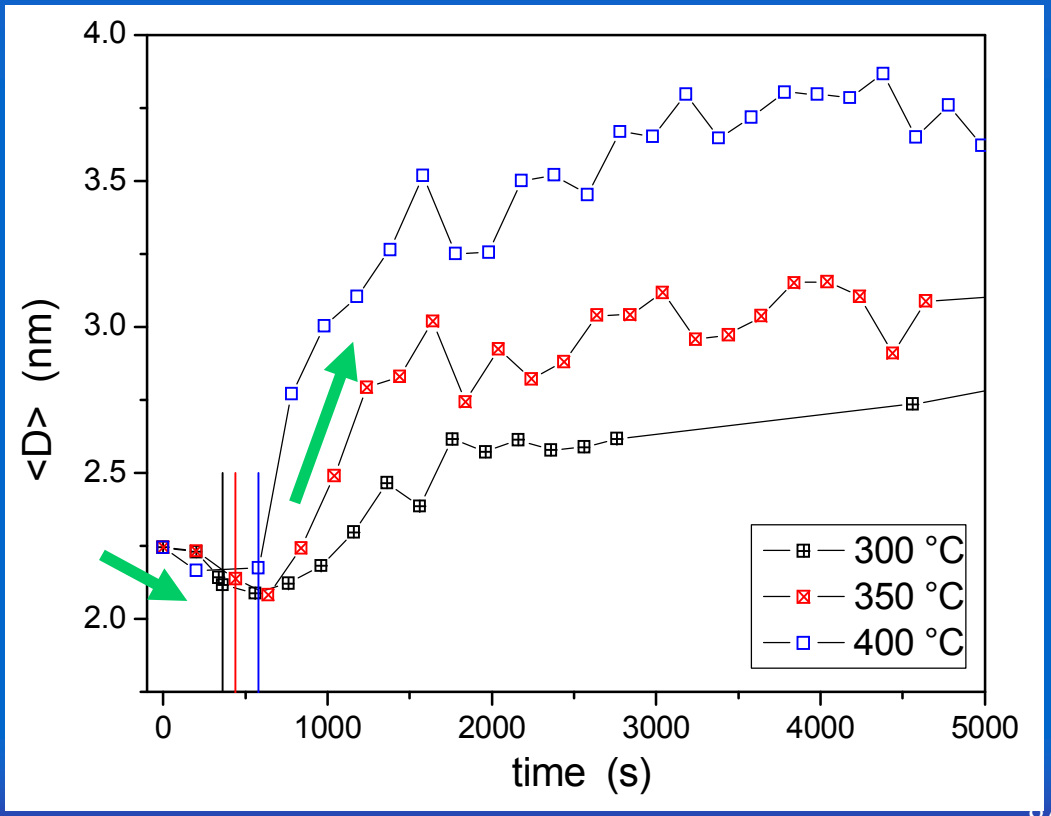

WPPM APPLICATIONS: NANOCRYSTALLINE CERIA

Nucleation during the heating stage: mean domain size initially decreases, before the grain growth starts

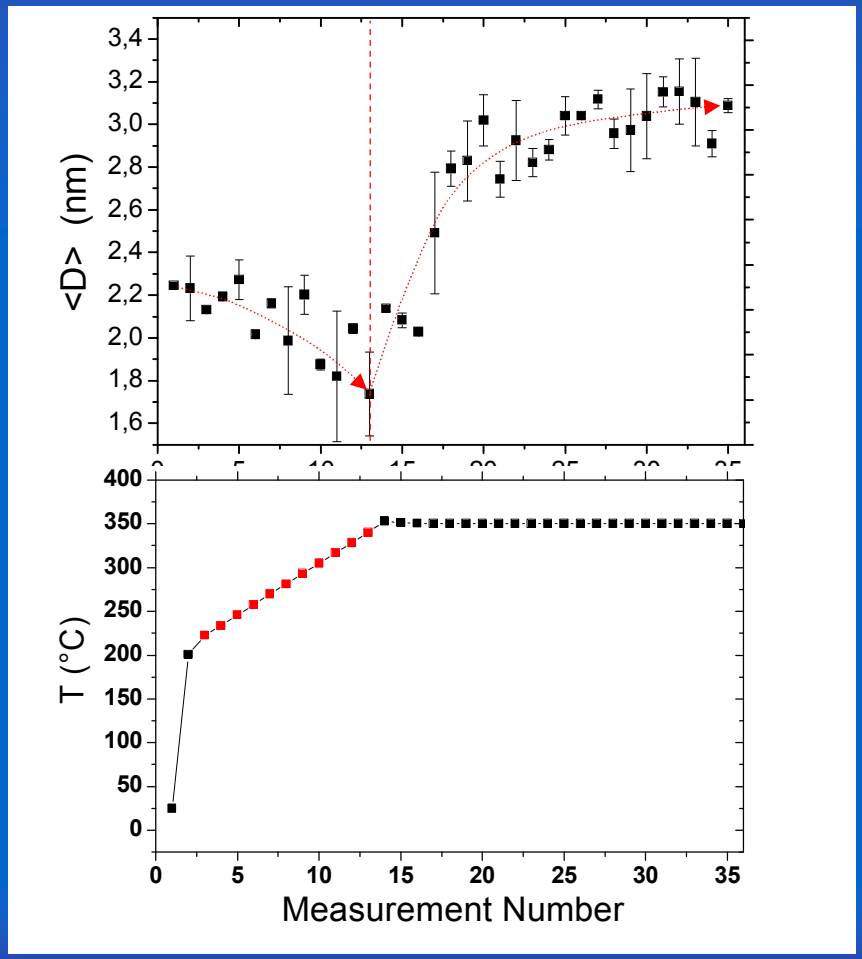

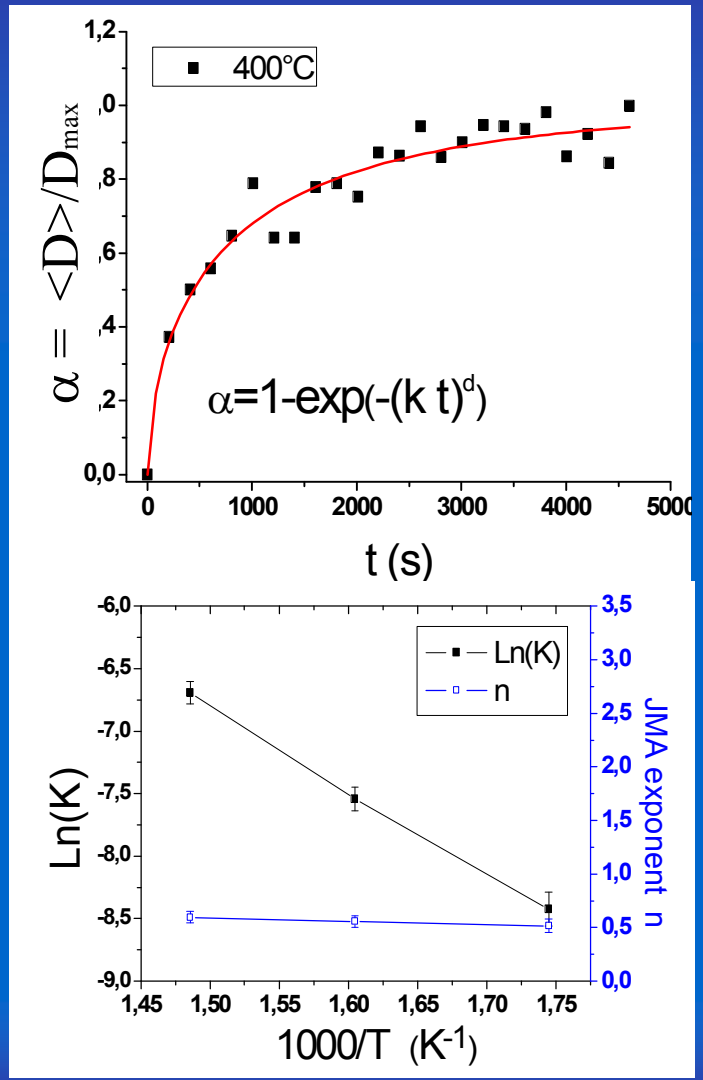

WPPM APPLICATIONS: NANOCRYSTALLINE CERIA

Heat treated 1h @ 400°C

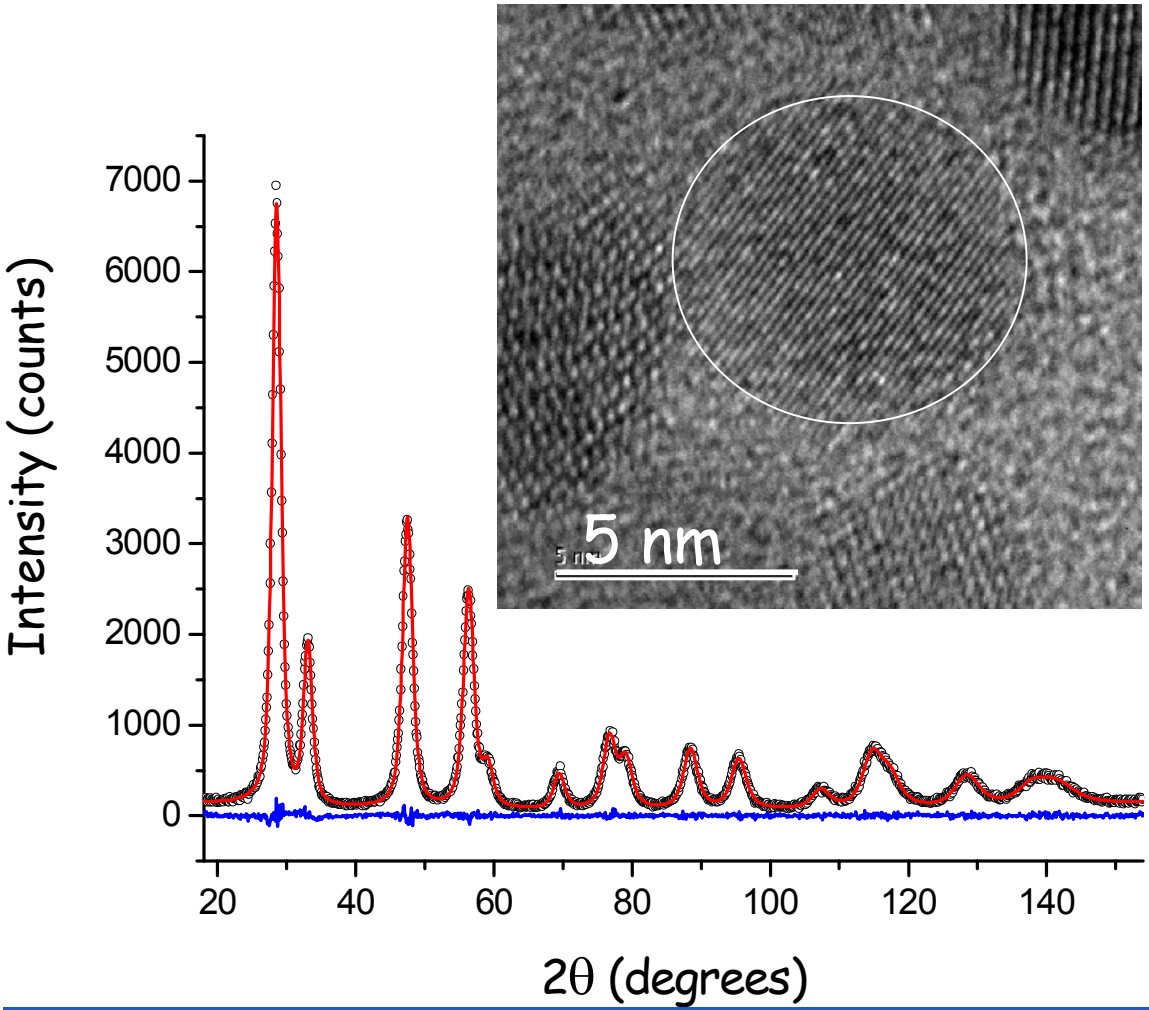

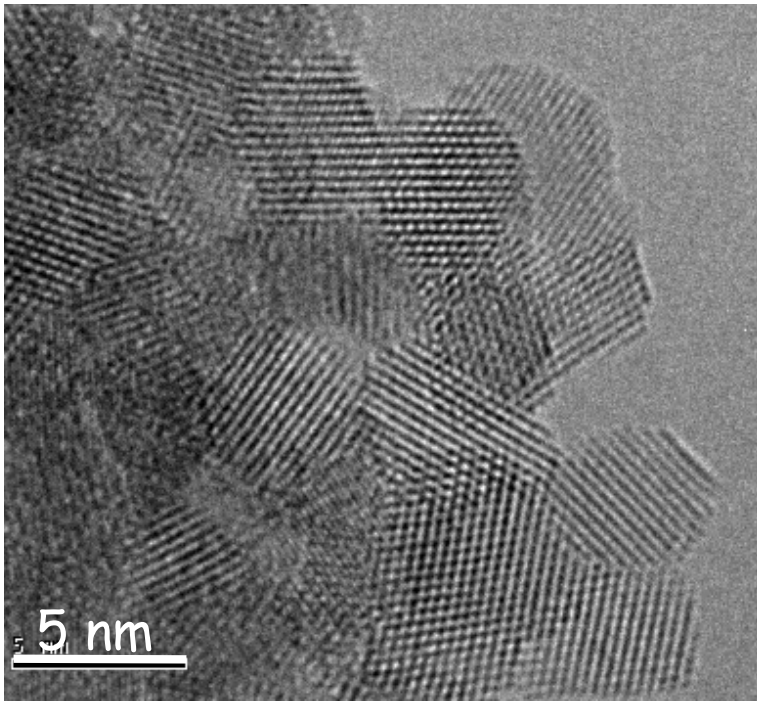

M. Leoni & P.Scardi, in *Diffraction Analysis of Materials Microstructure.* E.J. Mittemeijer & P. Scardi, editors. Berlin: Springer-Verlag. 2004

WPPM APPLICATIONS: NANOCRYSTALLINE CERIA

Heat treated 1h @ 400°C

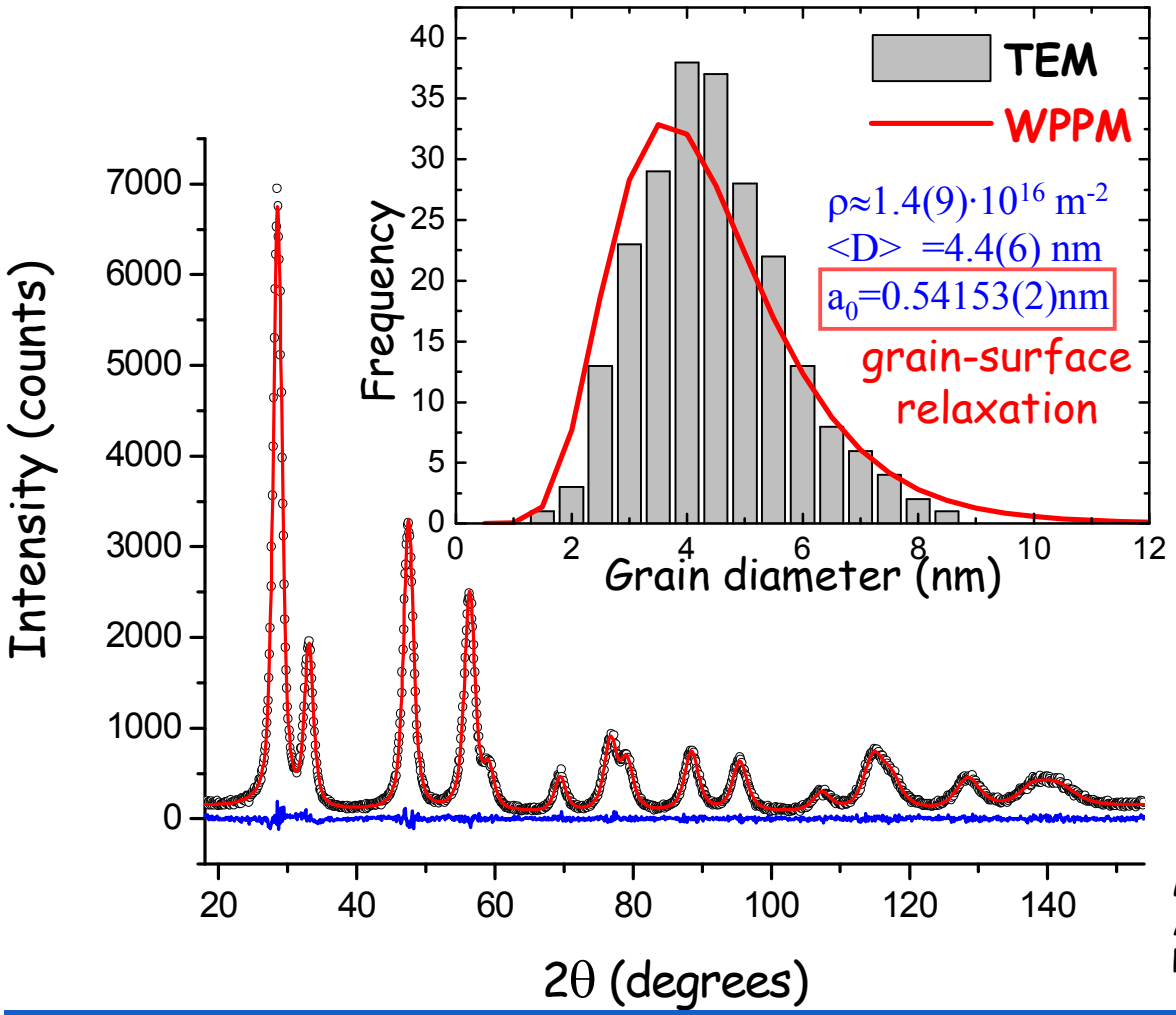

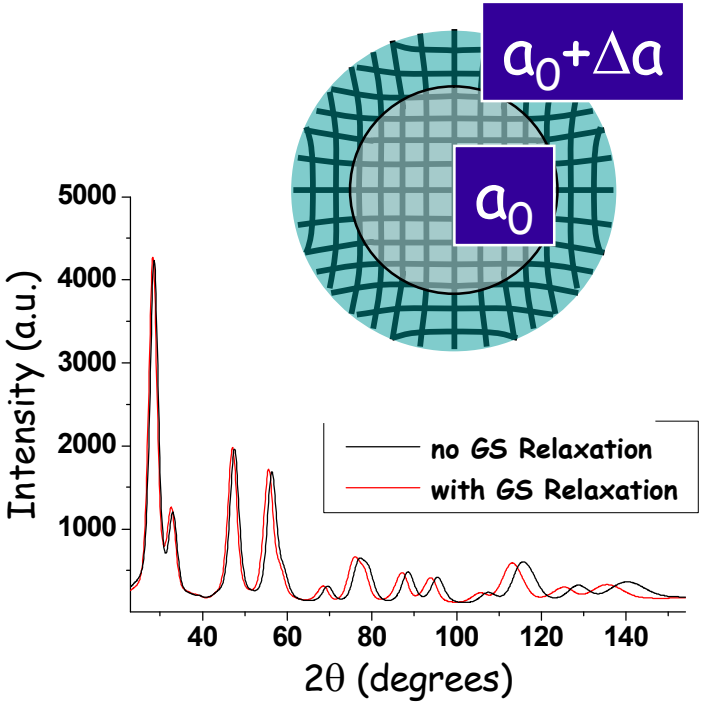

M. Leoni & P.Scardi, in *Diffraction Analysis of Materials Microstructure*. E.J. Mittemeijer & P. Scardi, editors. Berlin: Springer-Verlag. 2004

WPPM APPLICATIONS: NANOCRYSTALLINE CERIA

Highly-energy mechanical grinding ball-milled Fe-1.5%Mo

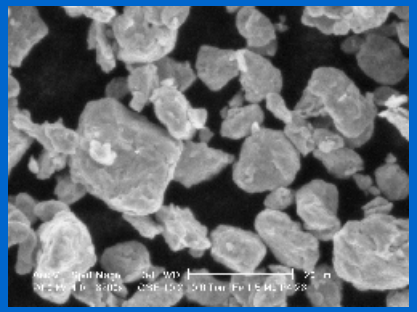

NANOCRYSTALLINE Fe-1.5%Mo POWDER

Planetary ball mill - process modelling & production

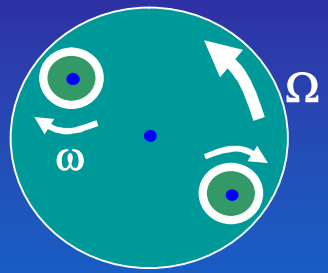

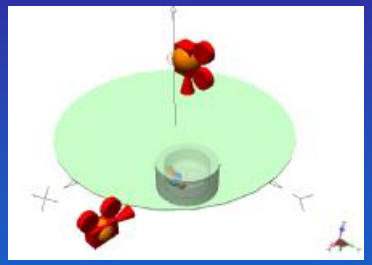

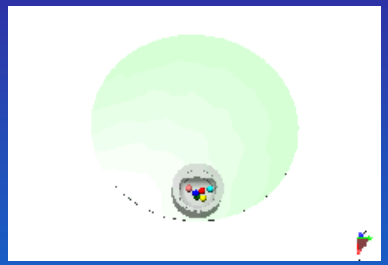

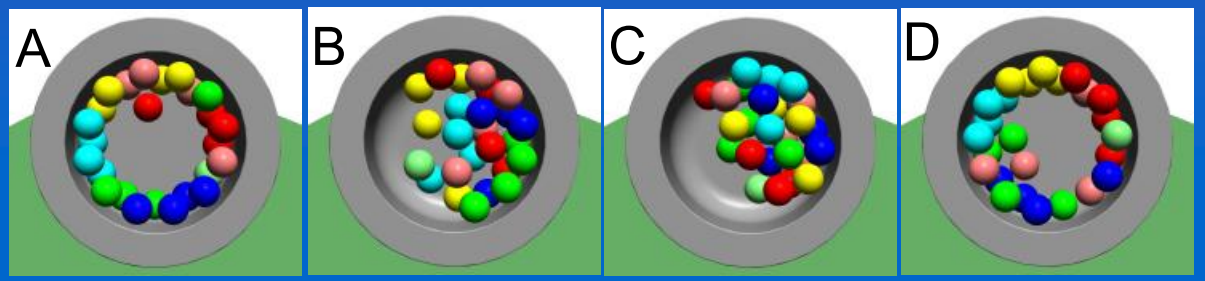

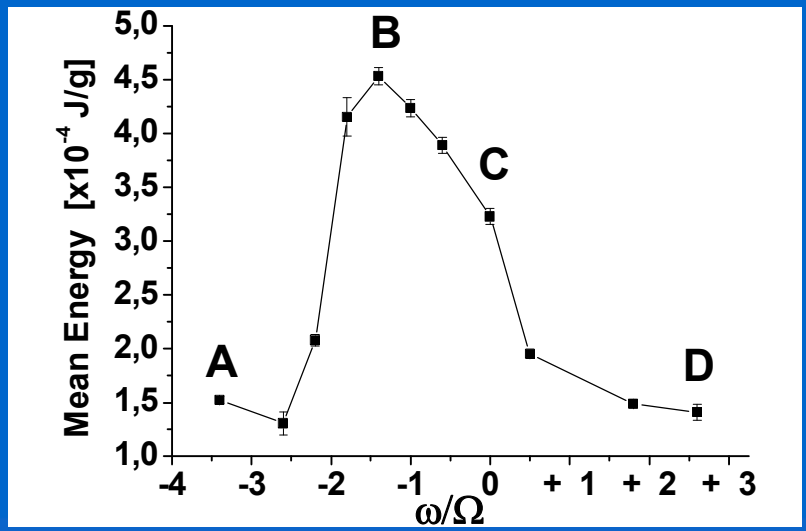

M. d'Incau,. Leoni & P. Scardi, J. Materials Research 22 (2007) 1744-1753.

NANOCRYSTALLINE Fe-1.5%Mo POWDER

Ball milled Fe1.5Mo (Fritsch P4) – data collected at ESRF – ID31 λ=0.0632 nm

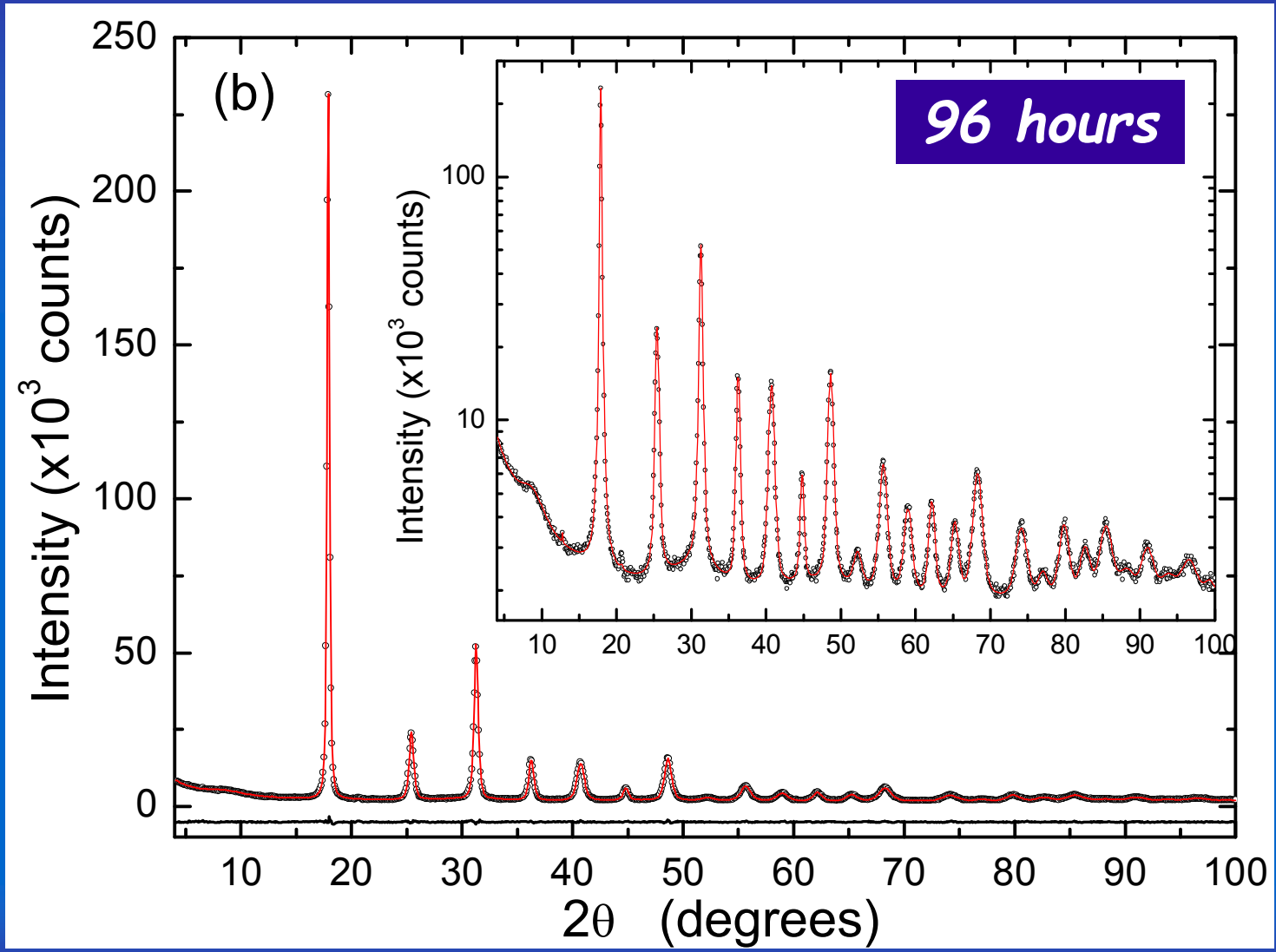

NANOCRYSTALLINE Fe-1.5%Mo POWDER

Ball milled Fe1.5Mo (Fritsch P4) – data collected at ESRF – ID31 λ=0.0632 nm

dislocation density/domain size vs. morphology

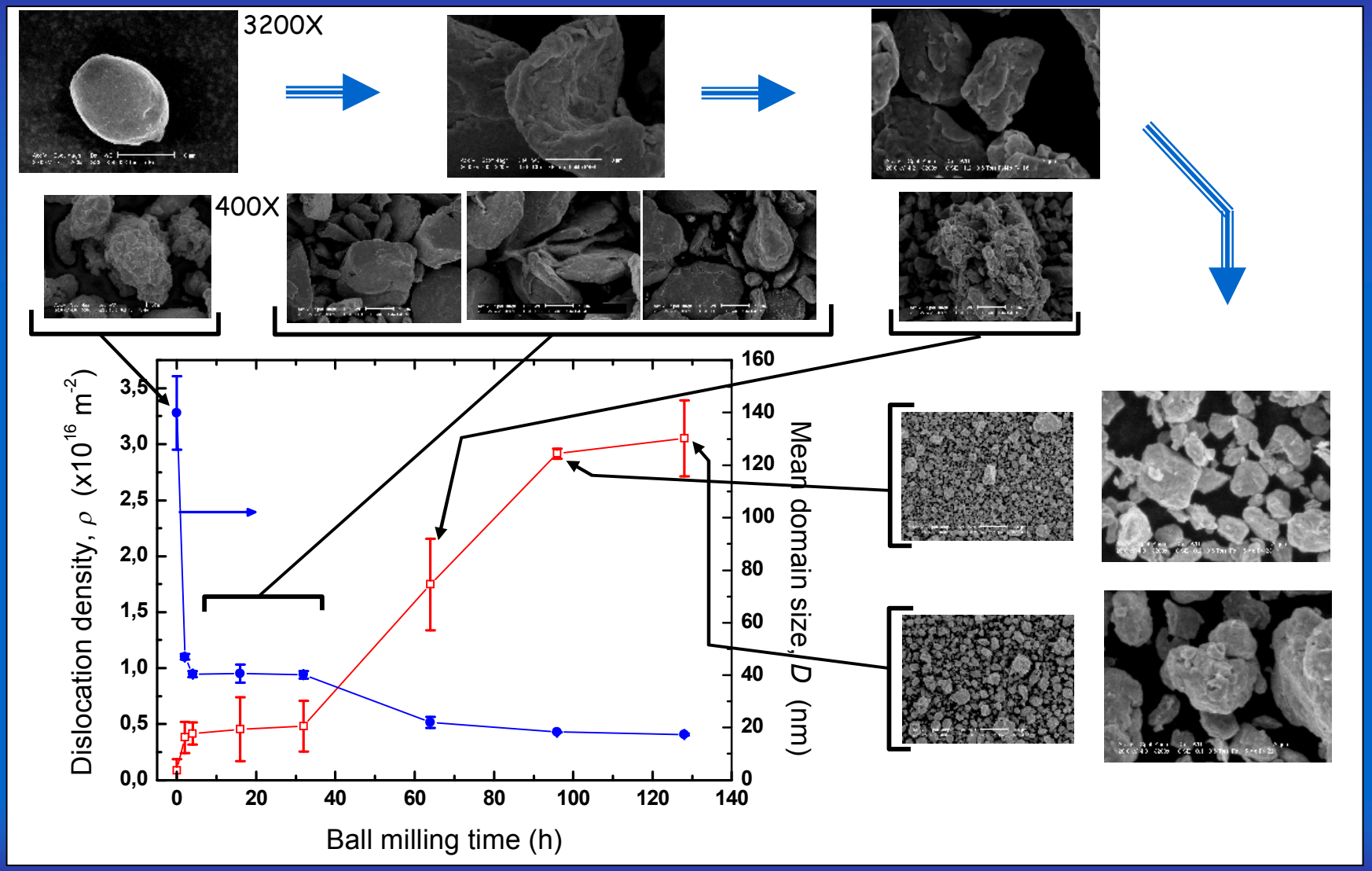

NANOCRYSTALLINE Fe-1.5%Mo POWDER

Ball milled Fe1.5Mo (Fritsch P4) – data collected at ESRF – ID31 λ=0.0632 nm

dislocation density/domain size vs. morphology

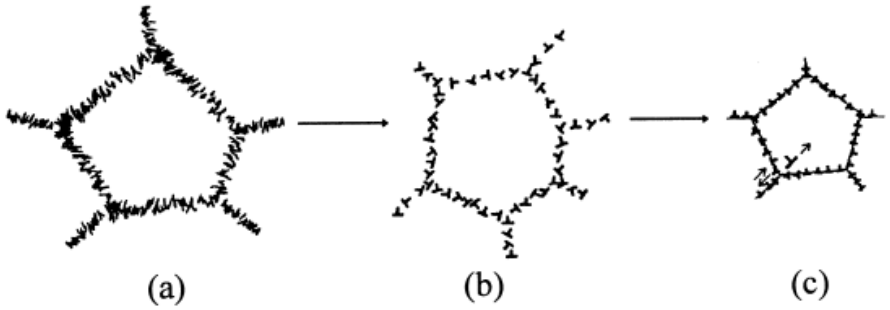

Fig. 15. Schematic model of dislocation structure evolution at different stages during severe plastic deformation.

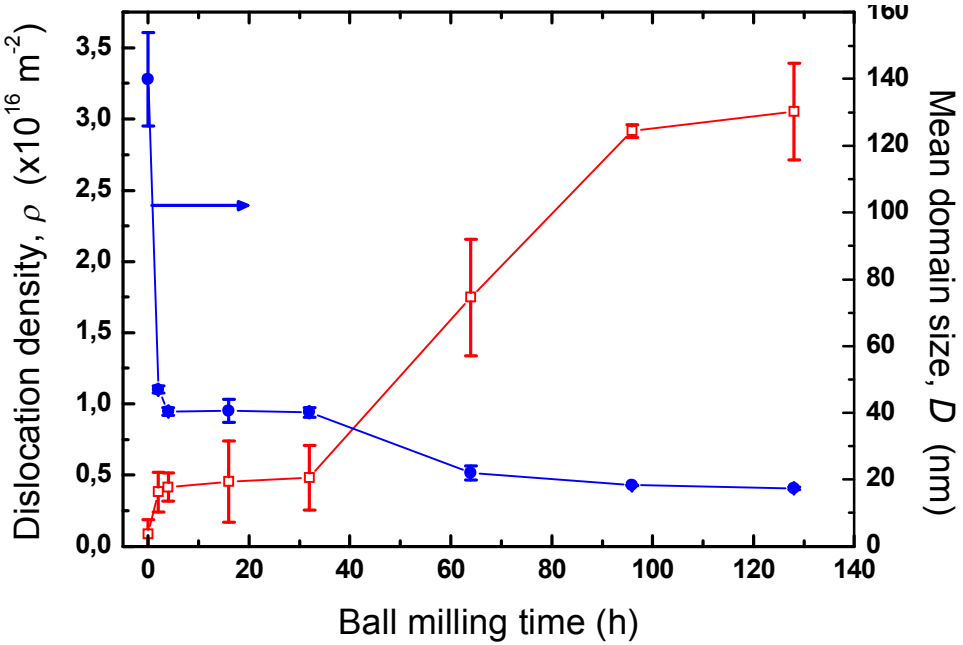

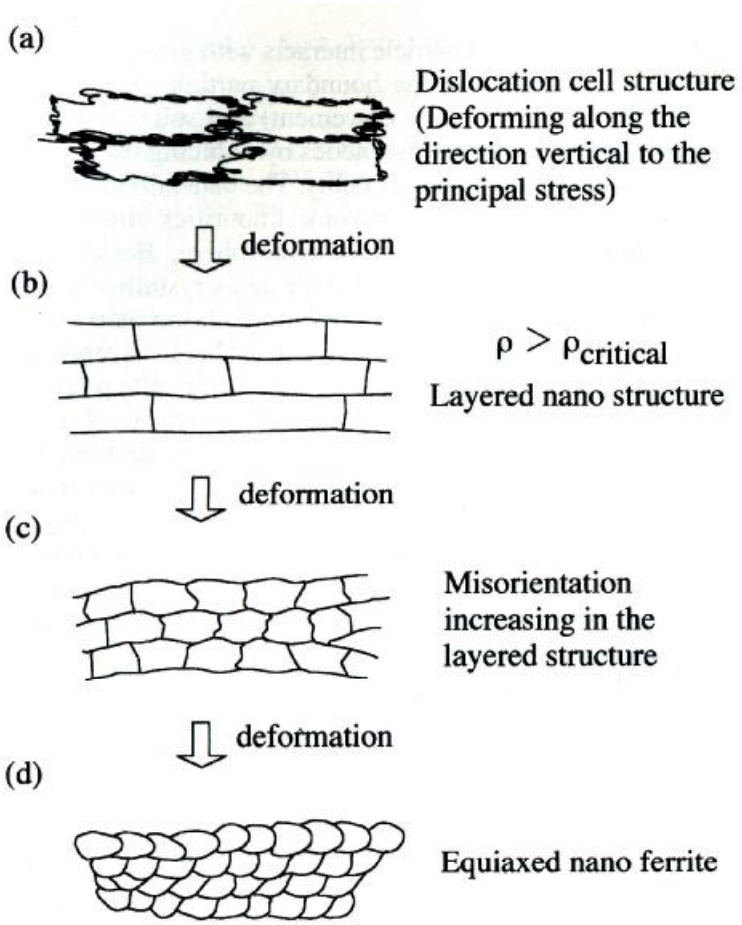

Fig. 11—(*a*) through (*d*) A schematic drawing of nanocrystalline ferrite formation by ball milling.

NANOCRYSTALLINE Fe-1.5%Mo POWDER

Ball milled Fe1.5Mo (Fritsch P4) – data collected at ESRF – ID31 λ=0.0632 nm

In addition to mean values, WPPM provides the size distribution

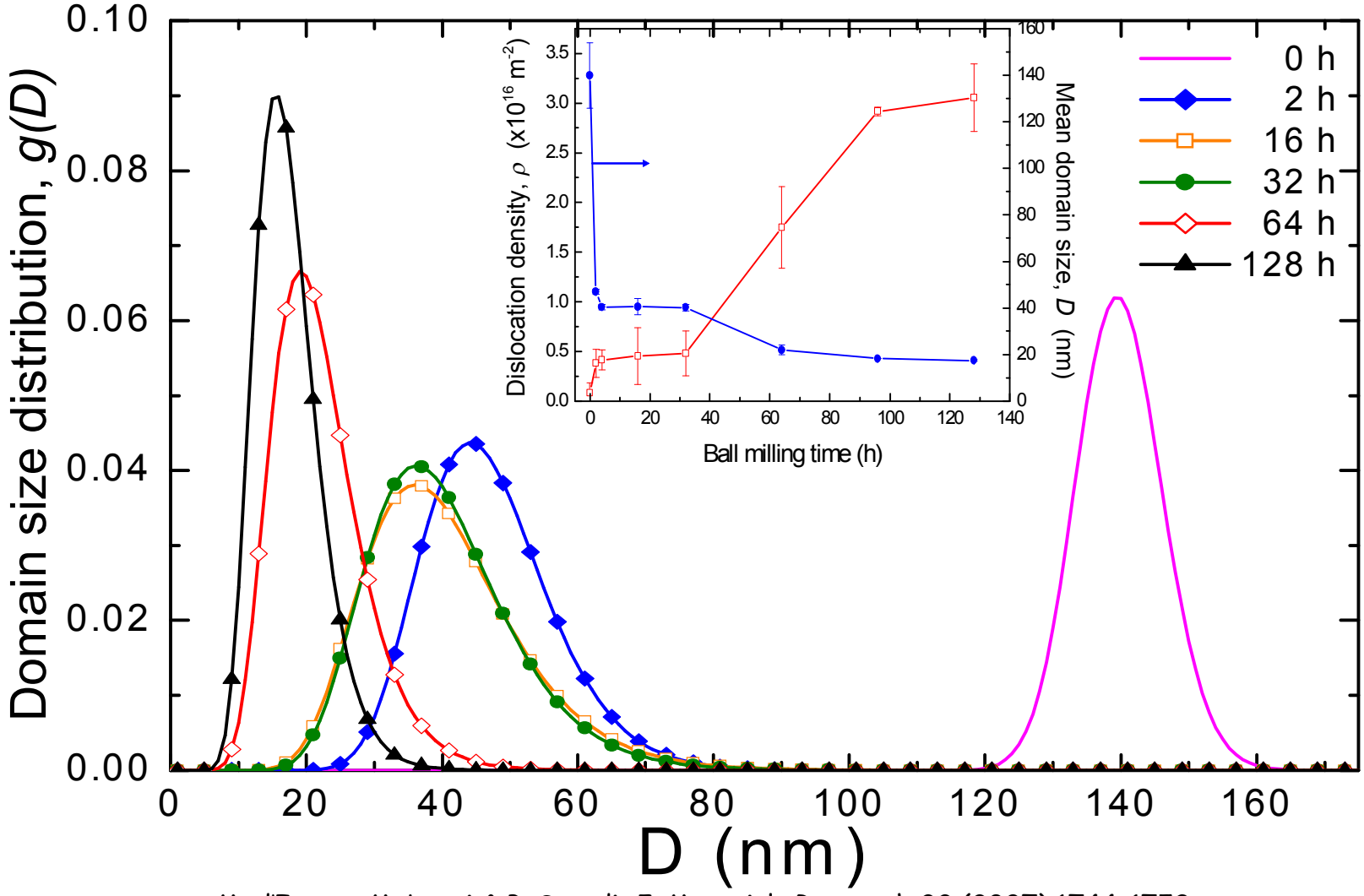

M. d'Incau,. M. Leoni & P. Scardi, J. Materials Research 22 (2007) 1744-1753.

PM2K SOFTWARE - email to: Paolo.Scardi@unitn.it

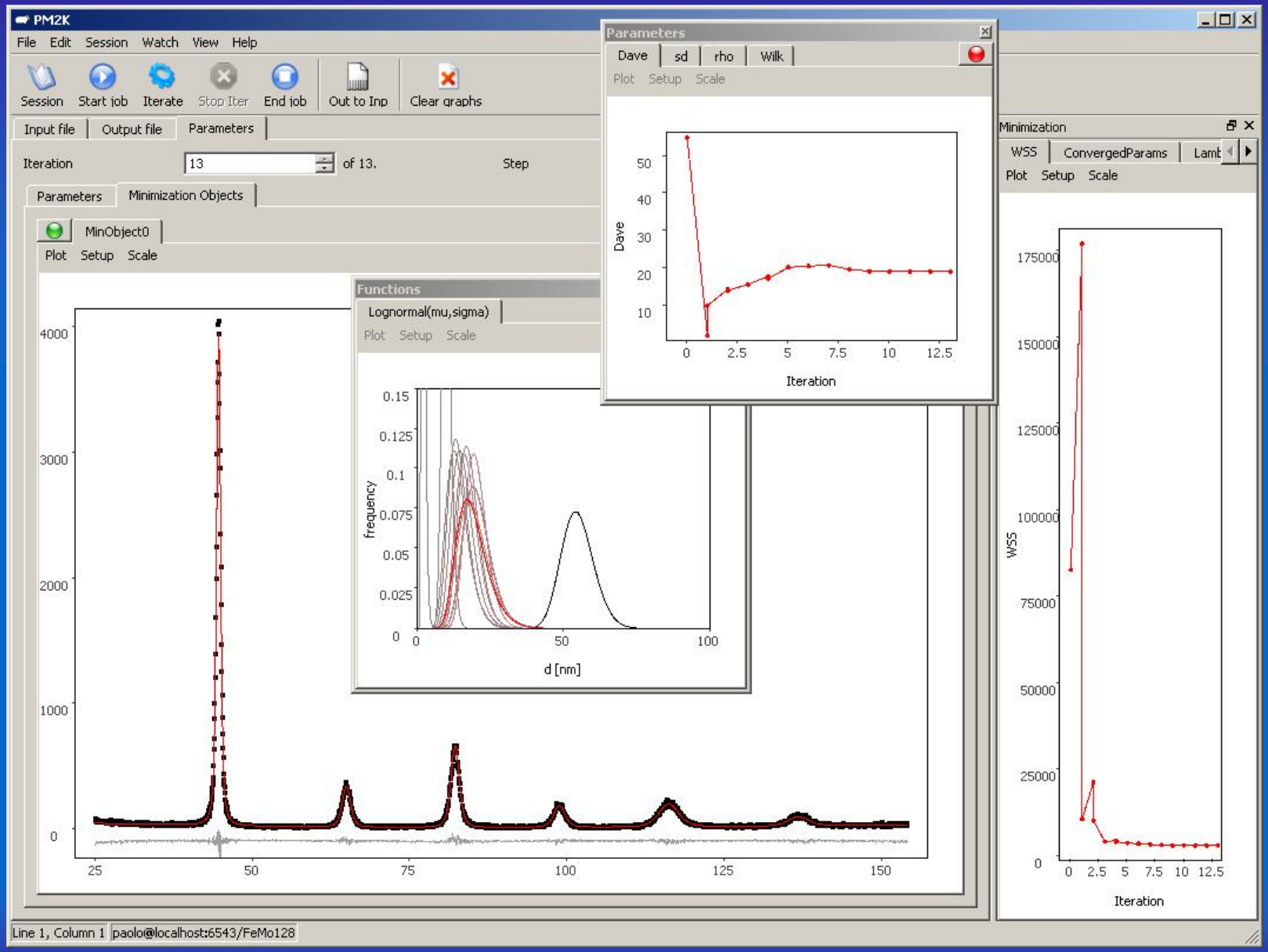

PART 2: REFERENCES - Paolo.Scardi@unitn.it

- P.Scardi & M. Leoni, *Acta Cryst.* A 57 (2001) 604
- P.Scardi & M. Leoni, *Acta Cryst.* A 58 (2002) 190
- P.Scardi, M. Leoni, R. Delhez *J. Appl. Cryst.* 37 (2004) 381
- M. Leoni, P. Scardi *J. Appl. Cryst.* 37 (2004) 629
- P. Scardi & M. Leoni, *Acta Mater.* 53 (2005) 5229.
- P. Scardi & M. Leoni *J. Appl. Cryst.* 39 (2006) 24.

Diffraction Analysis of Materials Microstructure
E.J. Mittemeijer & P. Scardi, editors.
Berlin: Springer-Verlag, 2004.

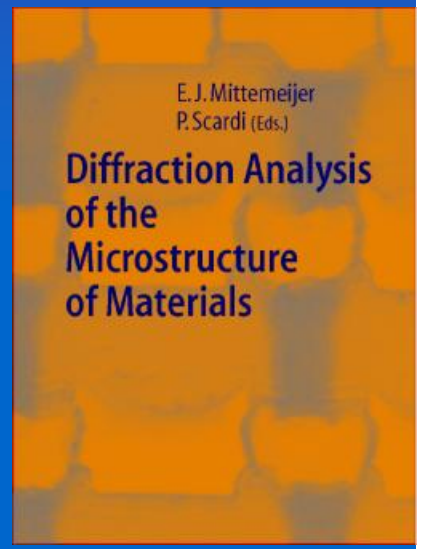

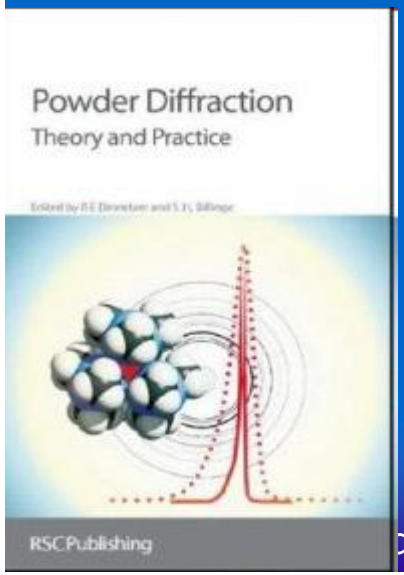

Powder Diffraction: Theory and Practice
R.E. Dinnebier & S.J.L. Billinge, editors.
Cambridge: Royal Society of Chemistry, 2008.

MCX - *A new beamline for Materials Characterization by XRD at ELETTRA (Trieste, Italy)*

G. Paolucci, E. Busetto, A. Lausi, J. Plasier (Sincrotrone Trieste), P.Scardi (Univ. Trento & INSTM)

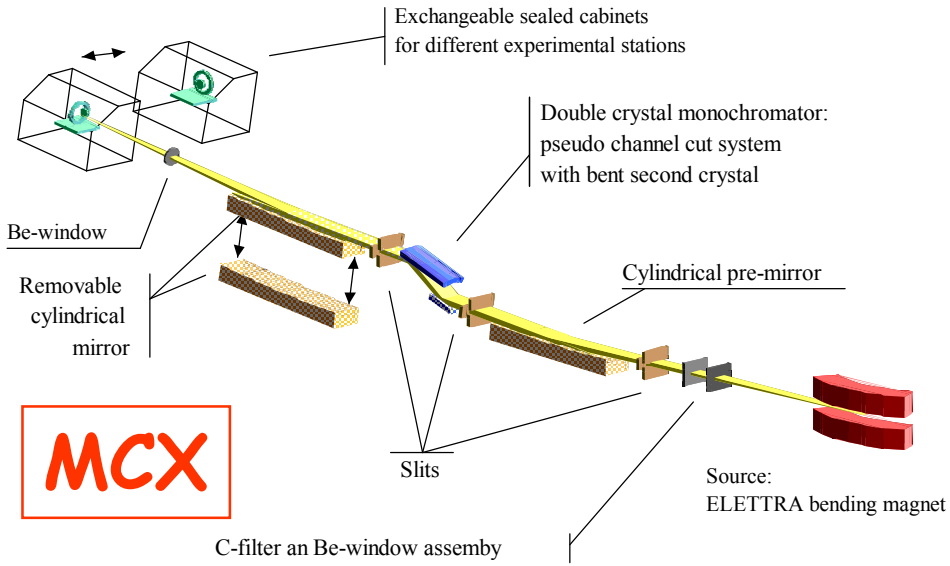

Examples of typical applications

- Residual stress and texture analysis in thin films by multiple wavelength XRD
- Surface analysis by grazing incidence XRD and reflectivity
- Medium-low energy (3.5÷20 keV) anomalous scattering XRD
- Line Profile Analysis (e.g., nanocrystalline, highly defected materials)
- Non-ambient studies (controlled atmosphere, high temperature kinetics)
- Surface mapping by microdiffraction (diffraction on small area)

University of Trento

International Doctoral School in Materials Science & Engineering

About 10 new positions per year
one bursary specific to MCX / ELETTRA

Information and applications:

http://www.mse.unitn.it

Paolo.Scardi@unitn.it

